The Phase Behaviour of Hydrogenated Phosphatidylinositol in Monolayers at the Air-Water Interface

Nancy Austin

A Thesis

in

The Department

of

Chemistry and Biochemistry

Presented in Partial Fulfilment of the Requirements of the Degree of Master of Science in
Chemistry at
Concordia University
Montréal, Québec, Canada

August 2005

Library and
Archives Canada

Published Heritage
Branch

395 Wellington Street
Ottawa ON K1A 0N4
Canada

Bibliothèque et
Archives Canada

Direction du
Patrimoine de l'édition

395, rue Wellington
Ottawa ON K1A 0N4
Canada

Your file Votre référence
ISBN: 0-494-10207-1
Our file Notre référence
ISBN: 0-494-10207-1

NOTICE:
The author has granted a non-exclusive license allowing Library and Archives Canada to reproduce, publish, archive, preserve, conserve, communicate to the public by telecommunication or on the Internet, loan, distribute and sell theses worldwide, for commercial or non-commercial purposes, in microform, paper, electronic and/or any other formats.

The author retains copyright ownership and moral rights in this thesis. Neither the thesis nor substantial extracts from it may be printed or otherwise reproduced without the author's permission.

AVIS:
L'auteur a accordé une licence non exclusive permettant à la Bibliothèque et Archives Canada de reproduire, publier, archiver, sauvegarder, conserver, transmettre au public par télécommunication ou par l'Internet, prêter, distribuer et vendre des thèses partout dans le monde, à des fins commerciales ou autres, sur support microforme, papier, électronique et/ou autres formats.

L'auteur conserve la propriété du droit d'auteur et des droits moraux qui protège cette thèse. Ni la thèse ni des extraits substantiels de celle-ci ne doivent être imprimés ou autrement reproduits sans son autorisation.

In compliance with the Canadian Privacy Act some supporting forms may have been removed from this thesis.

While these forms may be included in the document page count, their removal does not represent any loss of content from the thesis.

Conformément à la loi canadienne sur la protection de la vie privée, quelques formulaires secondaires ont été enlevés de cette thèse.

Bien que ces formulaires aient inclus dans la pagination, il n'y aura aucun contenu manquant.

Canada

Abstract

It has been suggested that phosphatidylinositol (PI), a precursor for a family of lipid messengers, forms lipid rafts in the membrane which are regulated by protein kinases and/or by the biophysical properties of this phospholipid. To better understand this raft formation, a simplified system comprising hydrogenated derivatives of soy PI was investigated. Analytical analysis using GC-FID and ESI-MS confirms that commercial PIH still contained 15% unsaturation. The effect of this unsaturation played a role in the phase behaviour, where a richer polymorphism for PIH compared to that of natural PI was observed. PIH phase separated at high pressures and all temperatures, which was confirmed by Brewster Angle Microscopy (BAM) at the air-water interface and AFM on Langmuir-Blodgett films deposited on mica. We report, for the first time, the presence of a condensed phase monolayer which was supported by the crystallographic data (GIXD) obtained for PIH. It was observed that phase separation of the monolayer becomes more apparent at all surface pressures as temperature increased. In our study, we report for the first time, the critical temperature above which a transition from a gaseous to a liquid-expanded phase occurs. The ability of PIs to form condensed phases plays a significant role in the miscibility with other membrane components, where a more condensed film is observed. Results suggest that intermolecular interactions between adjacent inositol headgroups affect the miscibility of PIH with phosphatidylcholine and phosphatidylethanolamine.

Acknowledgements

This thesis is dedicated to:

Dr. Rolf Schmidt, with whom I could not have done this without.

Dr. Christine DeWolf, my supervisor, who motivated and encouraged me from day one.

My brother and sister, Robert and Donna for kept me grounded.

My grandmother for her love and support

Last, but not least, my mother for believing in me when nobody else did.

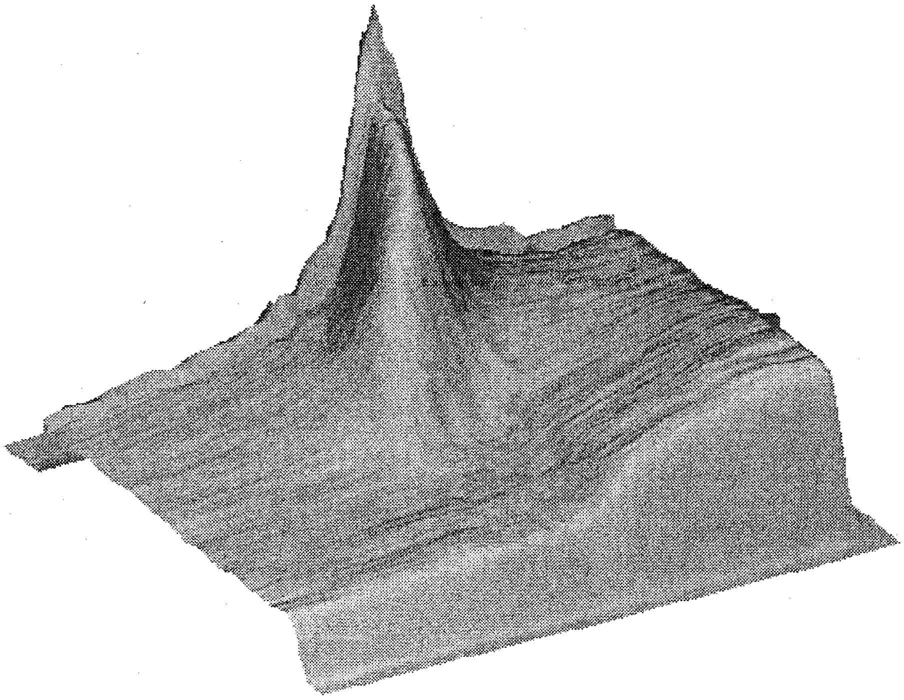

Table of Contents

List of Figures

List of Tables

List of Equations

List of Symbols

a: lattice constants

a_o: the cross sectional length of the headgroup

A: molecular area

A^E: excess area

A_c: critical area

A_{av}: the average/ideal area per molecule

A_o: cross-sectional area of chains

$A_{substrate}$: area of substrate immersed in water

A_{trough}: area of monolayer removed from subphase at constant surface pressure

A_1 and A_2: the areas per molecule

A_{12}: the difference between the actual and the ideal area per molecule

b: lattice constant

CS: crystalline phases

d_{hk}: d = repeat distance; h & k are miller indices

E: the incident and reflected vectors

G: Gibbs free energy

H_I: hexagonal

I: cubic

k: wavenumber

k: Boltzmann constant

K_{xy}: also known as Q_{xy}

K_z: also known as Q_z

L_{2d}: hexagonal rotator phase

L_2'': crystalline phase

$L\alpha$:lamellar phase

$L\beta$: gel phase

$L\beta'$: tilted gel phase

l_c: length of the hydrocarbon chains

LS: hexagonal rotator phase

n: number of molecules in the unit cell

n: number of moles (ideal gas law)

n_1: refractive indices of water

N_1 and N_2: mole ratios

N_{av}: Avogadro's number

O_v: hexagonal rotator phase

P: perimeter of the plate

P_b: rippled phase

Q_{xy}: an in plane component (GIXD)

Q_z: an out of plane component (GIXD)

R: reflection matrix

R: gas constant

R_s: resolution

S, L_2', L_{2h}: intermediate phase

T_R: transfer ratios

t: the tilt angle from the normal

V_{chain}: volume occupied by a single lipid molecule

w : work

w_T: is the total force and w_P is the force from plate

α subunit: one of the three subunits of PLC which make up the structure of this protein

α_f: the angle of the diffracted beam intensity

$\beta\gamma$ dimer: two of the three subunits of PLC which make up the structure of this protein

Δ: ellipsometric angle

$\delta\Delta$: the difference between the ellipsometric angle Δ of the film on the subphase and the subphase alone

γ: the surface tension

γ: lattice constants

γ^0: the surface tension with no amphiphile present

π: surface pressure

x: compressibility

2Θ: angle of diffraction

θ: the contact angle

φ: incident angle

ψ: the tilt azimuth angle

ψ and Δ: ellipsometric angles

λ: frequency

List of Abbreviations

AFM: Atomic Force Microscopy
BAM: Brewster Angle Microscopy
CMC: Critical Micellar Concentration
CPP: Critical Packing Parameter
DAG: Diacylglycerol
DMPI: Dimyritoylphosphatidylinositol
DMPC: Dimyritoylphosphatidylinositol
DPPA: 1,2-Dipalmitoyl-*sn*-Glycero-3-Phosphate
DPPC: 1,2-Dipalmitoyl-*sn*-Glycero-3-phosphocholine
DPPI: L-α-Dipalmitoylphosphatidylinositol
DPPI-3P: Dipalmitoylphosphatidylinositol 3-Phosphate
DPPI-4P: Dipalmitoylphosphatidylinositol 4-Phosphate
DPPI-5P: Dipalmitoylphosphatidylinositol 5-Phosphate
DSPC: 1,2-Distearoyl-*sn*-Glycero-3-Phosphatidylcholine
DSPE: 1,2-Distearoyl-*sn*-Glycero-3-Phosphatidylethanolamine
DSC: Differential Scanning Calorimetry
Elli: Ellipsometry
ESI-MS: electrospray ionization mass spectrometry
FAME: Fatty Acids Methyl Ester
FID: Flame Ionization Detector
FRET: Fluorescence Resonance Energy Transfer

FTIR: Fourier Transfer Infrared

GC: Gas Chromatography

GIXD: Grazing Incidence X-ray Diffraction

HEPES: N-[2-Hydroxyethyl]piperazine-N'-[2-ethanesulfonic acid]

IP_3: Inositol Triphosphate

IP_2: Inositol Bisphosphate

LB: Langmuir-Blodgett

LFB: Langmuir Film Balance

LS: Lung Surfactant

$(M-H)^-$: abundance peaks

NMR: Nuclear Magnetic Resonance

NN: Nearest Neighbours

NNN: Next Nearest Neighbours

PA: Phosphatidic acid

PC: Phophatidylcholine

PCSA arrangement: Polarizer-Compensator-Sample-Analyzer

PG: Phosphatidylglycerols

PI: L-α-phosphatidylinositol

PI(3)P: Phosphatidylinositol-3-Phosphate

$PI(3,4)P_2$: Phosphatidylinositol-3,4-Phosphate

$PI(3,5)P_2$: Phosphatidylinositol-3,5-Phosphate

$PI(3,4,5)P_3$: Phosphatidylinositol-3,4,5-Phosphate

PI(4)P: Phosphatidylinositol-4-Phosphate

PI(5)P: Phosphatidylinositol 5-Phosphate

PI(4,5)P_2: Phosphatidylinositol-4,5-Phosphate

PI-3 kinase: Phosphoinositide 3-Kinase

PKC: Protein Kinase C

PLA_2: Phospholipase A_2

PLC: Phospholipase C

PLD: Phospholipase D

PSD: Position Sensitive Detector

sn: stereospecifically numbered

SUV: Small Unilamellar Vesicles

TA: Tilt Azimuth

T_m: melting temperature

Chapter 1: Introduction

1.1 Bilayers/Membrane/Structure & Organization

A cell is one of nature's most unique assemblies given that it is highly organized with many functional units or organelles[1]. Each organelle consists of at least one membrane, which is vital to its function. Overall, a membrane is a dynamic complex structure that contains proteins, polysaccharides and lipids (see Figure 1). All membranes contain specific proteins that enable it to perform exceptional roles. The function and action of proteins are specific and vary depending on their type. These roles include: acting as anchoring sites, regulating transportation in and out of a cell or subcellular domains, regulating the fusion of the membrane with other membranes in the cell, cell recognition and signal transduction by providing transmembrane receptors that bind signalling molecules, providing a stable site for binding and catalysis of enzymes and providing a passageway across the membrane for certain molecules[1].

Another important contributor to cell membranes is the lipid component, which are the building blocks for many biological structures, such as vesicles, as well as many membranous compartments. Membrane proteins rely on lipid matrices to enable proper formation of their native state. What makes phospholipids special is their amphiphilic nature, where they contain a polar region and a non-polar region, the head and tail portion, respectively. Within membranes, they are present in a distinctive lipid matrix made up of two leaflets of closely packed lipid with the non-polar regions projecting inwards creating a 30-40 Å thick barrier[2]. Depending on the type of organelle, the proportion of protein to lipid will vary, where 25 to 75 % w/w of lipid is present within the membrane and the remaining proportion being protein, glycoprotein and/or lipoprotein[2]. Regardless of the various percentages of lipid present, the structural integrity of a membrane is attributed to the presence of this lipid matrix. The membrane has three major roles, where it: (i) provides a barrier for passive diffusional motion of small polar solutes, such as ions, sugar and low molecular weight metabolites. In addition it enables the passage of macromolecules, such as proteins, nucleic acids and other polysaccharides; (ii) provides a favourable environment for membrane proteins by increasing the solubility of proteins within a bilayer; and (iii) maintains the internal organization in the cell[2].

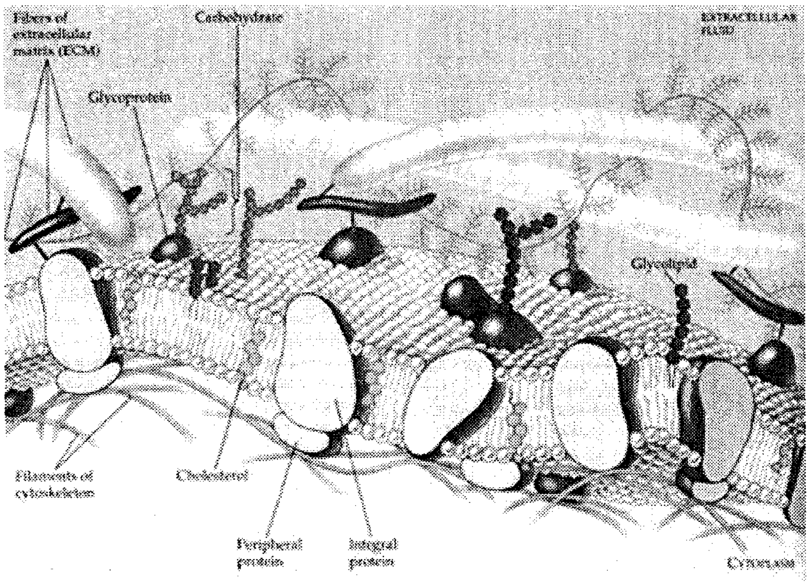

Figure 1 Schematic diagram representing structure of a plasma cell membrane in cross section[3]

Although proteins and polysaccharides are responsible for most of the chemical processes, their specific environment is created by lipids[2]. These lipids contribute to protein activity and function, where a multitude of processes in the living cell rely on a lipids distinctive and versatile properties. Despite this being considered a minor role, it is an important one in order to better understand protein functionality and activity.

1.1.1 Lipid Structure

The lipid components present in bilayers consist of phospholipids, cholesterol and glycolipids. Phospholipids are the principle types of membrane lipids in most organisms. Their structural motif is cylindrical in shape with a polar headgroup at one end of the hydrophobic diacylglycerol moiety. Phospholipids are classified as a glycerol derivative, which is designated by the prefix *sn* where the atoms of glycerol are *s*tereospecifically *n*umbered, starting with carbon atom 1 at the top of the formula, as indicated in Figure 2.

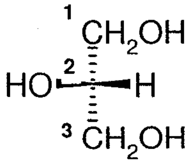

Figure 2 Schematic diagram of the correct labeling of glycerol derivatives[4].

Glycerol-based lipids are always accompanied by this prefix to differentiate this numbering system from others. For example, 1,2-dipalmitoyl-*sn*-glycero-3-phosphatidylcholine (DPPC), has a polar *sn*-3-glycero phosphodiester substituent and two hydrocarbon chains, each containing 16 carbons, at the *sn*-1 and *sn*-2 position (see Figure 3). In general phospholipids, at the *sn*-2-position, contain unsaturated hydrocarbon chains, while at the *sn*-1 position hydrocarbon chains are mainly saturated[2,5]. In addition, 10-20% of the lipids of a membrane have a charged headgroup[2] .

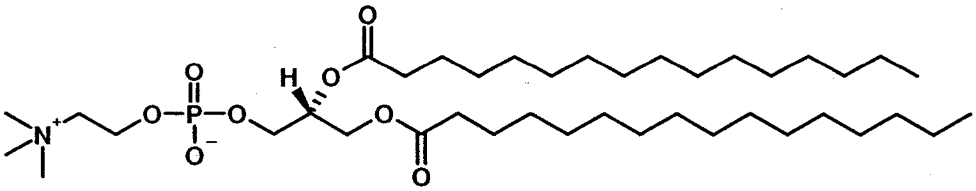

Figure 3 Chemical structure of 1,2-dipalmitoyl-*sn*-glycero-3-phosphatidylcholine (DPPC).

1.1.2 Lipid Organization[2]

The amphiphilic nature of phospholipids has a major influence on the organizational constraints of phospholipids. Consequently, a wide variety of organized structures, such as lipid bilayers can occur. This assortment of organized structures is dependent on the type of lipid aggregation (or phase separation) that can arise. In order for lipids to self-assemble in dilute solutions a favourable hydrophobic contribution, from the hydrocarbon chains must occur, where they sequester themselves within the interior of the aggregates. In addition, the hydrophobic interior of the aggregate must exclude water and headgroups, which limits the geometrical variability of the aggregate. In addition, these forms are dependent on the size of headgroup to hydrocarbon chains as well as the electronegativity of the headgroup. All three parameters predetermine the type of lipid packing (or packing parameter) based on the physical properties of an individual lipid molecule. This relationship is known as the critical packing parameter (CPP), which observes the ratio between the volume occupied by a single lipid molecule (V_{chain}) and the length of the hydrocarbon chains (l_c) multiplied by the cross sectional length of the headgroup (a_o) (see Equation 1).

$$CPP = \frac{V_{chain}}{l_c a_o}$$

Equation 1 CPP of aggregates to determine the type of organization.

Within lipid aggregates, long ranged and/or short ranged interactions can be present, where long range interactions are present between stacked lipid structures and short range interactions are present between neighbouring lipids. Depending on the physical properties of a lipid, short range and/or long range interactions order can occur.

The types of organized structures formed can be divided into two classes: (i) homogeneous and (ii) heterogeneous, which are dispersions of a pure lipid (single components) and dispersions of lipid mixtures, respectively. Homogeneous lipid dispersions have three subclasses based on order/organization of aggregation: (i) isotropic solutions, (ii) liquid crystalline/mesophases and (iii) solid phases. Isotropic solutions have short range and long range lipid disorder while liquid crystalline and solid phase both have short range and long range order.

Aggregates are associated with the formation of micelles. These liquid-like aggregates are categorized as liquid crystalline structures and are the building blocks for a wide variety of organized lipid dispersions, such as spherical micelles, elongated micelles, stacked micelles (lamellar micelles), inverted micelles, bicontinuous structures and vesicles. This multitude of aggregates can only be formed when the lipid concentration is above the critical micellar concentration (CMC). This critical lipid concentration is the point at which aggregation first appears. For micelle formation to occur, favourable hydrophobic effects between hydrocarbon chains, hydration of headgroup with polar solvent and the packing parameters must all be satisfied (as stated previously). Lipid chain length, structure, packing parameter, and the presence of branched chains as well as aromatics and unsaturations are all factors that contribute to the CMC.

There are two types of liquid crystalline structures: (i) thermotropic, where structures are heat induced and (ii) lyotropic, where structures are induced at favourable solute/solvent ratios. Lyotropic lipids can be subdivided into six categories, which are: (i) lamellar ($L\alpha$), (ii) gel ($L\beta$), (iii) hexagonal (H_1), (iv) cubic (I), (v) intermediate and (vi) nematic[6]. As a result of these solute/solvent ratios, various organized structures can be induced as shown in Figure 4.

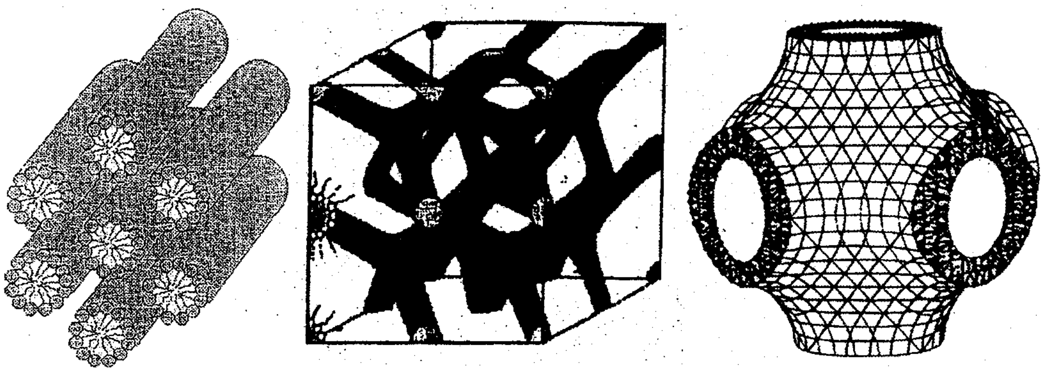

Figure 4 Schematic representation of examples of lyotropic aggregates of a (from left to right): hexagonal phase (H_I), cubic phase (I) and intermediate[6].

More importantly, lipid bilayers are categorized as liquid crystalline/mesophases and will be our topic of interest due to their biological relevance. More specifically, they are characterized as lamellar and/or gel (Figure 5). These two classes differ in that lamellar (L_α), a liquid-like structure, has long range but no short range order since free rotational mobility is present, while the gel phase (L_β) has long range and slight short range order, which implies that this phase has a limited amount of rotation about the long axis of the chain. These two phases are related in that a transition between a lamellar and gel phase can occur by applying heat to the solute/solvent gel phase mixture. During this transition an intermediate phase, which is referred to as a rippled phase (P_b) is induced.

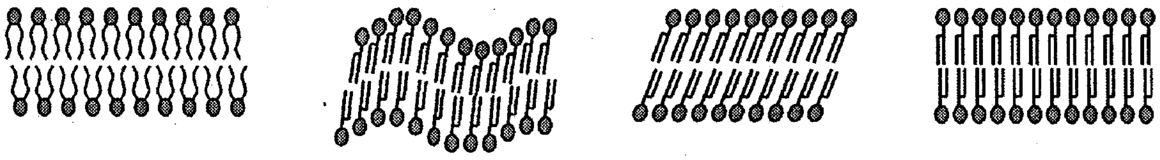

Figure 5 Phospholipid phases of liquid crystalline structures: a) lamellar phase (L_α), b) rippled gel phase (P_β'), c) tilted gel phase (L_β') and d) gel phase (L_β).

In addition, different types of gel phase can form and are dependent on the headgroup area to chain length ratio, thus its packing parameter. For example, at larger headgroup to chain length ratios, a tilted gel phase (L_{β}') is observed.

Phospholipids are usually characterized by their melting temperature (T_m); this is the temperature at which a phospholipid will change from a gel phase to a more fluid lamellar phase. It is important to note that the T_m is also dependant on solute/solvent mixtures as well. The unique physical properties of key phospholipids, phosphatidylinositides, will be discussed in relation to its T_m later in this chapter for the reason that some background information on phosphoinositides is required.

1.2 Phosphatidylinositol

Membrane phospholipids co-exist with slight variations in composition depending on their origin. For example, in bovine brain, 2% of the total phospholipid composition is attributed to phosphatidylinositol (PI), while 19% is found in soybean lecithins[4] (see Table 1). PI is known to comprise a group of minor lipid components of cell membranes and it also plays an important role in cell functioning and cell response[7].

Table 1 Phospholipid composition of lecithin versus that of bovine brain extracts[4].

Phospholipid	Soy lecithin	Bovine brain
Phosphatidylcholine	21	18
Phosphatidylethanolamine	22	36
Phosphatidylinositol	19	2
Phosphatidic acid	10	2
Phosphatidylserine	1	18
sphingomyelin	0	15

Phosphatidylinositol and its phosphorylated derivatives are collectively known as phosphatidylinositides and are usually confined to the inner leaflet of the plasma membrane. The most abundant of the phosphatidylinositides is phosphatidylinositol (PI), which has a myo-inositol attached to a polar *sn*-3-glycero phosphodiester substituent at the 1-position of an inositol ring (see Figure 6). Derivatives of PI are formed by sequential phosphorylation of hydroxyl groups at the 3-, 4-and 5-positions of the inositol ring using phosphatidyl kinases[8].

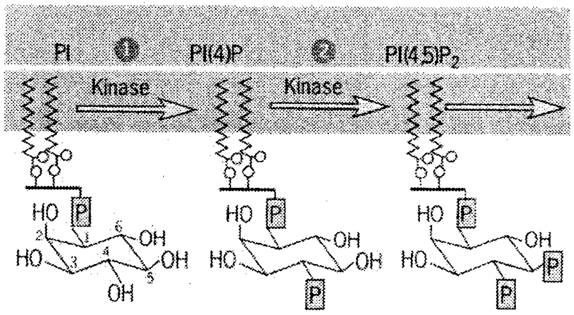

Figure 6 Schematic representation of the phosphorylation of PI using PI kinases[1].

Phosphatidyl kinases are responsible for specific phosphorylation of the hydroxyls along the inositol ring of PI. For example, the 4-position on the inositol ring can be phosphorylated to form phosphatidylinositol-4-phosphate (PI(4)P) by phosphatidyl kinase. Phosphatidylinositol-4-phosphate can then be phosphorylated to produce phosphatidylinositol-4,5-phosphate (PI(4,5)P_2). It has been recently found that animal cells use two different routes in the synthesis of PI(4,5)P_2[8]. For this process to occur the use of two kinases is required; type I and type II. Type I PIP kinase or PI(4)P 5-kinase, is known as 'the classical PI cycle'.

This process is reversible using other specific enzymes, such as phosphomonoesterases, which specifically remove phosphate from the 4-and 5-positions.

Phosphatidylkinase along with phosphomonoesterase control the lipid composition within a cell membrane, where the equilibrium between each derivative must be maintained for proper cell activity[8]. Therefore, the amount of PI and their derivatives is all regulated depending on cell signalling and trafficking.

There is a subfamily of kinases that will phosphorylate the hydroxyl group at the 3-position of the inositol ring[9]. These enzymes, phosphoinositide 3-kinase (PI-3 kinase), have regulatory roles and depend on their preferred substrate, which are PI(3)P, PI(3,4)P_2, PI(3,5)P_2 and PI(3,4,5)P_3. These phosphorylated lipids can bind[10,11]directly to a number of proteins and enzymes which can alter vesicular trafficking, protein kinases (involved in survival) and cell death[12].

1.2.1 The phospholipid effect

The most important of these lipids is phosphatidylinositol-4,5-bisphosphate (PIP_2), which is actively involved in the phosphatidylinositol cycle (also known as 'the phospholipid effect') (see Figure 6). This cycle entails a neurotransmitter or ligand binding to a receptor, which then activates a G-protein that triggers phospholipase C into its active form[13]. Once this occurs, PIP_2 is cleaved into diacylglycerol (DAG) and inositol triphosphate (IP_3). These derivatives are the second messengers that form very rapidly and at low concentrations. In order to emphasize the role and significance of phosphoinositides, the different aspects and key components of the phospholipid effect will be described in the following sections.

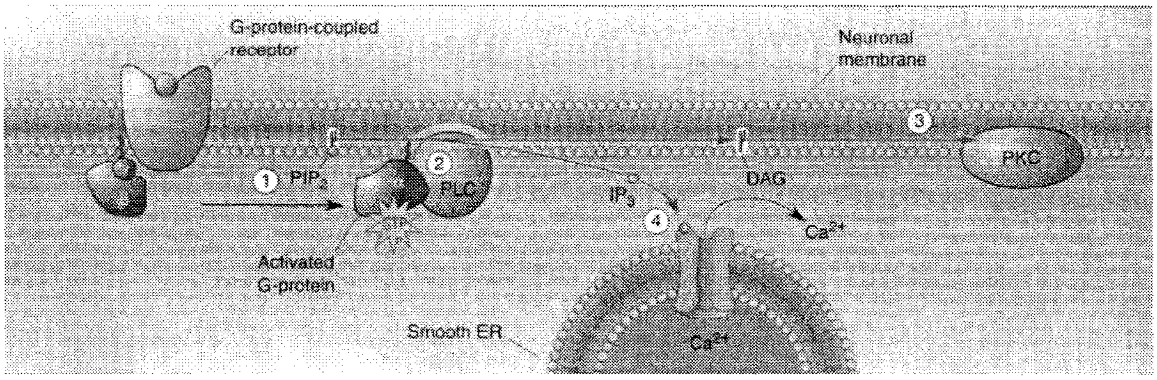

Figure 7 "Phospholipid effect" explains the phosphatidylinositol cycle where messengers are released and metabolized (Hokin and Hokin, 1953)[13].

1.2.1.1 Phospholipase C

Upon coupling of phospholipase C (PLC) with a G-protein, hydrolysis of PI(4,5)P_2 will occur between the *sn*-3 hydroxyl of the DAG backbone and the phosphatidylinositol bond, producing DAG and IP_3 (see Figure 8)[12].

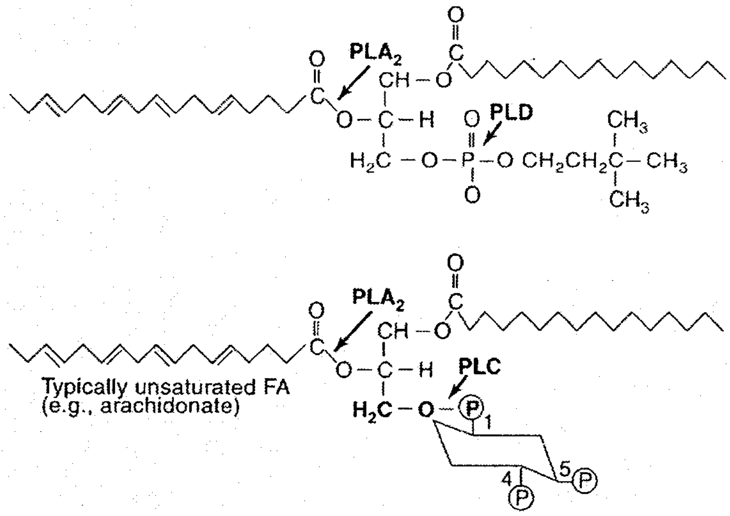

Figure 8 Main types of phospholipase activities[12].

There are three classes of PLC that hydrolyze PIP_2, PLCβ, PLCγ and PLCδ. All three classes contain similar catalytic domain structures however, differ in their regulatory properties[12]. PLCγ isoforms are activated by receptors with intrinsic tyrosine kinase activity, such as the epidermal growth factor and platelet-derived growth factor receptors. Also are activated by receptors with tyrosine kinase, such as the T-cell receptor. In contrast, very little is known about the regulatory factors of PLCδ [14]. The PLCβ isoform is activated by α subunits of G-protein. The G-protein will couple to variants of PLCβ, upon which initial stimulation of enzyme will occur[12].

1.2.1.2 Phospholipase A_2 (PLA_2)

Phospholipase A_2 (PLA_2) cleaves the fatty acid at the *sn*-2 position of the DAG backbone (see Figure 8)[12]. The fatty acid composition of bovine PIP_2 is largely composed of stearic acid, a saturated acyl chain, at the *sn*-1 position and arachidonic acid at the *sn*-2 position, 20 carbon *cis*-unsaturated acyl chain containing four double bonds. Arachidonic acid acts as a precursor for prostaglandins and leukotrienes. In addition, it can modulate potassium (K^+) channels, PLCγ and some forms of PKC[12].

1.2.2 Second messenger

The formation of second messengers occurs in one step, where three second messengers, DAG, arachidonic acid and its metabolites, and elevated levels of Ca^{2+}, are formed. Inositol triphosphate, unlike the second messengers listed above, does not actively contribute to cellular function. However, it is required for the production of Ca^{2+}[12]. Their roles within this mechanism are briefly discussed below.

1.2.2.1 Role of inositol triphosphate (IP_3)

IP_3 is recycled through an inositol phosphate cycle, where dephosphorylation of IP_3 to inositol bisphosphate (IP_2) is carried out. A similar mechanism using inositol bisphosphatase will cleave IP_2 to inositol phosphate (IP). The final step is required to free inositol for resynthesis, where the conversion of IP to myo-inositol (free inositol) by an inositol 1-phosphatase will induce the formation of PI. Upon liberation of inositol triphosphate into the cytoplasm, it is dephosphorylated. The released phosphate group binds to a calcium gated channel, activating a protein receptor creating an influx of free calcium (Ca^{2+}) from intracellular stores, such as endoplasmic reticulum, into the cytoplasm[8]. The production of Ca^{2+} enables many cellular activities, one of which is the activation of protein kinase C. Where upon activation, this enzyme induces phosphorylation of specific ion channels thus responsible to the opening and closing of channels. Complete dephosphorylation of IP_3 will terminate the release of Ca^{2+} and commence the biosynthetic pathway (formation of PI).

1.2.2.2 Role of Diacylglycerol

Diacylglycerol (DAG) has an important function in that it activates protein kinase C (PKC) [8]. PKC is a calmodulin-dependent enzyme that enables Ca^{2+} to modulate a large number of cellular processes by phosphorylation[15]. Calmodulin acts as a mediator between Ca^{2+} and PKC and is required for the activation of PKC[15].

Once PKC is activated DAG is converted to either phosphatidic acid (PA) or monoacylglycerol. The formation of PA is a result of the phosphorylation of DAG using diacylglycerol kinase[8]. Within the membrane there is an abundant amount of DAG present. The production of DAG is does not solely occur upon cleavage with PKC however it occurs upon cleavage with phospholipase D (PLD) as well. Alternatively, this enzyme will cleave phosphatidylcholine, which is a major lipid component in the membrane, at the phosphodiester bond to produce PA and choline (Figure 8). PA can then be dephosphorylated and converted to DAG[12]. Although the phosphatidylinositol cycle is well known[8], the biophysical conditions of this cycle is lacking. However, in the past couple of decades, further research has provided addition information pertaining to this pathway, which will be discussed in the following section.

1.3 Interfacial Activation of Enzymes

The majority of biological reactions in cells occur at the lipid-water phase boundary[16]. As a result, the activation of interfacial activation of enzymes has been of great interest. One of the most interesting findings is that the activity of an enzyme is dependent on the packing density of the lipid membrane[14,17-19]. There are two major theories pertaining to this packing density dependency, namely, the substrate theory and the enzyme theory[16,17]. According to the substrate theory the increase in enzyme activity at the interface is due to the characteristics of lipid substrate. Specifically, the concentration, hydration state, and conformation of the substrate are thought to play an important role[16] (see references within). For example, it has been suggested that the lateral lipid distribution, packing, orientation as well as its lateral phase separation contribute to enzyme activity[17,20,21]. In particular, enzyme activity in monolayers was found to be optimal around the borders of the liquid-ordered phase (analogous to gel phase), which is separated by a fluid lamellar phase[17]. In addition, it has been reported that the catalytic activity of phospholipase is dependent on the following: (i) aggregated lipid surfaces, (ii) elevated local substrate concentration[14,18,19], (iii) proper orientation of lipid molecules at the interface[22,23], (iv) optimal lipid packing and distribution, (v) favourable localized charge density and metal ion concentrations, and (vi) adoption of an active conformation by the enzyme upon penetrating the interface[14].

The enzyme theory claims that interfacial binding of the enzyme to a lipid induces a conformational change, which enables the substrate to bind to the active site, as is seen with the hinged region of lipases[16,24]. The two opposing theories have been extensively argued and supported. However, the substrate and enzyme theories are not mutually exclusive rather have a very different focuses on the same interfacial process.

1.4 Lipid Raft Formation

It is believed that enzymes modulate the assembly of lipid rafts as well as regulating the activity at the interface[21]. Submicron regions in cell membranes that are enriched in particular lipid and protein are referred to as rafts. These regions are thought to play an important role in the signaling, adhesion, endocytosis, apoptosis, protein organization and lipid regulation[25]. Raft formation is usually associated with a co-existence region of two phases, for example, between gel and lamellar phases. There are certain conditions where co-existence can occur, namely, in a lipid mixture: (i) which is at a temperature between the melting temperatures (T_m) of the individual components, (ii) which comprises lipids with a significant difference in chain length and (iii) which contains cholesterol[26].

Some specific lipids conform into highly concentrated localized regions, where its lateral lipid distribution can govern/alter protein-protein interaction, protein-lipid interaction[21] as well as rates of reaction and diffusion rates within a lipid bilayer[27]. If such lipid rafts exist, it will transform how the lateral organization of membranes is perceived and emphasize the importance of lateral organization in biomembranes for complex activities, such as signal transduction and membrane trafficking[28]. Over the two decade, raft formation became no longer speculation and several sightings had been reported in various shapes, sizes and compositions. For example, the occurrence of rafts within lung surfactant (LS) membranes, as well as sphingolipids and cholesterol containing membranes has been reported. Though there is numerous documented data for each raft event, only key reports relevant to our discussion will be introduced here.

Lung surfactants (LS) are composed of 1,2–dipalmitoyl-*sn*-glycero-3-phosphatidylcholine (DPPC), which contributes for 55 to 60% of total phophatidylcholine (PC) lipid, phosphatidylglycerols (PG), contributes to approximately 10% of total phospholipid and phosphatidylinositol, accounts for 2 to 5% of the total[10]. It has been found that raft formation among DPPC can be observed[29]. It has been suggested that this event may play a vital role on pulmonary and respiratory function within the lung and might be required for normal membrane activity to occur. As a result, this finding has sparked the interest of several researchers, where a better understanding of the behaviour of DPPC within LS is required in order to investigate this occurrence[10].

Sphingolipids are found in the extracellular leaflet of a plasma membrane. They consist mainly of long and saturated fatty acyl chains, which allow lipids to pack tightly and form lipid rafts[26]. They are associated with a high melting temperature, T_m, where its T_m is about 37 – 41 °C. In contrast, phospholipids have a T_m below 0 °C[26], and mainly consist of unsaturated acyl chains, which are not closely packed[30]. Sphingolipid-rich rafts are able to co-exist with phospholipids-rich domains in a loosely packed disordered state. Evidence suggests that sphingolipid-rich domains do exist in cell membranes and have been observed[26]. It was found that liposomes formed from artificial raft lipid mixtures showed fluorescence microscopy evidence for a more ordered phase co-existing with a disordered phase in the plane of the membrane[28]. Sphingomyelin and cholesterol combinations have been found to form a liquid-ordered phase in fibre cells[31]. The saturated nature of lipid rafts and glycolipids act to promote their interactions with cholesterol[28], which has an important effect on the behaviour of a membrane. It has been found that the addition of cholesterol, and not just sphingomyelin, to a phospholipid bilayer causes a disordered and ordered state to co-exist, thus, inducing lipid raft formation[30].

Caveolin is a cholesterol-binding protein that is associated with caveolae, a specific type of lipid raft[32,33]. Caveolae are usually found in the plasma membrane as invaginations, approximately 50-70 nm in diameter and are known to play important roles in signal-transduction processes and different transport mechanisms; one of which involving the formation of transport vesicles[26,31,33].

1.4.1 Lipid Rafts Involving Phosphoinositides

It has been suggested that phosphoinositides may not be uniformly distributed in the membrane[7,21,34,35]. This potential localization may be important in membrane trafficking[7,20,34,36-38] and, as a result, has given phosphatidylinositides a significant amount of recognition for the past two decades.

According to Cullen et al.,[7] regions of high phosphoinositide concentration are formed throughout the lipid membrane. The synthesis and production of phosphoinositol derivatives can be rapid in highly concentrated microdomains of phosphoinositides (or local regions with high phosphoinositide concentrations)[7]. For example, Tuominen et al.[39] postulate that a hydrophobic interface, or a cluster of PIP_2 headgroups is required for binding of $PI(4,5)P_2$ to interfacial proteins[40-42]. In addition, it was found that the presence of acidic lipids, which creates a hydrophobic interface, increases the stability of lipid-protein binding, within lipid rafts regions[39,40,43].

There are two opposing ideas regarding the interaction of phosphoinositide rafts with proteins. Gascard et al.[41] believe that compartmentalization of phosphoinositides is induced by the presence of interfacial proteins which sequester PI into separate domains. On the other hand, it has been suggested that PIP kinases are only active when PI is present in highly concentrated regions, or rafts[34]. Foster et al.[40] also report that lipid raft formation is favourable for protein activation. In fact, specialized regions of the plasma membrane may be highly enriched (>20%) in PIP. These findings suggest that clustering of inositol lipids in specialized regions of a lipid bilayer may be an important aspect of their ability to activate specific enzymes[40].

In addition, it is believed that the binding of phosphoinositides to these protein domains has a low affinity and is rapidly reversible. As a result, phosphoinositide-binding proteins constantly diffuse through the cytosol, searching for its substrate. To enable favourable interactions, the protein is translocated to specific regions in cells, where there is a high substrate concentration in the form of lipid rafts[7]. Similarly, PIP kinase has an activation loop or active site loop, that will complex with its substrate, phosphatidylinositol 4-phosphate, PI(4)P, or phosphatidylinositol 5-phosphate, PI(5)P. The pre-determined location of these inositides dictates the subcellular localization of the PIP kinase[34]. Since multiple lipids are required for protein-lipid binding interactions, encapsulating PI(4)P and PI(5)P with multiple lipids will induce the formation of raft-like clusters and as a result will activate the enzyme[34].

From these findings, it is evident that proteins are able to bind to phosphoinositide lipid rafts[20]. The relationship between lipid organization and membrane function requires knowledge of the magnitude of the lipid-lipid and lipid-protein interactions and their structural consequences. Membrane model systems are often used as a tool to study these interfacial interactions.

1.5 Membrane Model Systems

Bilayer matrices are complex structures, where the presence of numerous membrane proteins as well as lipids can make characterization difficult. A simplified system is needed, where phospholipid behaviour can be independently studied. Two model systems that are used as characterization methods are bilayers and monolayers. Monolayers are two dimensional self-organizing systems that imitate the behaviour of a bilayer leaflet and provide excellent models for studying lateral interactions between lipids.

1.5.1 Characterization of Monolayers

In monolayers at the air-water interface, the phospholipids are oriented such that their hydrophilic portion is submerged in water and its hydrocarbon chains are projected into the air (see Figure 9). In the following sections the theory behind surface tension and monolayer formation will be discussed. However, characterization techniques for this system will be presented in Chapter 2:.

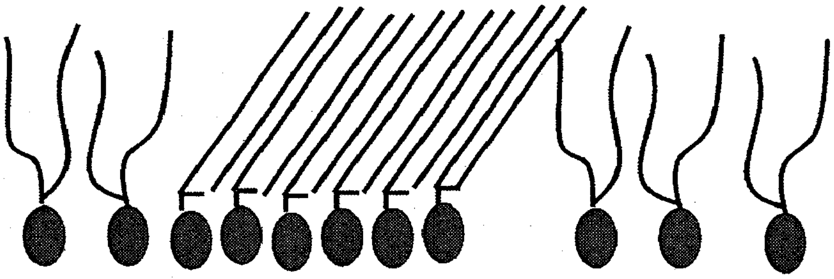

Figure 9 Monolayer of phospholipids at the air-water interface.

1.5.1.1 Terminology[2]

There are molecular interactions at the gas-liquid interface, where the pure liquid is in equilibrium with its vapour. A pure liquid phase, also known as the bulk phase, has net attractions that are fulfilled almost completely between adjacent molecules; therefore, there is no net force. In contrast, at the interface attractions are less completely fulfilled. There is a net resultant force away from the surface. In order to reduce this excess of energy and maximize attractive interactions, molecules will orientate themselves by minimizing the surface area as much as possible.

The work, **w**, required to create new surface area is also proportional to the number of molecules transported to the surface and thus to the increased area, A, which we can express in a basic linear defining equation as:

$$w = \gamma \Delta A$$

Equation 2 The work, w, required to create new surface area is also proportional to the number of molecules transported to the surface, γ, and thus to the increased area, A

where the proportionality constant γ is called the surface tension (see Equation 2). Therefore, γ can be viewed two ways: (i) as the free energy or work to create a unit area (energy/length^2) or (ii) as a force per unit length (which arises from the units which reduce to mN m^{-1}). The former considers the contribution of the work of increasing the area to the differential Gibbs free energy, in which case an increase in area will result in an increase in Gibbs free energy (see Equation 3). By including thermodynamic quantities, it can be expressed as

$$dG = \gamma dA$$

Equation 3 Increase in area, *A*, will result in an increase in Gibbs free energy the force and is required to define the surface tension, γ.

where

$$\gamma = \left(\frac{\partial G}{\partial A} \right)_{T,P}$$

Equation 4 The surface tension, γ, can be rewritten where the temperature and pressure remain constant.

The latter considers the force, which is required to define the surface tension, γ. It states that the amount of force required per unit length to prevent contraction of the surface, which is due to the surface tension. The surface tension is an intrinsic property of the material (see Equation 4).

1.5.1.2 Application to monolayer systems

The surface tension is lowered by the presence of adsorbed amphiphilic molecules, which orient at the interface. The surface pressure or lateral pressure, π, is defined as

$$\pi_s = \gamma^o - \gamma$$

Equation 5 Pressure or lateral pressure, π, is defined as the difference of the surface tension with no amphiphile present, γ^o, and the surface tension with an amphiphile added, γ.

where γ^o is the surface tension with no amphiphile present and γ when surface tension with an amphiphile added (see Equation 5). With Langmuir monolayers, small amounts of insoluble solute are quantitatively deposited onto the surface using a spreading solvent. The lipids are dissolved in a volatile solvent that spreads across a surface (taking the lipids with them) and then evaporates. Since lipids are insoluble in water and of low volatility, they remain confined to the surface resulting formation of a thin film of amphiphiles at the interface.

The lateral pressure, π, of a system can be obtained as a function of the molecular area, *A*. An isotherm defines the relationship between pressure and volume, at a constant temperature. This relationship can be seen in Figure 10, which displays a schematic of features of pressure-area isotherms observed for monolayers containing a single amphiphile.

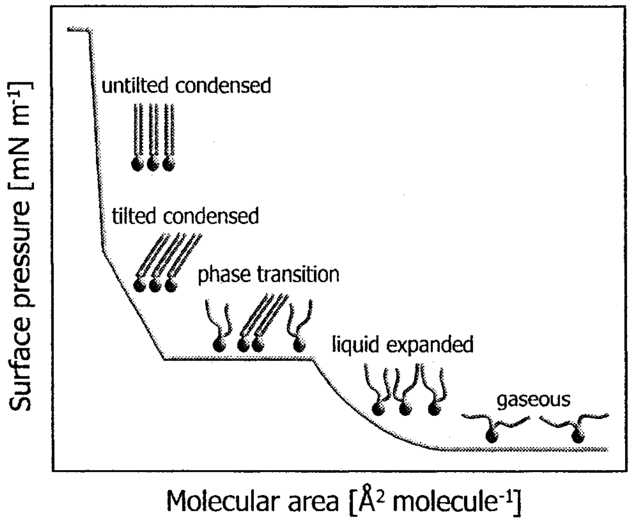

Figure 10 A schematic diagram of an idealized isotherm and the corresponding phases.

As the area available to the phospholipid monolayer is changed, the molecules will go through various phase transitions. These transitions are related to the behaviour of molecules at a given molecular area. At extremely low pressures, all monolayers exhibit gaseous behaviour, and as π approaches zero, we can apply a two-dimensional equivalent of the ideal gas law,

$$\pi A = nRT$$
$$or$$
$$\pi a_o = kT$$

Equation 6 The ideal gas law can be applied to a two dimensional system at very low surface pressures where the pressure, π, multiplied by the area *A* is equal to the number of moles, *n*, multiplied by the the gas constant, *R*, and temperature, *T*.

Where a_o, is the area that each molecule occupies, ($a_o = A/(n\mathrm{N}_{\mathrm{av}})$). Initially a horizontal slope can be observed at surface pressures designated 0 mN m^{-1} (negligible, non-measurable reductions in surface tension). This region is characteristic of a gaseous-like phase and is considered to correspond to hydrocarbon chains lying flat on the surface. In reality, aggregates can occur in this region but a coherent film with complete coverage of the surface does not exist. In the gaseous phase, molecules will have similar entropic energy levels with comparable rotational and translational motion this will be the dominant contribution to the free energy. Upon compression the monolayer (Figure 10), the transition from two-dimensional gas to two-dimensional liquid is observed. In the liquid-expanded state, molecules are assembled similarly to the lamellar phase that is found in bilayers. Here, molecules will diffuse rapidly along the surface and have considerable conformational disorder in the hydrocarbon chains, which leads to a highly compressible film[4] . The isothermal compressibility, x, of pressure-area (π, A) isotherms, is expressed as follows (see Equation 7)

$$x = -\frac{1}{\mathrm{A}}\left(\frac{\partial \mathrm{A}}{\partial \pi}\right)_T$$

Equation 7 Equation defining compressibility.

Further compression induces another distinct change in the slope, where it becomes horizontal. This transition region is associated with a first-order phase transition, where two phases, namely the liquid-expanded and condensed phases, co-exist. This region is ideally horizontal however, variations in the horizontal region can be observed. This occurrence could be due to the purity, temperature and compression speed at the air-water interface. Compressing the monolayer beyond the horizontal region causes the surface pressure to increase more steeply inducing a predominantly condensed phase. This condensed phase corresponds to molecules with maximum non-covalent interactions, where hydrocarbon chains are all-trans in conformation and packed together in an ordered state. This film is relatively incompressible, where $a_o \approx 0.19$ nm^2 for alcohols and esters[2].

In this phase adjacent molecules non-covalently interact through van der Waals and hydrophobic effect of their hydrocarbon chains as well as hydrogen bonding within the headgroup, which is comparable to the gel phase seen in bilayer systems. There are two general classes of condensed phases that can be observed: (i) tilted condensed phases and (ii) untilted condensed phases. These can be further subdivided into seven distinct monolayer condensed phases based on the packing parameters and the tilt direction. This arises because organic molecules have orientational and internal degrees of freedom. Within a monolayer, the molecular degrees of freedom are the tilt (relative to the water plane) of the long axis of the molecule, the orientation of the molecular backbones and the orientation of the headgroup. Consequently, the number of degrees of freedom is large enough to provide a rich polymorphyism. At a given temperature at low pressures, tilted phases can occur. As the pressure increased the tilt of the molecule with respect to its normal will continuously decrease. This process will continue until the molecule reaches an untilted state at which point a second order transition takes place. Within these two states, tilted and untilted, there are various types of phases, as summarized in Figure 11.

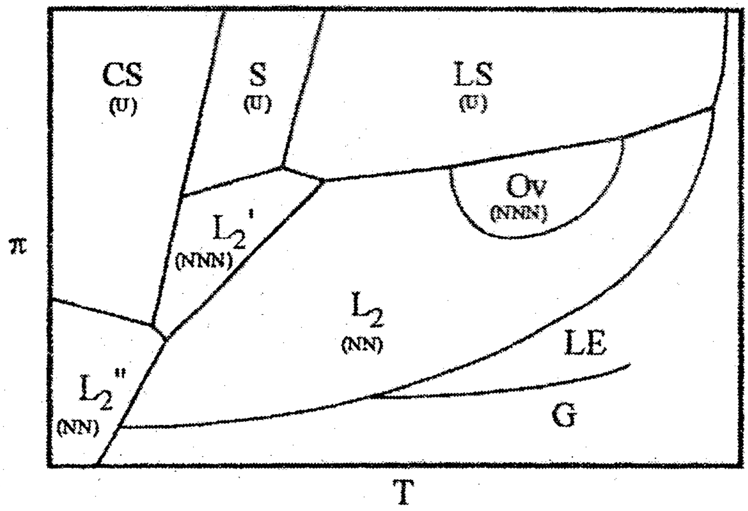

Figure 11 Schematic phase diagram demonstrating the various monolayer condensed phases formed by fatty acids. Note: L_2 phase can be subdivided into the L_{2h} and L_{2d}[44].

At low temperature, crystalline phases (L_2'' and CS) are found which exhibit long range ordering and herringbone packing. As the temperature increases, a set of intermediate phases (S, L_2', L_{2h}) can be observed, which have limited backbone order however, they do not have long range ordering similar to that of the crystalline phases. At high temperature, three phases (LS, O_v, L_{2d}) can be found in which the hydrocarbon chains have free rotation about their long axis, these are termed rotator phases such as hexagonal. In considering tilt phases, the tilted phases distort from hexagonal packing to a centered rectangular arrangement. Furthermore, the tilt can be directed toward nearest neighbours (NN), next nearest neighbours (NNN) or the tilt direction can be an intermediate between NN and NNN. This latter phase is not shown in the diagram, as it is not observed for fatty acids[44].

The packing density at even smaller areas causes re-orientation of the monolayer, where molecules submerge into the subphase or form multi-layers at the interface; this behaviour is characteristic of a collapse phase. It must be noted that the isotherm in Figure 10 is a schematic representation of features of pressure-area isotherms where in reality, depending on the structural characteristics of a phospholipids, an isotherm of its monolayer could consist of one or more of these phases.

There are some favourable advantages of this technique, compared to those of a bilayer system: The thermodynamic variables, which are temperature and surface pressure, can be directly controlled; you vary the molecular area and as a consequence the surface pressure, keeping the monolayer molecules at the interface but letting the water flow freely below it (see Figure 9). Such direct mechanical compression is not possible in any other bulk phase model system. By changing the length of a hydrocarbon chain or by changing the pH or ion content of the subphase, the intra-monolayer and the monolayer-subphase interactions can be widely varied.

1.6 PI in model systems

Both bilayer and monolayer model systems have been used extensively in the past two decades to obtain additional information about the role of PI within the plasma membrane. To better understand the biophysical contribution of PI, its aggregation properties are investigated using these systems. Preliminary findings have been successful in characterizing its phase behaviour as well as its enzymatic involvement and will be summarized here.

1.6.1 Interfacial Phosphorylation of Inositols

Model systems have also been used to study the interfacial phosphorylation of inositide lipids. Lipid-protein interactions have been found to influence the surface pressure and the membrane curvature[19,40]. For example, phosphorylation of PI affects the curvature of the membrane, by creating an increase in the size and electrostatic charge on the headgroups[19,35]. An increase in local concentration of phosphorylated lipids was shown to cause the membrane to curve further inwards, producing an invaginated structure[19]. This increase in membrane curvature directly affects the packing density (or pressure), in that the pressure decreases due to the repulsive interaction at the interface[19].

Similar enzymatic activity can be observed at the air-water interface, where lipid-protein interactions have been proven to influence the surface pressure in monolayer systems[14,15,17,18] (see section 1.3). The optimal conditions for enzymatic activity involving PI's are comparable and will be discussed here.

Hirasawa et al.[18] used PI monolayers as a substrate for phosphodiesterase to look at the conditions under which enzyme activity is optimal. It was found that partial penetration of enzymes is required for hydrolysis of substrate to occur. It was also proven that surface pressure influenced protein activity, where the activity was optimal at biologically relevant membrane pressures (~30 mN m^{-1}).

In addition to this, it was found that charges located at the interface, phospholipid composition of the interface as well as Ca^{2+} concentrations affected enzymatic activity[14,15,18]. For example, by adding increasing concentrations of acidic phospholipids, to a PI containing monolayer, an increase in enzymatic activity was seen for PLC[14,18]. Similar findings were acquired in bilayer systems, where upon addition of acidic lipid the activity of the enzyme increased[39,40,43].

Although the phosphatidylinositol pathway has been investigated[8], the lipid-protein interactions still remain unclear. The following questions still require further study: what is the mechanism of interfacial activation and associated conformational changes in enzymes at the lipid-water interface, how is this process dependent on lipid orientation; and most importantly, whether it is the protein's subcellular activity that induces protein raft formation or is the biophysical properties of the lipid that pre-determine the binding site and interaction with protein.

1.6.2 Phase Behaviour of PI

The phase behaviour of lipids is often used to characterize the biophysical properties. Differential scanning calorimetry (DSC) is often used to determine the phase behaviour of a particular lipid. From this, the stability of a lipid bilayer can be characterized by its melting temperature (T_m). T_m is the temperature at which a transition from a gel phase (L_β) to a lamellar phase (L_α) can be seen and is distinctive for a particular lipid bilayer system. Temperature studies were performed on soy PI in water (15% w/w) and a T_m -23 °C[10] was reported from DSC measurements. Similarly, a T_m of -17 °C was reported for wheat PI in water (15% w/w)[45]. Mansour also reports a T_m of -24.9 °C for dipalmitoylphosphatidylinositol (DPPI), which is surprisingly different from that of Redfern and Gericke, who reports at T_m of 41 °C for the same system[46]. In a saturated chain lipid such as DPPI, a T_m of -25 °C is unlikely especially if their reported value of soy PI has a higher T_m. On the other hand, Redfern's data is in agreement with

Hansbro who reports a T_m of 19-20 °C for dimyritoylphosphatidylinositol (DMPI) using ^{1}H NMR and polarized microscopy in addition to the DSC measurements[47]. The latter results are comparable to those for DMPC and DPPC, respectively[48]. Hydrated DMPI, on the other hand, remains crystalline up to 60 °C, which was determined by x-ray diffraction[49]. In addition a similar study was performed on a hydrated 50:50 DMPI/DMPC mixture which exhibited a L_α phase above 50 °C[49].

DPPI/DPPC mixed vesicles have observed a de-mixed system at physiologically relevant pH, using fluorescence resonance energy transfer (FRET)[46]. This has implications for membrane raft formation, which was proposed for inositols (see section 1.4). Redfern et al. have also studied mixtures of DPPC with derivatives of DPPI, namely DPPI-3P, DPPI-4P and DPPI-5P[46] using DSC and FRET. In all cases, these mixtures were also found to de-mix at a physiological relevant pH. In addition, this was also confirmed by FTIR in which two phase transitions were observed in a temperature study. Furthermore, the position of the phosphate on the inositol ring was shown to affect the stability of the vesicles. The influence of DPPC/DPPI-4P mixing ratios was studied and these systems remain de-mixed even at low percentages (1%) of DPPI-4P.

The phase behaviour of inositols has also been examined in monolayer systems. Several monolayer studies of a natural extract of PI report the appearance of a liquid-expanded phase (or fluid phase) all the way up to collapse at the air-water interface at room temperature[10,11,50]. These findings are in agreement with the DSC studies for which the T_m was reported between -17 and -25 °C (see above). Due to its high proportion of unsaturated chains, this multi-component system exhibits a fluid phase. In order to further characterize this system, its individual components can be isolated. Mansour et al.[10] have synthesized the dipalmitoyl component, DPPI, and solely observe a liquid-expanded phase up until the collapse[10] using fluorescence microscopy of monolayers. This in agreement with their DSC measurements however, contradicts the DSC findings of other groups (see above).

Monolayer miscibility studies can also yield additional information about a multi-component's phase behaviour. By introducing supplementary phospholipids, that have previously been characterized, changes in their individual systems can help determine the type of lipid mixture it is. A binary lipid mixture can exhibit ideal mixing (or complete immiscibility), where the average area per molecule of the individual components is the sum of the two individual systems (see Equation 8).

$$A_{ideal} = A_{av} = N_1 A_1 + N_2 A_2$$

Equation 8 When ideal mixing, A_{ideal}, between two components occurs the area covered is the average area of the individual components A_{av}.

A_1 and A_2 are the areas per molecule of each monolayer component at constant surface pressure and N_1 and N_2 are their respective mole ratios[10]. A binary mixture can also exhibit non-ideal mixing, where non-covalent interactions between adjacent lipids can create deviations in their miscibility. For example, the difference between the actual area per molecule, A_{12}, of the mixed system and that of the average/ideal area per molecule, A_{av}, will give the excess area, A^E and is defined as (see Equation 9)

$$A^E = A_{12} = \left(N_1 A_1 + N_2 A_2\right)$$

Equation 9 Equation used to calculate excess area, A^E at the air-water interface.

If a positive deviation from the ideal area per molecule, A_{ideal}, occurs, the individual components do not display favourable interactions, which means repulsive interactions occur. In contrast, if a negative deviation from the A_{ideal} occurs, the monolayer is able to compact into smaller areas, which implies that attractive interactions are present[10].

Miscibility studies obtained for binary mixtures of PI with DPPC, DSPC or DSPE show non-ideal mixing within small mixing ratios of PI[10,11,50]. It was observed that with an increase in the ratio of PI, an increase in unfavourable interactions occurred for mixtures with DSPE[50]. As a result this created an excess area at the air-water interface. In addition, binary mixtures of DPPI with DPPC also exhibit positive deviations from ideal mixing, which was attributed to unfavourable interactions[10].

The lipid phase behaviour is defined in part by the lipid orientation at the interface. Conformational studies have shown that the orientation of the inositol ring was neither parallel nor perpendicular to the plane of the membrane however somewhere in between[47]. This was determined by NMR studies of synthetic DMPI bilayers coupled with computational studies. It was later determined using neutron diffraction techniques, that orientation of the DMPI inositol ring was in fact perpendicular to the surface[22,49] as is seen with most sugar lipids[22,23,49]. In contrast, the phosphorylated derivative of DMPI, DMPI-4P, is tilted to enable a favourable orientation for subsequent phosphosphorylations[22,49]. Zhou et al. also determined that the inositol ring lies almost perpendicular to the surface which makes enzymatic attack of PLC more accessible[23]. These findings were determined by modeling of ^{1}H NMR data of diC$_6$PI and diC$_7$PI. These studies emphasized the importance of lipid conformation for the study of the enzymatic activity at the interface.

1.7 Objective

PI's biophysical contribution to cellular function in a lipid membrane still remains a relatively new area of research. In more recent years, researchers have been trying to resolve the current question: are phosphoinositides localized in regions of high PI concentration (in other words, lipid rafts) within the membrane? The raft hypothesis proposes that certain naturally occurring lipids aggregate in the plane of the membrane driven by distinctive intermolecular interactions, including van der Waals interactions between the long, nearly fully saturated chains as well as hydrogen bonding and electrostatic interactions between adjacent headgroups[28]. For example, PI(4,5)P_2 is located in enriched areas of PI[20] where PI alone contributes to 80% of the total inositol composition, while the remaining 20% are phosphorylated derivatives of PI.

Since PI is the major inositol component and the key component in the production of PI(4,5)P_2, our investigations have begun with an extract of soybean PI. Soy PI, in itself, is a complex structure where its hydrocarbon chains in the *sn*-1 and *sn*-2-position can contain 16 and 18 carbon atoms with a range from 0 to 3 double bonds. Consequently, this makes it difficult to interpret the phase behaviour of PI. To facilitate complete characterization of this system, a simplified system is needed, where pure extracts of all possible components could be investigated individually. However, most of this these components are not readily available and if so, are very expensive. An alternative is to study a hydrogenated soy PI product, in which hydrocarbon chains are saturated. Since fewer components are present, this derivative enables us to study the contributions of hydrocarbon chain and headgroup structures on the phase behaviour.

In particular the objectives of this thesis are to: (i) qualitatively and quantitatively analyze hydrogenated PI (PIH), (ii) study the phase behaviour of PIH over a range of temperatures, (iii) study the miscibility of PIH with key membrane lipids.

The aim of these studies is to understand the occurrence of localization of inositides within membranes, and will lead to a better understanding raft formation within the PI components. In the longer term, these results will support the study of lipid-protein interactions, as well as the signal transduction pathways.

Chapter 2: Experimental Methods

2.1 Langmuir Film Balance

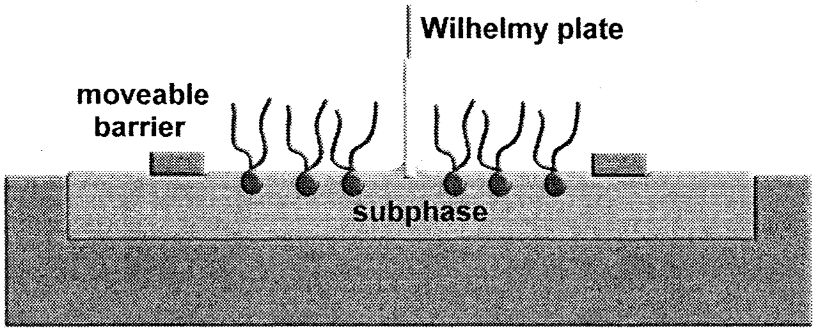

Figure 12 Schematic diagram of a Langmuir Film Balance.

A Langmuir film balance, which has a fabricated Teflon trough, contains an aqueous liquid (or subphase) (see Figure 12). The changes in surface tension are monitored using a Wilhelmy plate, which is simply a filter paper, suspended from a copper wire and is dipped into the liquid. Once brought into contact with a liquid, the surface tension manifests itself in the meniscus that forms around the perimeter of the plate. A vertical force balance will occur, indicating that the weight for the meniscus must equal the upward force provided by the surface. This force in turn equals the vertical component of the surface tension ($\gamma \cos\theta$, where θ equals the contact angle) times the perimeter of the plate, P (see Equation 10). Since the surface tension is a force per unit length of the surface edge, we have

$$w = \gamma P \cos\theta$$

Equation 10 This force, w, equals the vertical component of the surface tension times the perimeter of the plate, P.

however, if the Wilhelmy plate has a contact angle of zero (Equation 11), then the equation can also be rewritten as

$$w_T - w_P = (2l + 2w)\gamma$$

Equation 11 w_T is the total force and w_P is the force from plate and is equal to the perimeter of the plate, its length, l, and width,w, multiplied by the surface tension γ.

Where w_T is the total force and w_P is the force from plate. This is equal to the perimeter of the plate, its length and width, multiplied by the surface tension.

This equation can be rewritten, where the total force (the plate plus its surroundings) minus the force of the plate is equal to the force of its surroundings, F. Therefore, The surface tension, γ,

$$\gamma = \frac{\mathrm{F}}{2l} = \frac{w_T - w_P}{(2l + 2w)}$$

Equation 12 The surface tension, γ, divided by the length of the wire, l.

The changes in the film molecular area are controlled by two movable barriers that travel laterally across the interface compressing the monolayer to smaller surface areas. As a result, the surface tension will change, where the surface becomes more densely packed and a decrease in free energy as well as the surface tension will occur. The surface tension at the interface is expressed as the surface pressure, π, of the monolayer which can be directly measured as a function of the molecular area, Å^2 molecule^{-1}.

2.1.1 Langmuir Film Balance Instrumentation

Surface pressure-area isotherms, at the air/water interface, were obtained on a thermostated Langmuir film balance (Nima Technology Ltd., Coventry, UK) at 15, 25, and 35 °C with a compression speed of 10 $cm^2 \cdot minute^{-1}$ (equivalent to approximately 6 $\AA^2 \cdot molecule^{-1} \cdot minute^{-1}$). Surface pressure measurements were made using a filter paper Wilhelmy plate (see section 2.1) to ensure a contact angle of zero with water. Troughs made out of Teflon are engineered in a round-edged rectangular shaped platform. The movable barriers as well as the Wilhelmy plate are connected to a computer interface.

2.2 Brewster Angle Microscopy

This technique enables one to visualize monolayers at the air-water interface, where it provides additional information that cannot be obtained from a Langmuir film balance alone. Brewster angle microscopy (BAM) observes, in real time, the morphology (or lipid aggregation) of a monolayer. Images of the morphology are obtained as the surface pressure, π, and molecular area, $\AA^2$ $molecule^{-1}$ change.

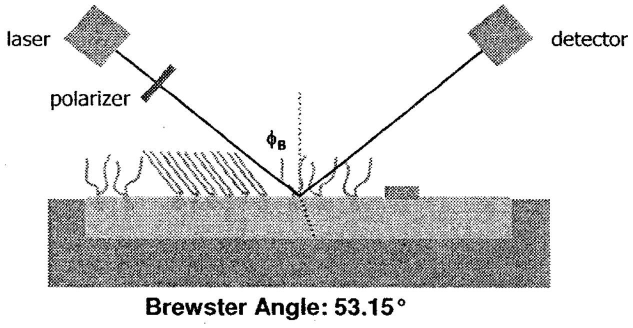

Figure 13 Schematic diagram of an Elli2000I.

In this method (see Figure 13), the incident laser beam illuminates the surface at the Brewster angle (53.15° for water). At this angle, a p-polarized beam of light will not reflect therefore, all light is refracted into the subphase. The angle is related to the refractive indices, n, of two materials (see Equation 13).

$$\tan\alpha = \frac{n_2}{n_1}$$

Equation 13 Equation used to determine the Brewster angle.

Where, n_2 is the refractive index of the subphase and n_1 is that of air. By placing a thin film on the surface, the Brewster angle equation is no longer satisfied. As a result, reflections at both interfaces occur. All beams are superimposed to produce a signal and are detected with a sensor, such as a CCD camera, where at the air-water interface the physical properties of that monolayer, will give rise to different contrasts thus creating a colour intensity change (see Figure 14).

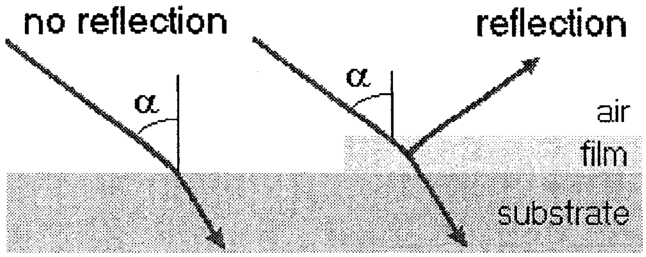

Figure 14 Properties of the Brewster angle[51].

Therefore in compressing a monolayer to smaller molecular areas BAM will give direct visualization to the phase transitions of a monolayer. There are different types of arrangement in a film that can arise, where in a condensed phase molecule can tilt in different directions. As a result what appears as texture in a BAM image, can be due to the different polarizations of each tilted direction[44].

2.2.1 BAM Instrumentation

Brewster Angle Microscopy (BAM) and ellipsometry measurements were carried out with an I-Elli2000 imaging ellipsometer (Nanofilm Technologie GmbH, Göttingen, Germany) equipped with a 50 mW NdYAG laser (ν=532 nm). All experiments were performed using a 20× magnification with a lateral resolution of 1 μm. BAM experiments were performed at an incident angle of 53.15° (Brewster angle of water) and a laser output of 50% (analyzer, compensator and polarizer were all set to 0).

2.3 Ellipsometry

Ellipsometry is a method that measures optical properties of a surface. Similar to BAM it utilizes the change in reflection of polarized light induced by the surface. Its high sensitivity is very useful in imaging thin films as well as quantitatively determining changes in the optical properties of the films.

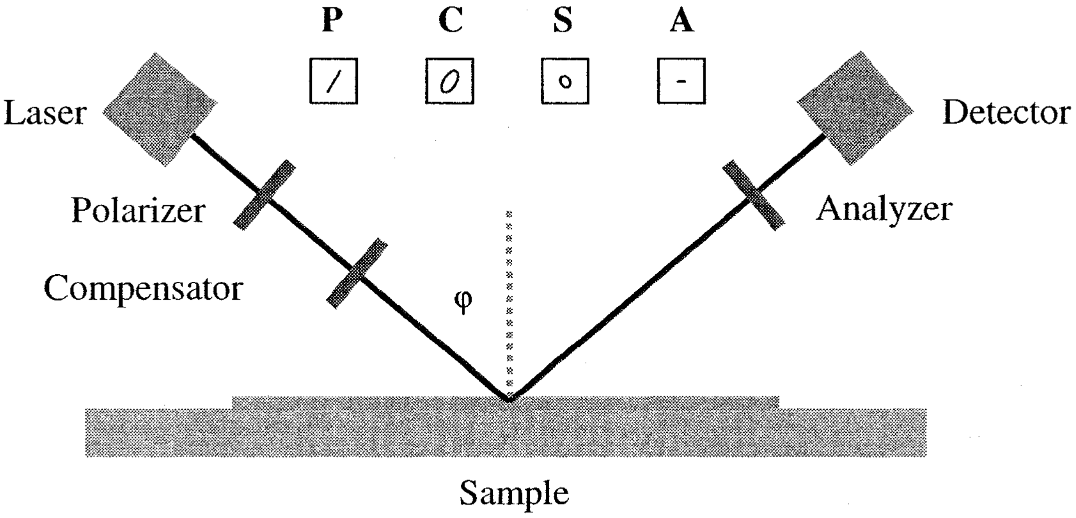

Figure 15 Schematic diagram of a standard PCSA (polarizer-compensator-sample-analyzer) ellipsometer arrangement.

In the PCSA arrangement (Polarizer-Compensator-Sample-Analyzer, see Figure 15), light passes through a polarizer and a compensator before being reflected off of the sample surface at an incident angle, φ. The reflected beam goes through an analyzer and is collected in a photodetector. If this photodetector is a sensitive CCD camera, imaging can be added to the ellipsometer.

In an ellipsometric measurement, elliptically polarized light is produced by the compensator which induces a phase shift of one component of the incident, linearly polarized light beam. Different elliptical states of polarization can be obtained by rotating a compensator in variable amounts.

The reflected light wave will have an altered state of polarization, where vectors p (parallel to incident beam) and s (perpendicular to beam) undergo different overall shifts and will exhibit different reflectivities. As a result, the form and size of the ellipse of polarization is changed and is a measure of the optical properties of the sample (see Figure 16).

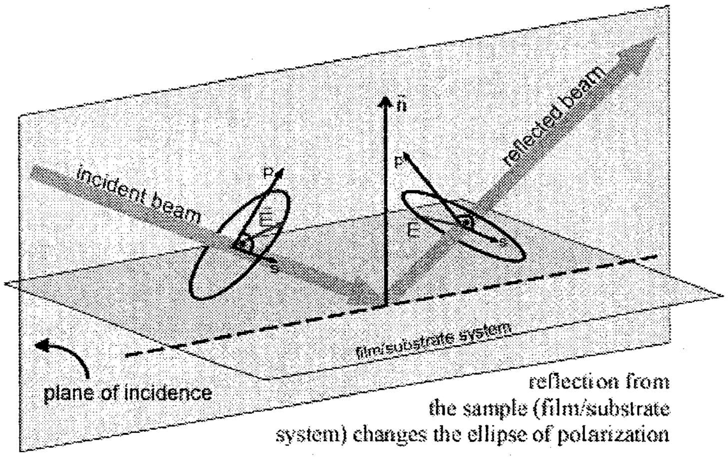

Figure 16 Schematic diagram showing the effect the sample has on the ellipse of polarization[51].

The incident and reflected E vectors are connected by a reflection matrix R of the sample, which describes these optical properties (Equation 14):

$$\frac{E_{p,out}}{E_{s,out}} = \begin{pmatrix} R_{pp} & R_{sp} & E_{p,in} \\ R_{ps} & R_{ss} & E_{s,in} \\ & & \end{pmatrix}$$

Equation 14 The incident and reflected E vectors are connected by a reflection matrix R.

In order to measure the reflection matrix R (i.e. the change in state of polarization state of the incident light), the optical components have to be set so that the intensity of the reflected light wave is minimized. In order for this to occur, the polarizer, P, will be rotated until a linearly polarized reflection is produced. This can be determined by rotating the analyzer until a minimum signal for the reflected light is found. This procedure is also referred to as 'nulling' (see Figure 17).

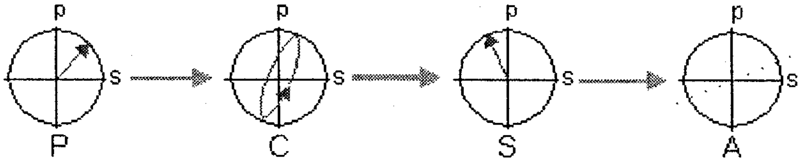

Figure 17 Schematic representation of the nulling of the sample[51].

The result of nulling is a set of angles P, C and A for the optical components which are used to calculate the reflection matrix R. The reflection matrix R of the sample is diagonal (R_{sp}, $R_{ps} = 0$) for isotropic materials. The reflection coefficients, R_{pp} and R_{ss}, are related to the ellipsometric angles, ψ and Δ (see Equation 15):

$$R_{pp} = \frac{|R_{pp}|}{|R_{ss}|} Exp[i(\delta_{pp} - \delta_{ss})]$$

$$\tan\psi = \frac{R_{pp}}{R_{ss}}$$

$$\Delta = \delta_{pp} - \delta_{ss}$$

Equation 15 The relation of ψ and Δ to the ellipsometric coefficients, R_{pp} and R_{ss}.

To calculate the optical properties of a film on a substrate, like refractive index or optical thickness, is very complex. An optical model must be developed and applied as the formula that describes R as a function cannot be inverted. In all, with a single nulling, two measurable real quantities are obtained, which are ψ and Δ. From these measurements the index of refraction, the film thickness or another combination of two real numbers can be modeled by mathematical fitting.

2.3.1 Ellipsometry Instrumentation

Ellipsometric measurements were carried out on the IElli 200 instrument which was previously described in section 2.2.1. In this case the incident angle was set at 50.00° and a laser output of 100% with utilized with the analyzer and compensator set to 20.00°. The reported Δ values are an average of 10 measurements each taken at the same location on the monolayer and are consistent for multiple samples. The ellipsometric isotherm is reported in terms of $\delta\Delta$, which is defined as the difference between the ellipsometric angle Δ of the film on the subphase and the subphase alone ($\delta\Delta = \Delta_{\mathrm{film}} - \Delta_{\mathrm{subphase}}$).

2.4 Langmuir-Blodgett Film Balance

Langmuir-Blodgett (LB) films are deposited/transferred monolayers which provide a way to construct mono/multilayers on solid surfaces. This setup comprises a dipping device to lower or raise the substrate perpendicular to the lipid-water interface, movable barriers to maintain a controlled surface pressure, π, and a surface pressure sensor. Consequently, this modification facilitates the transfer of a monolayer, from the surface of water to a solid substrate. This technique enables one to design and construct structured materials one monolayer at a time. Repeatedly dipping a solid substrate through a monolayer, builds multilayers.

Figure 18 illustrates the formation of an LB film where a lipid monolayer is being transferred. This process is achieved by gradually drawing a solid substrate from the lipid-water interface causing the monolayer to physisorb to the solid substrate through non-covalent interactions. As the monolayer is transferred, the surface pressure is kept constant through an automated barrier device repositioning itself to enable a constant pressure.

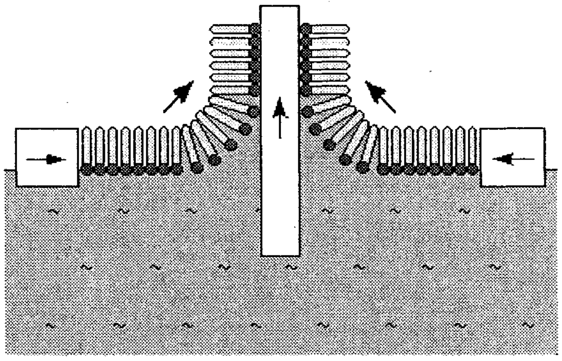

Figure 18 Schematic diagram showing a Langmuir-Blodgett transfer[52].

The organization and the topography of amphiphilic molecules adsorbed onto solid surfaces are observed through AFM, which will be discussed in section 2.5.

2.4.1 LB-transfer Instrumentation

Monolayers were transferred at a constant pressure onto freshly cleaved mica, purchased from Ted Pella Inc. (Redding, California), for topographical analysis by AFM, on the upstroke using the Langmuir-Blodgett technique with a dipping speed of 0.5 cm·minute^{-1}. All transfers were carried out under symmetric compression and transfer ratios, T_R, were recorded.

$$T_R = \frac{A_{trough}}{2 \times A_{substrate}}$$

Equation 16 Transfer ratios, T_R, formula

Transfer ratios are defined as, area of monolayer removed from subphase at constant surface pressure, A_{trough}, divided by area of substrate immersed in water, $A_{substrate}$ (see Equation 16). T_R values were always close to 1.

2.5 Atomic Force Microscopy

Atomic Force Microscopy (AFM) can be used as an imaging tool, a pico force sensor, molecular tweezers and a specialized chemical sensor. The imaging capabilities at the air-lipid interface on a solid substrate are of great interest in lipid monolayer studies. AFM provides three-dimensional images of surfaces that approach molecular or even atomic resolution. This technique was used for its enhanced resolution compared to most optical microscopy techniques as well as its ability to scan non-conducting surfaces.

For non-conducting materials, such as lipids, AFM is applied where its resolution depends on the diameter of the tip; the smaller the diameter, higher resolution, R_s, is acquired. It is also dependent on the frequency of oscillation the tip. A detailed map of the surface can be obtained, from this technique, at the molecular level.

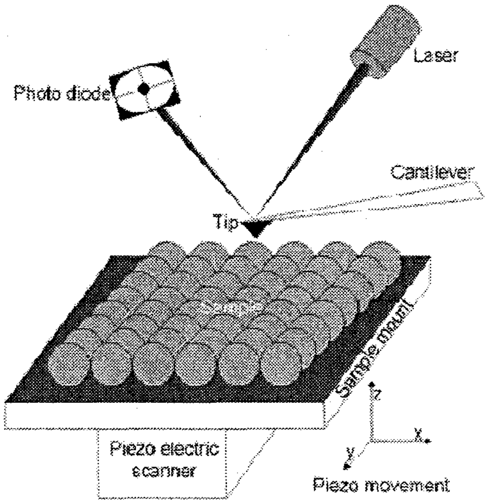

Figure 19 Schematic representation of an AFM apparatus[53].

Figure 19 shows a schematic representation of an AFM apparatus. The morphology of a surface is recorded with a tip that is usually made out of diamond or silicon nitride (Si_2N_4). This tip is mounted onto a mirrored cantilever spring. A laser beam is reflected off the back of this cantilever, and the reflected light is received by a photodetector. Depending on the topography of the surface, the reflected beam will shift accordingly. The signal from the photodetector goes to an electronic feedback loop that raises or lowers the tip so as to maintain constant deflection/amplitude. This process also ensures that the tip does not damage the surface, since constant amplitude must be maintained. The feedback controller has two parameters; proportional feedback and integral feedback. Proportional gain is related to the change in tip height which is proportional to the error signal, which is the difference between the current you wish to maintain (the setpoint) and the actual current. The integral feedback is the change in height proportional to accumulated error signal.

The tip is able scan over the surface of a substrate, in the x and y direction in two different scanning modes; it can either scan in contact with the surface or oscillating over the surface in a tapping motion. In contact mode, a large force is applied to the sample. In contrast, tapping mode has a limited amount of sheer forces. Depending on the sample one mode will be preferential over another, for example if the sample being scanned is physisorbed to a solid substrate, it would be ideal to scan the surface of the sample in the tapping mode where the integrity (morphology) of the sample will remain relatively the same.

2.5.1 AFM Instrumentation

A Nanoscope IIIa (Digital Instruments, Santa Barbara, CA) was used to capture AFM images in air at room temperature using tapping mode at a scan rate of 1 Hz using etched silicon cantilevers (RTESP NanoProbe, Veeco, Santa Barbara, CA) with a resonance frequency of ~300 kHz, a nominal spring constant of 20-80 N/m, and tip radius of <10 nm. Oscillation amplitude of 175 mV and medium damping (~25%) were employed for these measurements.

2.6 Grazing Incidence X-ray Diffraction at the air-water Interface

Grazing Incidence X-ray Diffraction (GIXD) is a technique which provides information on the molecular arrangement and packing of the alkyl chains in condensed phases of monolayers at the air-water interface. As seen in section 1.5.1.2, there are several variations of condensed phases, which can be distinguished from one another. These phases can be differentiated with the use of not only BAM imaging (see section on BAM) but with the use of GIXD as well[54]. GIXD has an increased precision since the distinction between phases through the orientation of molecules relative to the unit cell of a molecule can be determined (in other words, unit cell parameters), where additionally the tilt direction (ex. NN, NNN) as well as the angle of tilt can be identified.

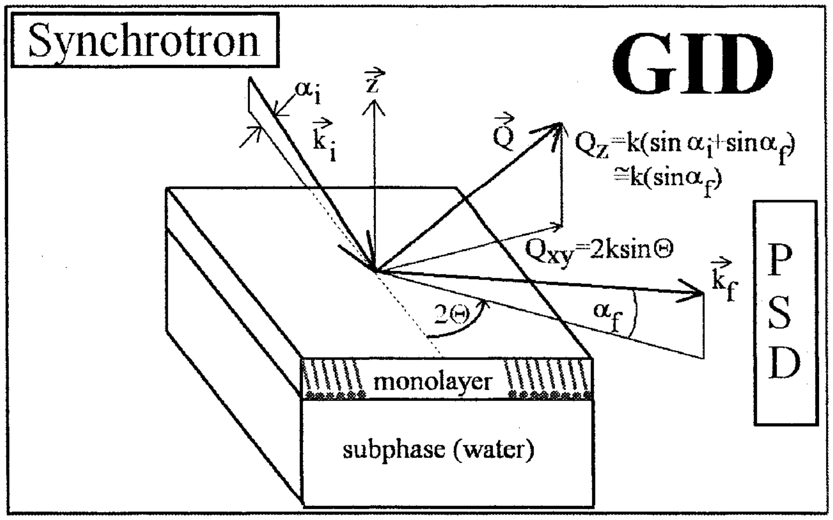

Figure 20 Schematic diagram of the geometric components determined through an analysis of grazing incident diffraction (GID) data using a position sensitive detector (PSD)[55].

In order to obtain information on the molecular arrangement and packing of the alkyl chains of a condensed phase, an x-ray beam hits the monolayer at an angle, α_i, less than that of the critical angle total external reflection (Figure 20). The diffracted beam intensity can be described by an out of plane component, Q_z, which is defined by the angle α_f, and an in plane component, Q_{xy}, defined by the angle 2Θ. Bragg peaks, can be observed when the monolayer exhibits lateral periodicity (or repeat structure) between the alkyl chains as is found in the condensed phases. However, these condensed phase structures can be considered two-dimensional powders of individual crystals that are packed randomly relative to each other, displaying a limited lateral short order chain range. With the used of the geometric components defined in Figure 20, the component are then defined in Equation 17 as

$$Q_{xy} = k\sqrt{\cos^2 \alpha_i + \cos^2 \alpha_f - 2\cos \alpha_a \cos \alpha_f \cos 2\theta}$$

$$Q_{xy} \approx 2k \sin \theta$$

$$Q_z = k\left(\sin \alpha_i + \sin \alpha_f\right) \approx k \sin \alpha_i$$

$$Q_{xy} \approx 2k \sin \theta_{\max} = \frac{2\pi}{d_{hk}}$$

$$k = \frac{2\pi}{\lambda}$$

$$d_{hk} \approx \frac{\lambda}{2k \sin \theta_{\max}}$$

Equation 17 Geometric components of the beam of light from GIXD.

Q_{xy} gives information about the lattice constants a, b and γ, which are required to determine the dimensions and structure of the unit cell (see Figure 21), while Q_z provides tilt angle from the normal and tilt azimuth (direction of tilt relative to the unit cell ex. NN, NNN) (See Figure 22). The unit cell is defined when considering a molecule and its six nearest neighbours. When the molecules have perfect hexagonal packing, the lattice constants a, b and c are equal. The resulting diffraction pattern yields all peaks at the same Q_{xy} value (see Figure 23 and section 1.5.1.2). Such a packing is usually obtained for untilted molecules which additionally means that there will only be one peak at $Q_z = 0$. Note in Figure 23 a schematic characterization of these peaks is given, where in this figure Q_{xy} and Q_z are represented as K_{xy} and K_z, respectively.

As the tilt of the alkyl chains increases from its normal, the unit cell is distorted from hexagonally packed molecules, where as a result multiple peaks can be observed. If the molecules tilt towards either nearest neighbours or next nearest neighbours (i.e. along a symmetry axis) a centered rectangular (orthorhombic) packing is achieved when a is not equal to however b and c are equal (see Figure 21). The resulting diffraction pattern comprises 2 peaks, one degenerate and one non-degenerate (see Figure 21). Note that if the tilt is towards nearest neighbours, the degenerate peak is out-of-plane and the non-degenerate peak is in-plane (Figure 23b). Note that if the tilt is towards next nearest neighbours, both peaks are at $Q_z > 0$, that is out-of-plane, with the degenerate peak is at lower Q_z values (Figure 23c). If the tilt direction has an intermediate tilt, between nearest and next nearest neighbours, an oblique unit cell arises where a, b and c all have different lengths. The diffraction pattern then shows three peaks and each peak is not equivalent (Figure 23d).

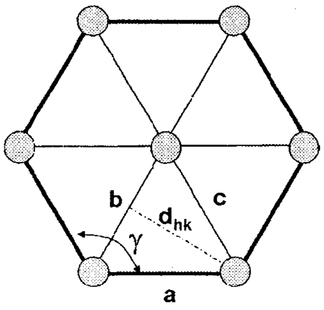

Figure 21 Schematic of a unit cell showing the lattice constants a, b and γ.

The lattice constants allow us to determine the molecular area within the plane of the water surface. Equation 18 is used to determine the molecular area, A_{xy}, where it must be divided by the number of molecules, *n*, in the unit cell.

$$A_{xy} = \frac{ab\sin\gamma}{n}$$

Equation 18 Molecular area, where it must be divided by the number of molecules, *n*, in the unit cell.

Perpendicular to the air-water interface a molecules tilt angle is determined by its Q_z position, where at $Q_z = 0$, the alkyl chains are untilted. The tilt angle, t, from the normal and the tilt azimuth angle, ψ, to the a-axis can be calculated using Equation 19

$$Q_z^{\max} = Q_{xy}^{hk} \cos(\psi) \tan(t)$$

Equation 19 The tilt angle, *t*, is determined by its Q_z position.

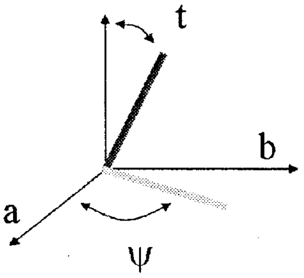

Figure 22 Peak position analysis

Once the tilt angle is determined, this along with the lattice constants will also allow us to determine the cross-sectional area of chains, A_0. In Equation 20, the molecular area is multiplied by the cosine of the tilt angle, *t*, where

$$A_o = A_{xy} \cos t$$

Equation 20 The cross-sectional area of chains, A_0 is the molecular area multiplied by the cosine of the tilt angle, *t*.

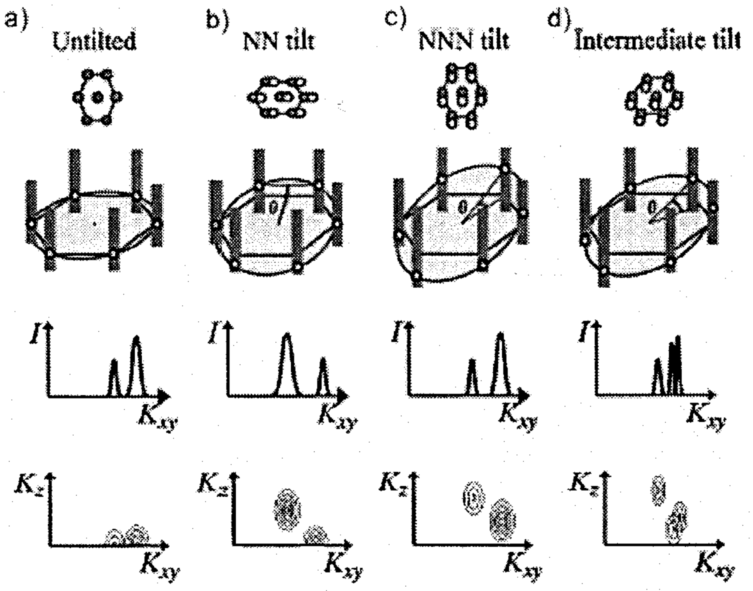

Figure 23 Schematic diagram of characteristic diffraction patterns when a) molecules are untilted, b) tilted towards nearest neighbour (NN), c) tilted towards next nearest neighbour (NNN) and d) tilted intermediately between NN and NNN (oblique)[54].

2.6.1 GIXD Instrumentation

It should be noted that samples were sent to Gerald Brezesinski at the Max-Planck-Institute of Colloids and Interfaces in Berlin, Germany, who performed the experiments at 25 °C on the liquid-surface diffractometer on the beam line BW1 at HASYLAB, DESY in Hamburg, Germany. A brief description will be provided however, exact details pertaining to the experimental setup can be found in for example, Kaganer et al [54]. Although collection of data was performed by Gerald Brezesinski the analysis was carried out at Concordia as part of this thesis.

The diffracted beam of the vertical scattering angle α_f is detected by use of a linear position sensitive detector (PSD) (OED-100M, Braun, Garching, Germany). The vertical full width at half-maximum (fwhm) was 0.005 Å^{-1}, while Q_{xy}, the in-plane component ($Q_{xy} = (4\pi/\lambda)\sin(2\theta_{xy}/2)$), has a resolution of 0.009 Å^{-1}. The intensities of arbitrary points were compiled and fitted using model peaks. The intensity of each peak is obtained in the Q_{xy} direction (Figure 10), where they are analyzed using a least-squares fitting tool in the Q_{xy} direction by use of Lorentzian, which is parallel to the air-water interface. The intensity of each peak is also compiled in the Q_z direction and fitted by use of Gaussians, which is out of plane and normal to the interface. This is performed in order to decide base on fits the number of peaks present, their position and full width at half maximum.

2.7 Analytical techniques

Standard analytical techniques, namely gas chromatography-flame ionization detector (GC-FID) and electrospray ionization mass spectrometry (ESI-MS), were used to qualitatively and quantitatively analyze the fatty acid composition of PIH. It should be noted that the instrument manipulations and data analysis of the GC data was done by Alexandre Ouellet while the ESI-MS instrumentation was operated by Alain Tessier.

2.7.1 Gas Chromatography Instrumentation

All samples were analysed using an Agilent Technologies GC-FID instrument (model 6890N) fitted with a 30 m long x 0.32 mm inner diameter column of HP-5 (polysiloxane 95% and 5% phenyl) polarity and film thickness of 0.25 µm coupled to a flame ionization detector (FID). In order to obtain quantitative data a few important steps must be taken to ensure complete and accurate data: Firstly, optimisation of the GC method including FAME standards identification. Secondly, the calibration of standards and detection limits determination. Finally, the analysis of the method blank as well as PIH is performed. Note that all of these steps were carried out by Alexandre Ouellet. However, sample preparation was supervised.

2.7.1.1 Optimization of Method

2.7.1.1.1 Temperature ramp and the flow rate used

A six temperature ramp is used to optimize resolution of closely eluting peaks. Table 2 is the method that was carried out for the standard as well as the sample.

Table 2 Temperature ramps used for GC method

Temperature (°C)	Rate (°C/min)	Hold time (min)	Total time (min)
45	N/A	1	1
140	15	0	7.33
214	4	0	25.83
216	0.5	0	29.83
219	4	0	30.58
223	0.5	0	38.58
260	10	12	54.28

2.7.1.1.2 FAME standards identification.

A fatty acids methyl ester (FAME) standard, Supelco37 was used to identify derivatized fatty acids. A bacterial standard was initially used to identify all Supelco37 fatty acid methyl esters standards since 13 derivatized fatty acids were common to both the Supelco37 and the bacterial standards. Overlapping the Supelco37 spectrum and the bacterial standards was performed to identify all Supelco37 fatty acid methyl esters standards.

2.7.1.1.3 The calibration of standards and detection limits determination

Each peak obtained for the FAME standard has different responses therefore, the highest and lowest values obtained for the bacterial sample mixture served as a guide to determined the detection limits expected. Once this is completed, all peaks that were analysed in the unknown samples which were quantified by subtracting the method blank fatty acids.

2.7.2 Electrospray Mass Spectrometry (ESI-MS) Instrumentation

Experiments was conducted in the negative mode on a Micromass Q-Tof-2^{TM} and analyzed with Mass Lynx 4.0 software. The source temperature and the desolvation temperature were set at 60 and 100 °C, respectively. The flow rate was 0.5 μL/min. Note that only the instrumentation portion of this experiment was done by Alain Tessier.

Chapter 3: Methodology (Preparation and Characterization Methods)

3.1 Substances

The following substances were used without any further purification.

3.1.1 Phospholipids:

Reagents Used	Form/Purity	Company	Method of Analysis
Hydrogenated Soy L-α-Phosphatidylinositol (PIH)	Powder/ 99.0%	Avanti Polar Lipids Inc.	LFB, LB, BAM, Elli, ESI-MS, GC, DSC, PLA_2
1,2-Distearoyl-*sn*-Glycero-3-Phosphatidylcholine (DSPC)	Powder/ 99.0%	Avanti Polar Lipids Inc.	LFB, LB, BAM, Elli, ESI-MS, GC
1,2-Distearoyl-*sn*-Glycero-3-Phosphatidylethanolamine (DSPE)	Powder/ 99.0%	Avanti Polar Lipids Inc.	LFB, LB, BAM, Elli, ESI-MS, GC
1,2-Dipalmitoyl-*sn*-Glycero-3-Phosphate (DPPA)	Powder/ 99.0%	Avanti Polar Lipids Inc.	ESI-MS

3.1.2 Structures

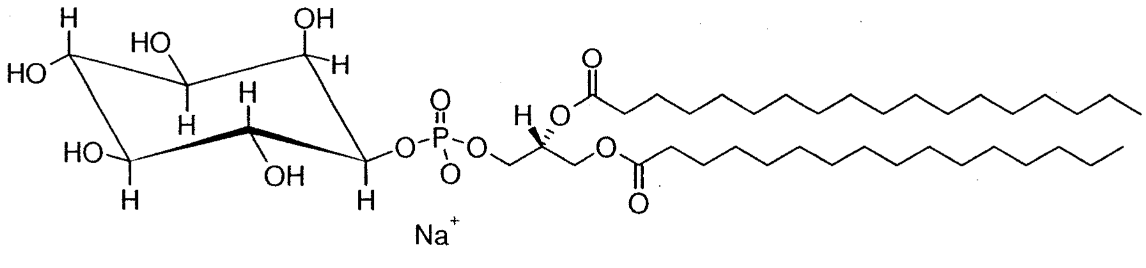

Figure 24 Hydrogenated Soy L-α-Phosphatidylinositol (PIH).

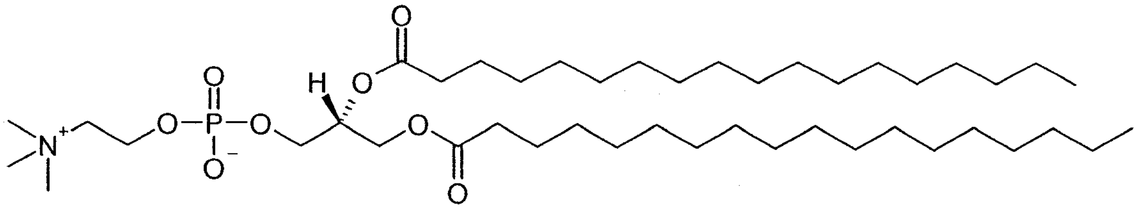

Figure 25 1,2-Distearoyl-*sn*-Glycero-3-Phosphatidylcholine (DSPC).

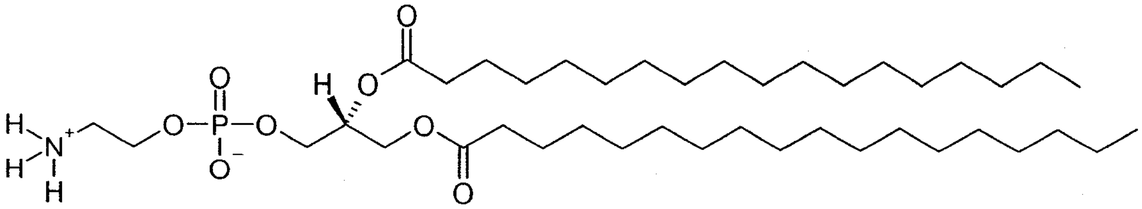

Figure 26 1,2-Distearoyl-*sn*-Glycero-3-Phosphatidylethanolamine (DSPE).

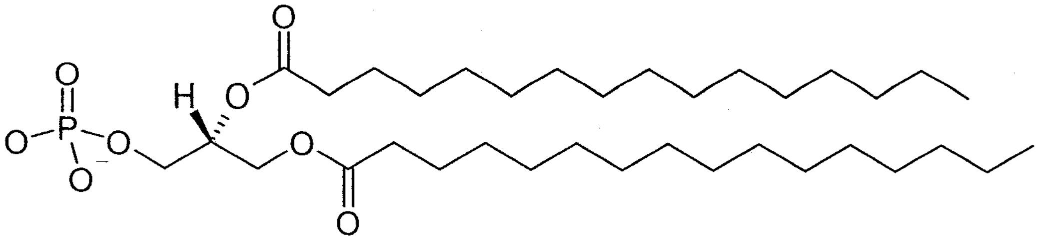

Figure 27 1,2-Dipalmitoyl-*sn*-Glycero-3-Phosphate (DPPA).

3.1.3 Other substances used:

Reagents Used	Purity/Grade	Company	Applications
HEPES buffer	99.5%	Sigma	LFB, LB, BAM, Elli
Sodium Chloride	98%	Sigma-Aldrich	LFB, LB, BAM, Elli, GC (Base Hydrolysis & FA Methylation), PLA_2
Sodium Hydroxide	97%	Sigma-Aldrich	LFB, LB, BAM, Elli, PLA_2
Chloroform	HPLC grade	Fisher Scientific	LFB, LB, BAM, Elli, ESI-MS, DSC,
Methanol	99.9%	Fisher Scientific	LFB, LB, BAM, Elli, ESI-MS, GC (Base Hydrolysis & FA Methyl.), DSC,
Ultrapure water	resistivity: 18.3MΩ-cm	EasyPure II LF system	LFB, LB, BAM, Elli, ESI-MS, GC (Base Hydrolysis & FA Methyl.), DSC, PLA_2
Acetonitrile	99.5 %	EM Science	ESI-MS
Ammonium hydroxide		Chemical Stores	ESI-MS
Dichloromethane	≥ 99.5%	Fisher Scientific	Base Hydrolysis
Potassium Hydroxide (KOH)	90%	Aldrich	Base Hydrolysis
Anhydrous Na_2SO_4	99.0%	Sigma	Base Hydrolysis
Hexanes	≥ 99.9%	Fisher Scientific	FA Methylation
10% BCl_3 in ethanol		Sigma-Aldrich	FA Methylation
Phospholipase A_2 (P9279)	1 283 units/mg protein pH 8.9 at 25 °C	Sigma-Aldrich	Hydrolysis of PIH

The subphase for monolayer experiments were buffered using 10 mM HEPES (see Figure 28) and 100 mM NaCl which was adjusted to pH 7.0 using 1M NaOH.

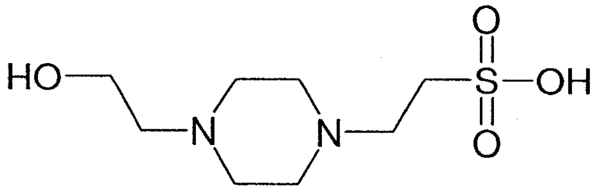

Figure 28 HEPES: N-[2-Hydroxyethyl]piperazine-N'-[2-ethanesulfonic acid].

LB films were prepared using freshly cleaved mica obtained from Ted Pella Inc. (Redding, California).

3.2 Sample preparation

To ensure an accurate measurement, a few important guidelines must be followed: (i) all samples are weighed in tin or silver capsules using a microbalance, (ii) a microbalance is used to weigh samples, since accurate measurements are always required, (iii) silver capsules instead of tin capsules are used if a solvent mixture is required and/or when sonication is required to dissolve compound into solution. It is important to use silver capsules because tin capsules will degrade in acidic conditions and when sonicated extensively (more than 15 min) and (vi) solutions are always stored at -20 °C and sealed with chloroform resistant Teflon tape to slow evaporation of $CHCl_3$.

3.2.1 DSPE

Pure: Preparation of 10 mL stock solution. Between 6 mg and 8 mg of 1,2-distearoyl-*sn*-glycero-3-phosphatidylethanolamine (DSPE), a synthetic phospholipid, is dissolved in 8: 2 chloroform/methanol solution. DSPE is weighed in a silver weighing capsule and placed in a chloroform-rinsed 10 mL volumetric flask. 2 mL of methanol followed by 3 mL of chloroform was then added. Once solvents are added and mixed, and solution is cloudy, it is sonicated until clear (approximately five minutes). Once solution is no longer cloudy the remaining amount of chloroform is added. Once a DSPE solution is stored and taken out of the freezer, solution is always cloudy. Therefore, before every use, the DSPE solution is brought to room temperature then sonicated until clear.

3.2.2 DSPC

Pure: Preparation of 10 mL stock solution. 1,2-distearoyl-*sn*-glycero-3-phosphatidylcholine (DSPC), another synthesized lipid, dissolves readily in pure chloroform. Approximately 6 mg to 8 mg of DSPC is weighed using a microbalance for accuracy in a tin weighing capsule. The capsule, containing DSPC, is placed in a chloroform-rinsed 10 mL volumetric flask followed by the required amount of chloroform. The same sample preparation was applied to 1,2–dipalmitoyl-*sn*-glycero-3-phosphatidylcholine (DPPC).

3.2.3 PIH

Hydrogenated soy L-α-phosphatidylinositol (PIH) is extremely hygroscopic which makes weighing samples inaccurate. As a result, all samples must be handled with care. To ensure an accurate measurement, gloves must be removed prior to sample usage to reduce the amount of electrostatic charges and achieve good accuracy.

The physical properties of PIH make its miscibility low in pure chloroform; therefore a solvent mixture of 1:3 methanol/chloroform must be used as was done for PE. In addition, PIH must be sonicated for complete dissolution in solution as was PE. Also, to ensure complete solubility, less material is used. Since PIH is unable to readily dissolve in solution, the concentration is lower than usual (0.8 mM to 1.0 mM). Therefore, approximately 0.5 mM (or 0.400 mg/mL) solution of PIH is prepared. In all, a special sample preparation is required for proper dissolution of PIH: (i) initially the flask, containing PIH, is filled to half its total volume with a 1:2 methanol/chloroform mixture; (ii) this mixture is sonicated for 15 minutes; (iii) An aliquot (equivalent to 6% of the total solution volume) of pure methanol is added; (iv) the mixture is sonicated for an additional 15 minutes; (v) an aliquot (equivalent to 26% of the total solution volume) of 1:15 methanol/chloroform mixture is added at this point. (vi) Finally, a drop of Millipore water is added and the solution is sonicated for an additional 15 minutes or until the solution becomes clear. Note mixtures are formed by addition of appropriate amounts of relevant stock solutions.

3.3 Electrospray Ionization Mass Spectrometry (ESI-MS Negative mode)

PIH preparation. 1 mL of a 1 mM was prepared in chloroform/methanol/water mixture (70:26:4). The lipid and solution mixture are sonicated for 30 minutes at 30 °C at 66 sonics per minute. This sample is then diluted in an acetonitrile/water mixture (70:30) with 0.1% ammonium hydroxide to produce a final concentration of 1 μM. If solution appears cloudy, it must be sonicated until clear. At this point, 2 mL of this solution was placed in a separate vial for analysis. The stock solution was stored at approximately 4 °C. Similarly, 1,2-dipalmitoyl-*sn*-glycero-3-phosphate (DPPA), which is used as a standard, undergoes the same sample preparations.

3.4 GC sample preparation

3.4.1 Base Hydrolysis of PIH (Saponification)[56].

Approximately 1 mg of PIH is weighed and placed in a 3 mL vial. No more than 1 mL of 0.5 N KOH in methanol was added along with 0.2mL of Millipore water and a stir bar. Prior to reaction the pH of the mixture was determined, with the use of litmus paper, to ensure basic condition is achieved (pH~10). The solution was refluxed for two hours at 100 °C in a sand bath. After this time, the sample is cooled to room temperature and pH is adjusted to 2 by adding 6N HCl dropwise (approx. 6-8 drops were required). The organic phase is then extracted with three 1 mL portions of dichloromethane then washed with three 1mL portions of 5% NaCl solution. The organic phase, containing the fatty acid derivative, is then dried with anhydrous sodium sulphate (Na_2SO_4). The sample was purged with N_2 gas and left at room temperature overnight.

The following day, the sample is decanted into a clean 3 mL vial. The anhydrous sodium sulphate is then rinsed three times with 1 mL portions of dichloromethane. The sample along with rinsings are combined and evaporated by heating the solution to 40 °C using a heating block and flowing N_2 gas over the surface of sample. Similarly, a blank was prepared using the same method.

3.4.2 Fatty Acid Methylation (Derivatization)[56].

Following the base hydrolysis of PIH, the fatty acid products were methylated in order to create a lipid with an increased volatility. The sample preparation is as follows:
In a 3 mL vial 10% BCl_3/CH_3OH is added to the fatty acid products, which was previously evaporated to dryness with N_2 gas. Once the reagent is carefully poured into vial, it is purged with N_2 gas for 30 seconds then sealed with a Teflon-lined cap. The solution is placed in a heating block and allow to heat at 100 °C for 2 hours. After 2 hours, reaction vial is removed from heating block and allowed it to cool to room temperature. The organic phase is extracted with hexanes (1×100μL followed by 1×200μL) and combined. The combined organic phase is washed three times with 1 mL 5% NaCl solution portions. The organic phase is then collected in a clean vial.

Anhydrous sodium sulphate (Na_2SO_4) is used as a drying agent and is added to the hexanes solution followed by purging with N_2 gas and leaving overnight.

The next day, the sample is decanted into a clean 3 mL vial. The anhydrous sodium sulphate (Na_2SO_4) is then rinsed three times with 1 mL portions of hexane. The sample along with rinsings are combined and evaporated by heating the solution to 40 °C using a heating block and flowing N_2 gas over the surface of sample. Similarly, a blank was prepared using the same method.

Prior to injection the sample is dissolved in 1.0 mL of dichloromethane and transferred to a GC vial.

3.5 Hydrolysis of PIH with PLA_2

3.5.1 Vesicle Preparation[57,58]

A 35 mM KCl and 10 mM $CaCl_2$ medium at pH 8.4 is added to dry PIH to form a 6.0 mM (or ~ 5 mg/mL) lipid dispersion. The temperature of the dispersion remained between 35 °C and 40 °C. For proper vesicle formation to occur, the temperature must be kept above the melting temperature of pure PIH (32–37 °C[59]). To induce multilamellar vesicles, this dispersion is agitated on a bench vortex for approximately 1 hour followed by a 30 minute cycle period of 2–3 minutes sonication and 1 minute cooling at 40 °C. To remove large multilamellar liposomes, these vesicles are centrifuged for 30 minutes at 10 000 g at 24 °C. They were centrifuged again at 16 000 g for 3–4 hours at aprroximately 30 °C. The supernatant or Small Unilamellar Vesicles (SUV) are removed without disrupting the bottom of test tube. To ensure vesicle dispersion, the temperature is kept at

40 °C until samples were ready for use. Once the desired amount of vesicles is removed, they are incubated at the reaction temperature (30 °C) for at least 4 hours.

3.5.2 Hydrolysis Reaction[57,58]

A 0.01 mg/mL stock solution of the enzyme was prepared by dissolving PLA_2 in a 35 mM KCl and 10 mM $CaCl_2$ solution (pH 8.4). The desired amount of vesicles is placed in a microfuge tube and left to incubate for at least 4 hours at 30 °C (the reaction temperature) at pH 8.4 against the medium. Once the incubation period is complete, the enzyme solution is added to the reaction mixture. Approximate 5 minutes was alloted for the reaction time. Upon completion of the reaction, the pH was adjusted to 2 using 6N HCl solution (~ 6-8 drops required) and fatty acid was extracted using hexanes (3 × 400 μL). It was then evaporated to dryness with N_2 gas at 40 °C.

3.5.3 Base Hydrolysis of Lyso-PIH

Base hydrolysis for the lyso-PIH, which is water soluble, was performed. See section 3.4.1 for procedure.

3.5.4 Fatty Acid and Lyso-PIH Methylation (Derivatization): (see 3.4.1 and 3.4.2)

Both samples are derivatized as described previously. See section 3.4.2 for procedure.

Chapter 4: Qualitative and Quantitative analysis of PIH

Hydrogenated soy L-α-phosphatidylinositol (PIH) was provided by Avanti Polar Lipids with a certificate of its fatty acid composition. In order to determine the fatty acid composition, phospholipids are hydrolyzed and their fatty acid derivatives were then analyzed by gas chromatography (GC)[60]. In Figure 29, the fatty acid composition of PIH is reported as being 30% palmitoyl (16:0), 60% stearoyl (18:0) and 10% other. Despite the provided analysis, some information was lacking and left two main concerns.

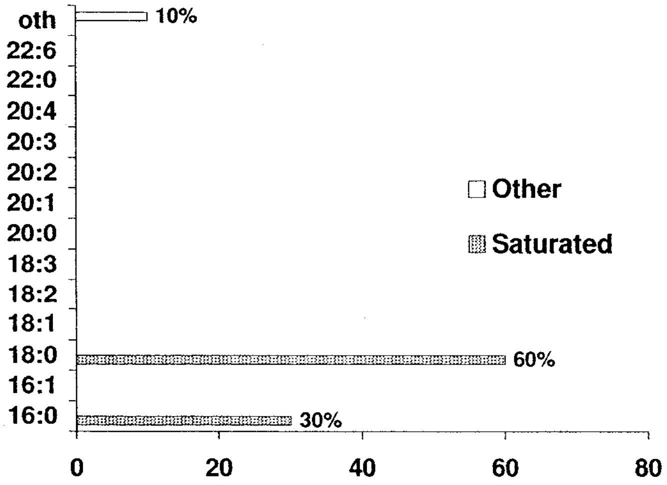

Figure 29 Fatty acid composition of PIH reported by Avanti[60].

First of all, 10% other was reported in their analysis. According to Avanti, PIH is 100% inositol however, in their quantitative assessment there were some fatty acid derivatives that could not be identified with their standards. It is postulated that this 10% other is inositol however could indeed be attributed to the formation of lyso-PIH or other side products. Secondly, the percentage of asymmetric versus symmetric phospholipids in the mixture still remains unidentified. For example, 30% of PIH is allocated to palmitoyl fatty acid. Whether a fraction of this is symmetric, dipalmitoyl (C16:0/16:0), or asymmetric, palmitoyl-stearoyl (C16:0/C18:0) was not indicated. In order to study the biophysical properties of PIH and interpret its phase behaviour these questions must be answered. These concerns will be addressed through a qualitative analysis of PIH followed by a quantitative analysis of the fatty acid derivatives of PIH.

4.1 Electrospray Ionization Mass Spectrometry (ESI-MS) -Negative mode

This technique was used as a qualitative method to analyze the fatty acid composition of PIH. In this analysis, the negative mode was chosen over the positive for two reasons: (i) First of all, in the positive mode, several abundance peaks can be obtained, where $(M\text{-}H)^+$ and $(M+H)^+$ ions are formed resulting in overlapping of peaks. (ii) Secondly, in the negative mode, $(M\text{-}H)^-$ions are the only abundance peak observed. Since PIH is an extract composed of multiple components, the positive mode would produce several overlapping peaks. In order to limit this occurrence, the selection of parent ion and its fragmentation pattern can be simplified using the negative mode[61]. Unlike the fatty acid composition of PIH, soy PI is composed of other components (see Figure 30) and as a result a number of possible m/z ratios can arise (see Table 3).

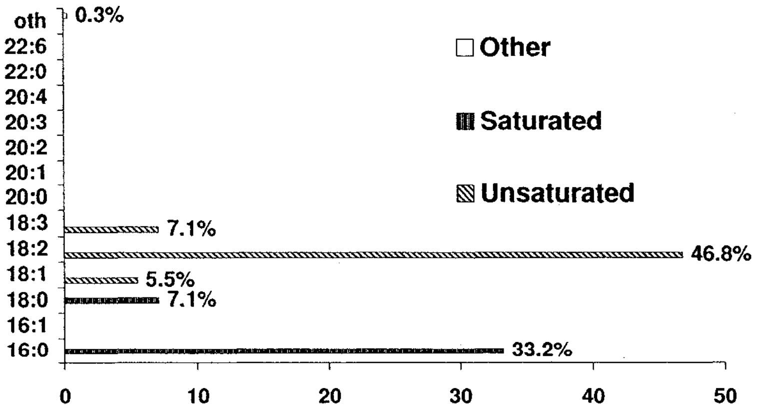

Figure 30 Fatty acid composition of soy PI reported by Avanti[60].

Table 3 Summary of possible m/z ratios in soy PI including those that have been identified by FAB-MS (indicated with an asterisks).

Alkyl Chains	m/z
16: 0/18: 0 PI	837
16: 0/18: 1 PI	835
16: 0/18: 2 PI	833*
16: 0/18: 3 PI	831*
16: 0/16: 0 PI	809
18: 0/18: 0 PI	865
18: 0/18: 1 PI	863
18: 0/18: 2 PI	861*
18: 0/18: 3 PI	859*
18: 1/18: 1 PI	861*
18: 1/18: 2 PI	859*
18: 1/18: 3 PI	857*
18: 2/18: 2 PI	857*
18: 2/18: 3 PI	855
18: 3/18: 3 PI	853

Among these possibilities, the m/z 831, 833, 857, 859 and 861 ions were observed using Fast Atom Bombardment-MS (FAB-MS) for soy PI[61] (indicated in Table 3 with an asterisk). Note that the m/z 809 ion, which corresponds to 16:0/16:0 PI components (or dipalmitoyl-PI), is not observed for soy PI by Jensen et al. In addition, the fatty composition reported by Avanti clearly displays no existence of unsaturated C16 lipid in the extract (see Figure 30). Therefore, from these results, one can postulate that m/z ratios at 837 and 865 will arise for PIH, which corresponds to 16:0/18:0 PI or 18:0/16:0 PI (also referred to as palmitoyl-stearoyl-PI or stearoyl-palmitoyl-PI) and 18:0/18:0 PI components (or distearoyl-PI), respectively. A qualitative analysis on PIH, was performed and will be presented and analyzed in the following sections. 1,2-dipalmitoyl-*sn*-glycero-3-phosphate (DPPA) was also analyzed as a reference compound.

4.1.1 1,2-Dipalmitoyl-*sn*-Glycero-3-Phosphate (DPPA)

An ESI-MS spectrum of DPPA was obtained to aid in the analysis of PIH by comparison of fragmentation patterns. Both DPPA and PIH have similar physical properties, where its hydrocarbon chains are dipalmitoyl (or 16:0/16:0-PA) and its headgroup is a negatively charged phosphate. The only major difference between these two lipids is the absence of an inositol ring in DPPA (see Figure 31).

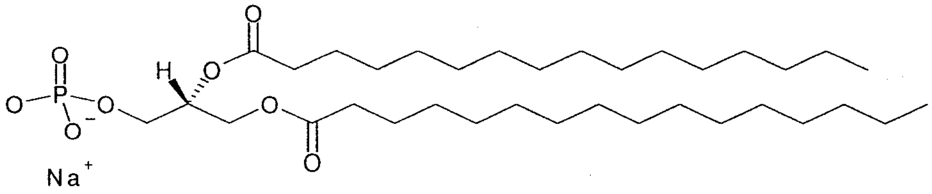

Figure 31 1,2-Dipalmitoyl-*sn*-Glycero-3-Phosphate (DPPA).

ESI-MS-TOF spectra of DPPA indicate the parent ion ([M]$^-$) m/z ratio to be 647, which is confirmed in an ESI-MS-TOF MS/MS performed at 647.6 m/z (Figure 33). In this spectrum, the fragmentation pattern of the parent ion ($[M]^-$) contains the m/z 391 ion and is followed by another dissociation to form the m/z 255 ion. These ions are referred to as the daughter ions, where the appearance of the m/z 391 ion ($[M-R_{16}CO_2-H]^-$) is due to a neutral loss of a fatty acid at the *sn*-2 position ($[R_{16}CO_2-H]$) while the m/z 255 ion is a carboxylate anion ($[R_{16}CO_2^-]$) which reflects a loss of the *sn*-1 palmitoyl fatty carboxylate anion ($[R_{16}CO_2^-]$)[62]. In addition, the hydrolysis of m/z 391 causes the carbon-oxygen bond of the methyl ester to cleave and form the m/z 152 ion. This fragmentation pattern clearly indicates that the parent ion is indeed the m/z 647 ion.

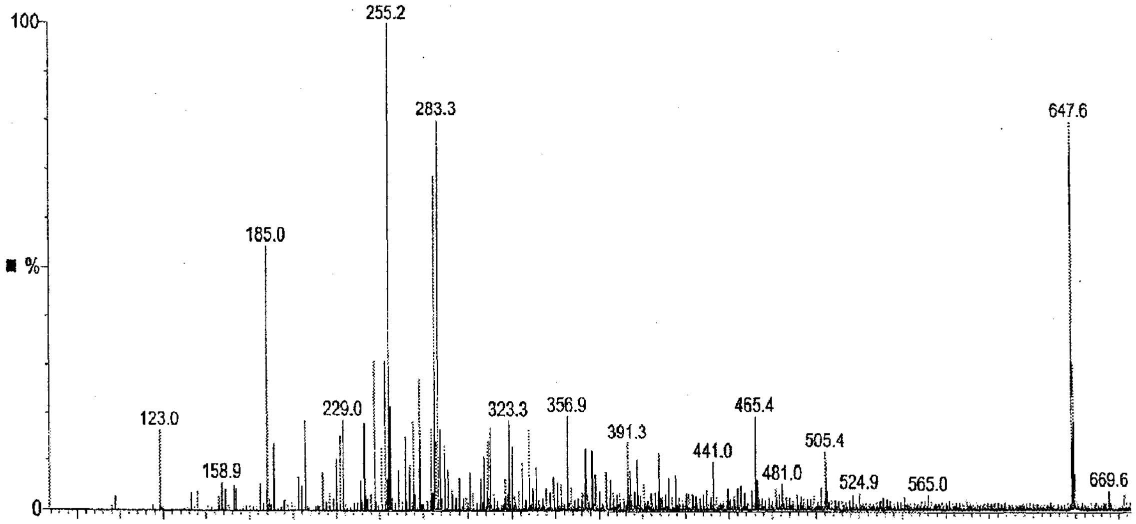

Figure 32 ESI-MS-TOF spectra of DPPA.

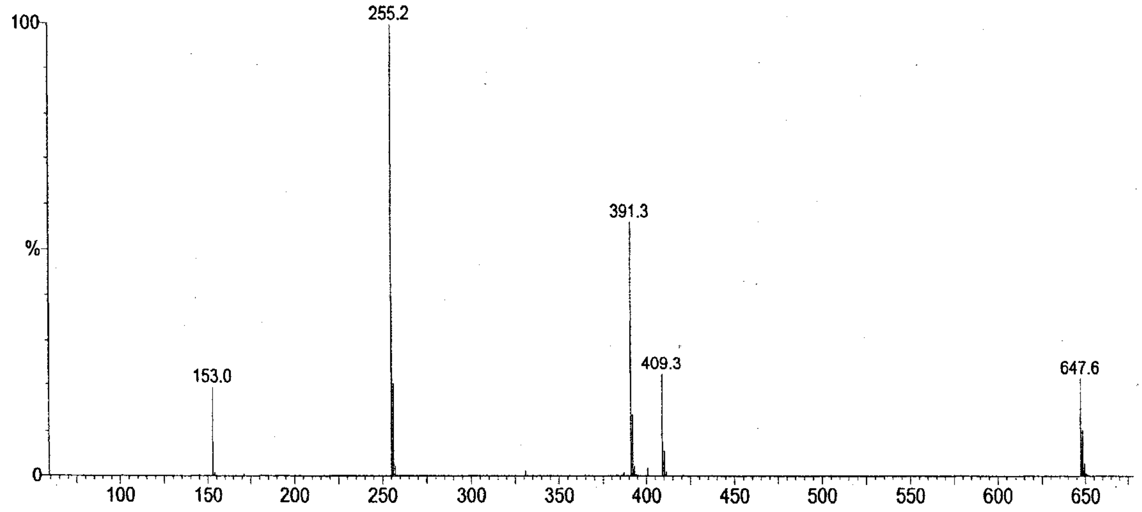

Figure 33 ESI-MS-TOF MS/MS at 647.6 m/z spectra of DPPA

4.1.2 PIH

Since PIH is an extract, there are several parent ions that can arise (see Figure 29). As postulated in section 4.1, the appearance of two parent ions ([M⁻]) should be seen however, in Figure 34, parent ions at 837.7 m/z and 865.7 m/z along with m/z 835.7 and 863.7 ions are observed. These unexpected ions are the parent ions of the unsaturated components of soy PI, namely 16:0/18:1 PI (or 18:1/16:0 PI) and 18:0/18:1 PI (or 18:1/18:0 PI), which corresponds to the m/z 835.7 and 863.7 ions, respectively (see Table 3). These peak associations were confirmed in the MS/MS at 835.7 and 863.7 m/z where analogous fragmentation patterns were observed to those of the unsaturated DPPA (Figure 35 and Figure 36). In addition, the m/z 809 ion was not observed (data not shown), which indicates that dipalmitoyl PI is not present, which coincides with reported data[61]. Moreover, the m/z 861 and 859 ions may be present in trace amount however, from the spectra does not allow one to conclusively determine their presence. Keeping this in mind, we cannot completely rule out any of the parent ions indicated with asterisks in Table 3.

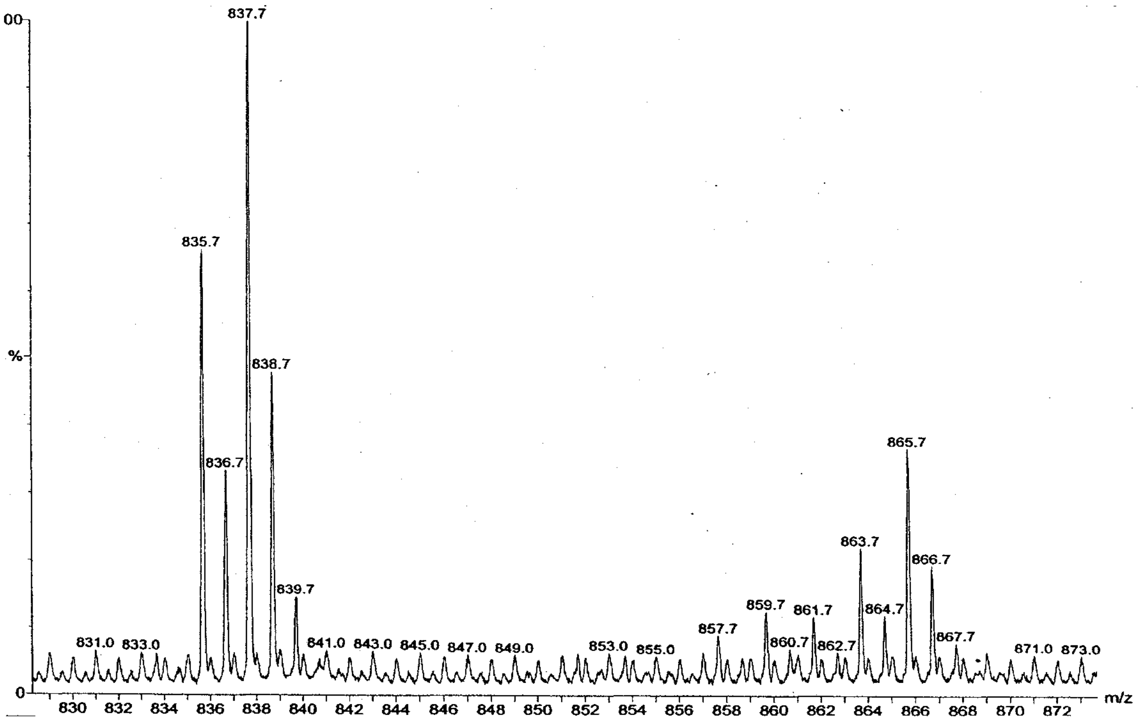

Figure 34 Time-of-flight (TOF) MS spectra of PIH

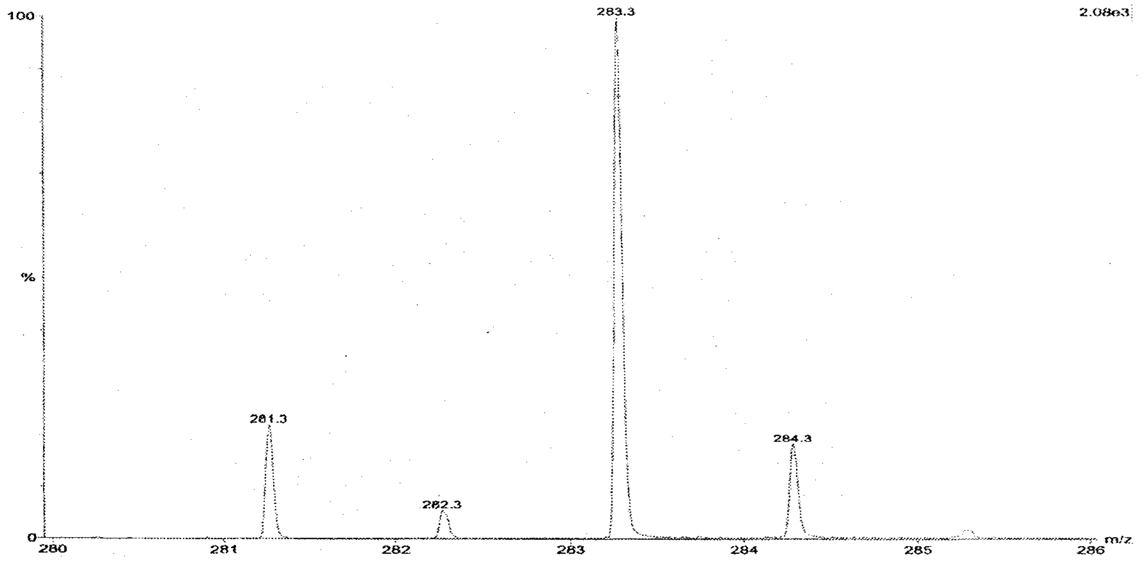

Figure 35 Time-of-flight (TOF) MS/MS spectrum of PIH at 863 m/z

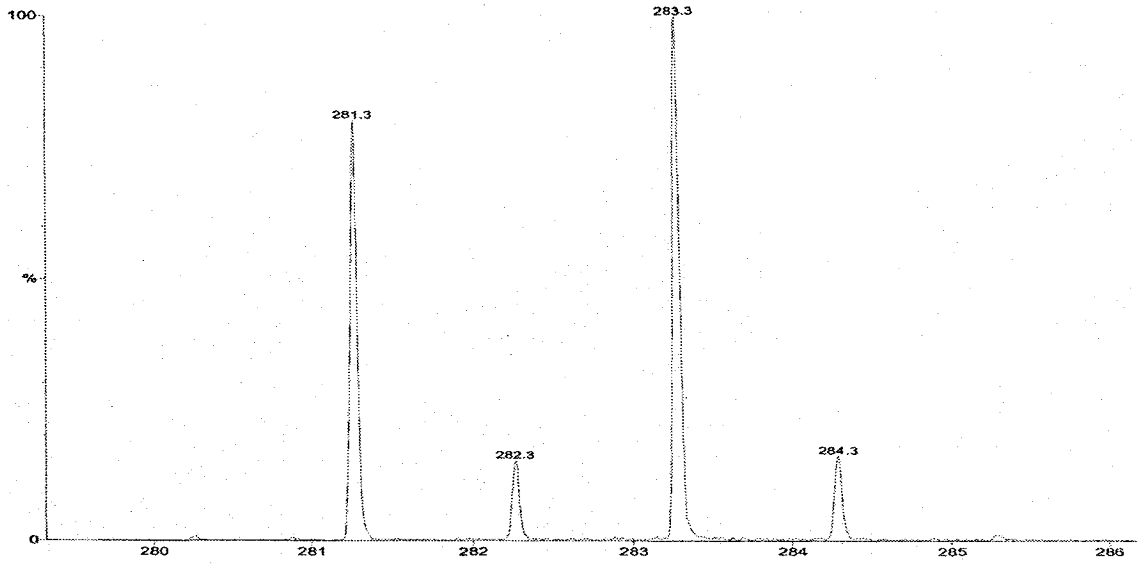

Figure 36 Time-of-flight (TOF) MS/MS spectrum of PIH at 835 m/z

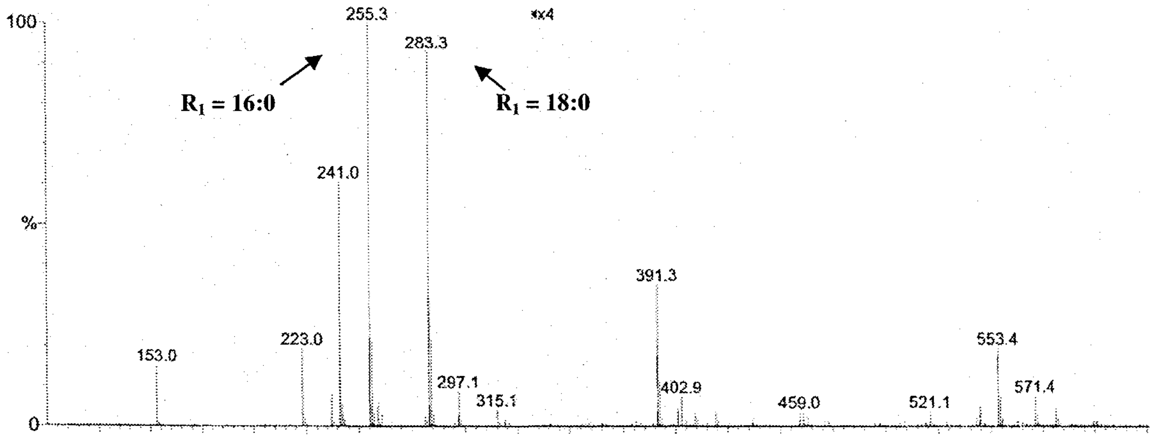

Figure 37 Time-of-flight (TOF) MS/MS spectrum of PIH at 837.8 m/z

Figure 37 is the MS/MS of the $[M]^-$at 837.8 and the principle daughter ions that are observed are due to fatty acid carboxylate formation, which are the m/z 241 and 297 ions. The m/z 241 ion is due to the loss of both hydrocarbon chains along with the loss of water while the m/z 297 ion is due to a loss of both hydrocarbon chains. In addition, the fragmentation patterns as well as daughter ions observed for DPPA at m/z 391, 255 and 152 are similar to those observed for PIH (see Figure 37 and Figure 38), except the m/z 283 ion which is a distearoyl carboxylate anion (18:0 hydrocarbon chain)[61,62]. Moreover, this spectrum contains ions at m/z 553.7 which is due to a neutral loss of the *sn*-2 fatty acid substituent ($[M–R_2CO_2{}^{-}H]^{-}$). Also, ions arising from a neutral loss of ketene at the *sn*-2 ($[M–R'_2CH=CO]^{-}$) are found to be m/z 571.7 ions[62].

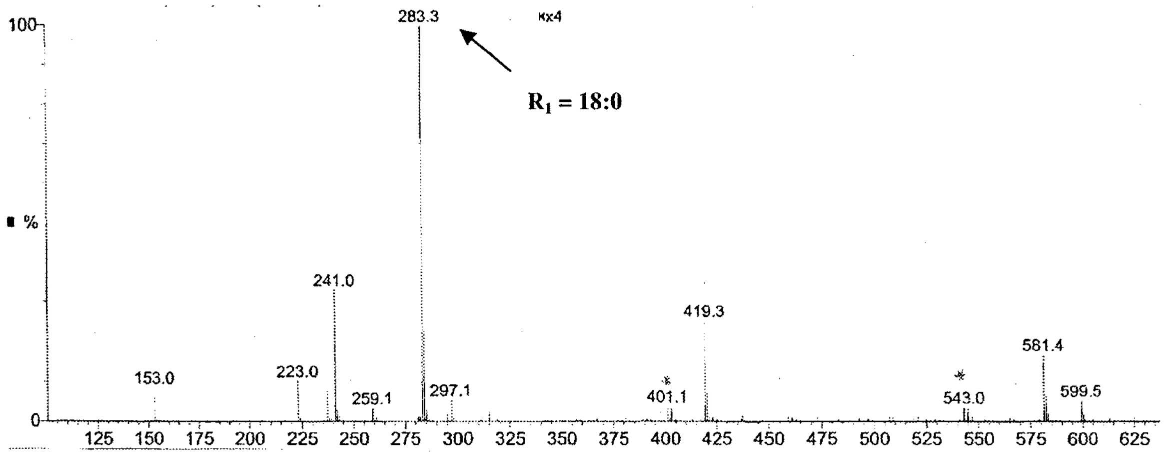

Figure 38 Time-of-flight (TOF) MS/MS at 865.8 m/z

Similarly, a MS/MS spectrum at 865.8 m/z was obtained and analogous peaks were observed except the daughter ion at the m/z 255 (see Figure 38). This indicates that this component is solely saturated distearoyl-PIH (or 18:0/18:0 PI). The occurrence of ions at m/z 581 is due a neutral loss of a carboxylate fatty acid that undergoes a hydrogen exchange[62].

From these results in is confirmed that our sample of PIH does indeed contain unsaturated components of PI. Although it is still a simplified system, to be able to fully understand the monolayer phase behaviour a quantitative study is required to determine the amount of unsaturation present in PIH and this was performed using gas chromatography (GC).

4.2 Gas Chromatography (GC)

In accordance with the base hydrolysis reaction experiment (saponification) followed by the methylation reaction (derivatization), which is outlined in Chapter 3, a fatty acid analysis of the derivatized PIH was carried out. In order to quantitate the results, a fatty acid standard, a method blank along with a PIH sample is required. In Figure 39, a GC-FID spectrum of PIH fatty acid derivatives and a method blank is given. The red spectrum is the method blank while the blue spectrum is the PIH derivatives. As indicated on the spectrum, two peaks were identified at 22.9 and 27.43 minutes, which corresponds to a palmitoyl fatty acid (16:0) peak and stearoyl (18:0) peak, respectively. The unsaturated fatty acid components were identified and are amplified, for visual purposes, in Figure 40. In this spectrum, three peaks were identified at 26.73, 26.94 and 27.02 minutes, which represent the cis C18:1n9, C18:2n6 and C18:3n3, trans C18:1w9 and cis C18:2w6 peaks, respectively. These peaks confirm that unsaturation is indeed present in the PIH sample. They also confirm that the peaks at 861 and 859 in the ESI-MS are indeed representative of trace amounts of the respective components. Moreover, the quantitative analysis of these peaks tells us that the saturated portion is 85% from the total amount of PIH and that the unsaturated portion corresponds to 15% (quantitative analysis done by Alexandre Ouellet). The reagent used in this experiment was 10% BCl_3 in ethanol, which consequently created an ethyl ester bond instead of the desired methyl ester. As a result, two side reaction product peaks at 30.21 and 37.19 minutes are seen. These peaks were identified, with the use of a database, as saturated fatty acids, palmitoyl fatty acid (16:0) and stearoyl (18:0), respectively. The total amount of unsaturated fatty acid observed could possibly explain the 10% other Avanti reports, which indicates that their hydrogenation experiment did not react to completion. Although it is clear that 15% of the fatty acids are unsaturated, we still do not know how many lipids contain one chain with units of unsaturation, how many lipids have both chains containing units of unsaturation and finally how many degrees of unsaturation per chain are present. Consequently, this means that up to 30% (15/50 lipids) of PIH could have at least one unit of unsaturation, which will indeed contribute to the phase behaviour at the air-water interface. However, while the theoretical maximum percentage of lipids containing one or more units of unsaturation is 30%, it is likely that the actual percentage is less if there are lipids that contain a unit of unsaturation on each chain, in which case a minimum of 14% (7/50 lipids) of PIH could be unsaturated. In light of this finding, the MS did not allow us to rule out components with units of unsaturation on each chain, e.g. 18:1/18:1, 18:1, 18:2 or 18:2/18:2. In addition, the chain distribution at each position (i.e. *sn*-1 and *sn*-2) of each PIH component is not known. As a result, a quantitative analysis will be attempted using enzyme hydrolysis with PLA_2 to determine these uncertainties.

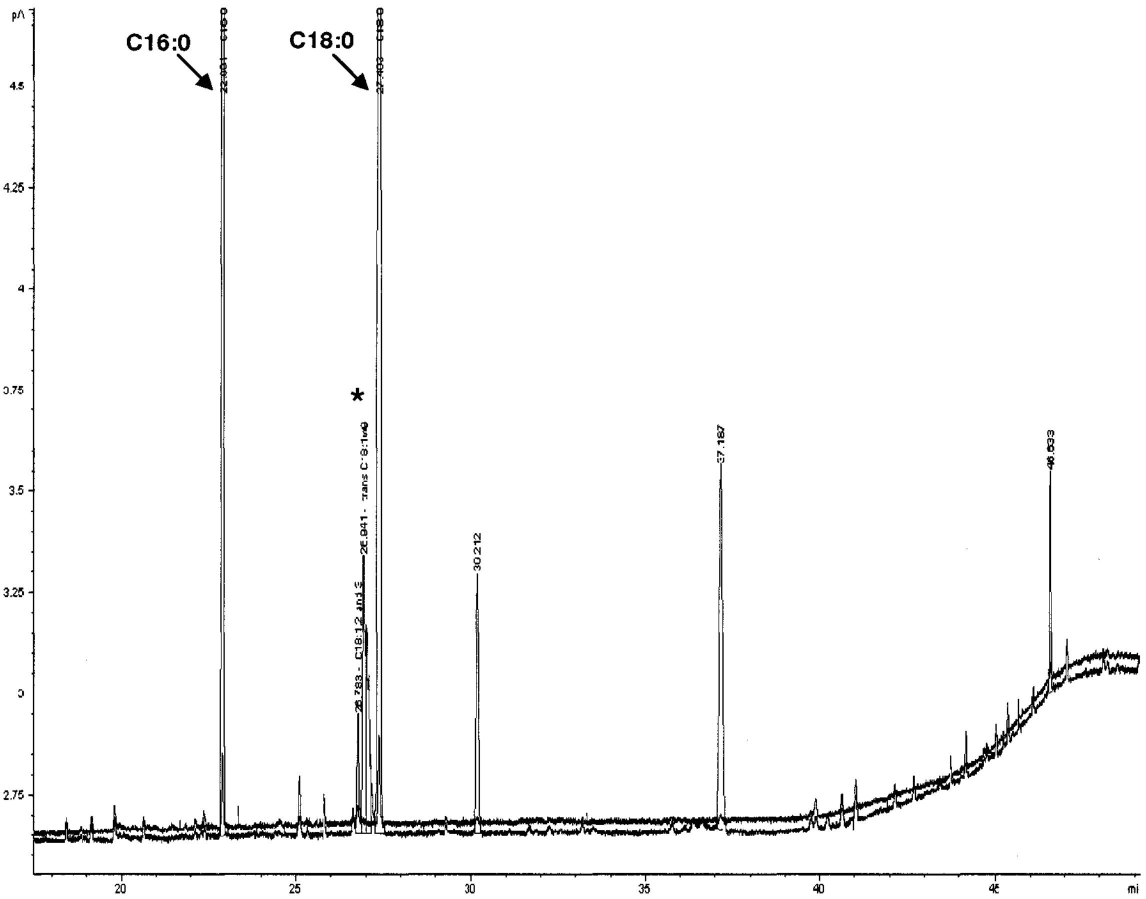

Figure 39 GC-FID spectrum of PIH fatty acid derivatives: red spectra is the method blank and blue spectra is PIH derivatives

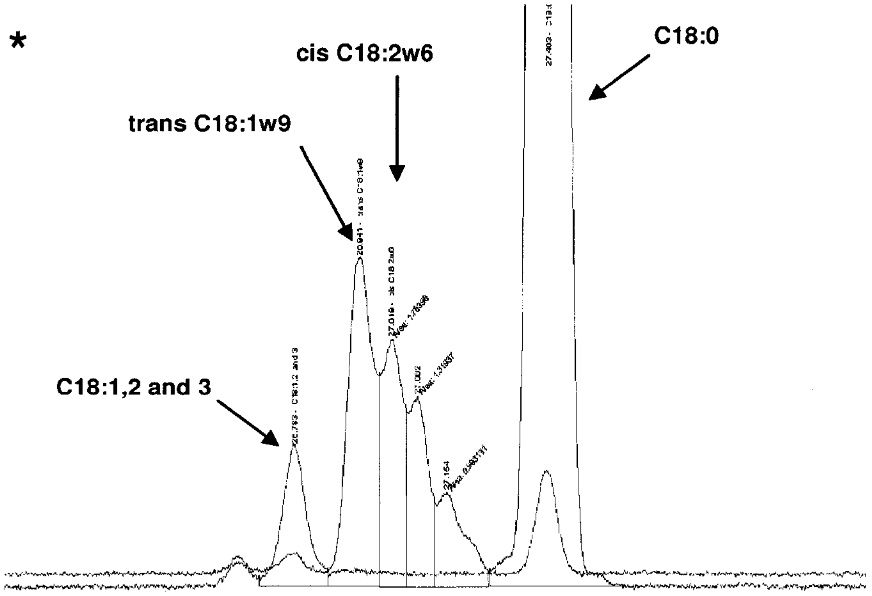

Figure 40 GC-FID spectrum of PIH fatty acid derivatives

4.3 Hydrolysis of PIH with PLA_2

The fatty acid composition of lyso-PI has been previously recorded, where a hydrolysis reaction was performed using PLA_2[60]. The procedure entails the cleavage of a hydrocarbon chain at the *sn*-2 position (see Figure 8) leaving lyso soy PI intact (see Figure 41). The composition of the lyso-PI was found to contain 65% saturated palmitoyl and 35% C18, where only 11% of this is attributed to its saturated component (see Figure 42)[60].

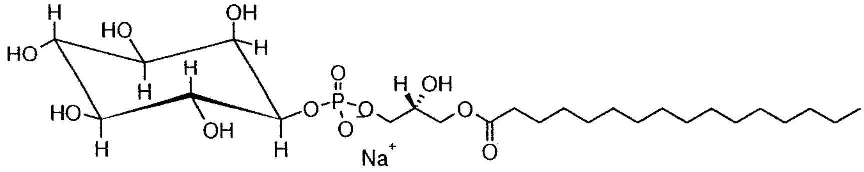

Figure 41 Lyso Soy Phosphatidylinositol.

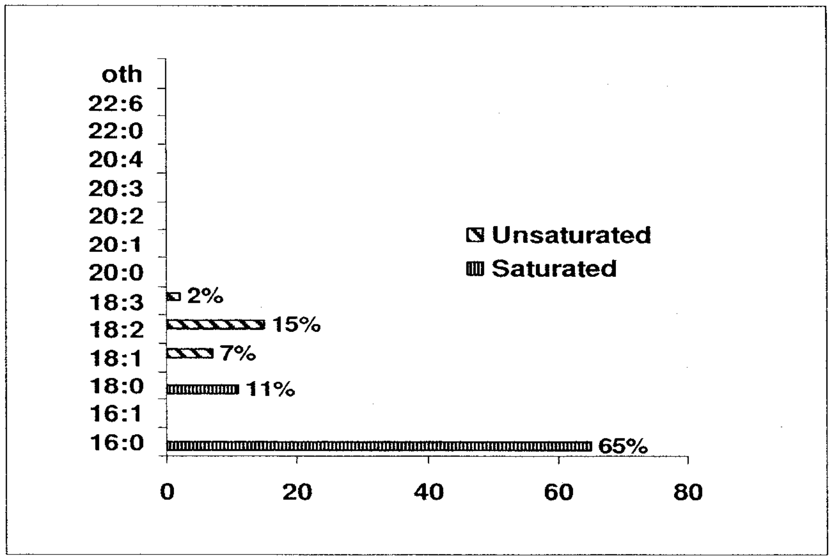

Figure 42 Fatty acid composition of soy lyso PI reported by Avanti.

As discussed in section 4.1, it is known that the dipalmitoyl-PI component, the m/z 809 ion, is not observed[61] and was confirmed in our data as well (see 4.1.2). This implies that limited traces of dipalmitoyl lipids are found and the palmitoyl chains must predominantly contribute to the asymmetric component of PI. If all palmitoyl chains are though to be associated with a stearoyl-PI component, then half of the stearoyl fatty acid (30%) must be present as distearoyl-PI (see Figure 29), which corresponds to 1/3 of the total PIH lipid comprising distearoyl PI. From Figure 42, 35% lyso-PI has C18 at the *sn*-1 position, which confirms that 1/3 of PIH should be indeed distearoyl-PI. The remaining 2/3 of PIH are then asymmetric inositols namely, palmitoyl-stearoyl-PI or stearoyl-palmitoyl-PI. The results obtained in the ESI-MS spectrum along with the fatty acid composition of lyso PI (which showed predominantly palmitoyl fatty acids at the *sn*-1 position) and that of soy PI leads us to believe that the *sn*-2 position is mainly composed of C18-PI (see Figure 30). This reasoning is confirmed when a quantitative analysis of the fatty acid derivatives was performed for bovine. From the results obtained, there was a clear indication that trace amounts of palmitoyl lipid are found at the *sn*-2 position however is mostly found at the *sn*-1 position[5,63]. Whether the quantitative analysis of soy PI will differ from bovine brain PI will be investigated using enzymatic digestion as will be seen in the next section.

4.3.1 Fatty Acid and Lyso-PIH derivatives

The procedure was carried out, as outlined in Chapter 3, section 3.5, and two GC-FID spectrums, one of the fatty acid portion and the other of the lyso-PIH portion, were obtained (see Figure 43 and Figure 44, respectively). In Figure 43 a GC-FID spectra of the fatty acid derivative is shown, where no peaks were observed. However, in Figure 44 two peaks at 22.9 and 27.43 minutes are seen, which correspond to a palmitoyl fatty acid (16:0) peak and stearoyl (18:0) peak, respectively. This hydrolysis data obtained clearly shows that a few problems were encountered. These problems will be addressed where possible reasoning behind the data collected followed by a few suggestions for future experimentation will be discussed.

The ability to predetermine whether vesicles are formed requires a technique such as light-scattering microscopy, which we were not set-up for. Without this information, we do not know for certain if vesicle formation occurred. In order for hydrolysis to occur at the lipid-water interface, the formation of the small unilamellar vesicles (SUV) is vital for successful hydrolysis with PLA_2 on PIH.

Secondly, once the enzyme solution is added to the reaction mixture, approximately five minutes was allotted for the reaction to occur based on the predetermined specific activity of the enzyme. Perhaps at this point enzyme activity was minimal or insufficient time was provided for enzyme to bind to the interface and hydrolyze PIH. This would suggest that a significant decrease in reaction product is likely.

Also, in allowing the PLA_2 to react, PIH is cleaved between the carbonyl carbon and the ester bond. At this point, the resultant fatty acid was extracted with hexanes. Using hexanes as a solvent might have been too non-polar of a solvent and therefore complete extraction of resultant fatty acid was not successful.

Finally, PLA_2 was not extracted from the lyso-PIH prior to saponification (see, Chapter 3: for procedure). Only after saponification was PLA_2 removed from product during extraction with dichloromethane. From the data in Figure 15, two peaks at 22.9 and 27.43 minutes are seen, which correspond to a palmitoyl fatty acid (16:0) peak and stearoyl (18:0) peak, respectively. These peaks are very small but present, which indicates that the quantity of sample is minimal. This loss can be due to the fact that not all PIH weighed initially reacted with the enzyme, since only SUV were extracted, thus lowering the total quantity of lipid. Also, the unsaturated fatty acids might still be present however, is in extremely small quantities. If they are indeed present they are not identified by GC.

In order to obtain agreeable result, the procedure for this experiment will have to be improved. A similar experiment was reported, however for bovine PI, where the procedure for their PLA_2 experiment is outlined[5]. This entails an incubation of 1 μmole of PI with 0.2 mL of 0.1% aqueous bee venom (which contains the enzyme of interest) in 1.6 mL 0.01M Tris-HCl buffer adjusted to pH 7.2. After incubation, 3.0 mL of ether is added, stoppered and kept at room temperature for an allotted time (approximately twenty hours). The time will vary depending on the specific activity (units/mL) of enzyme.

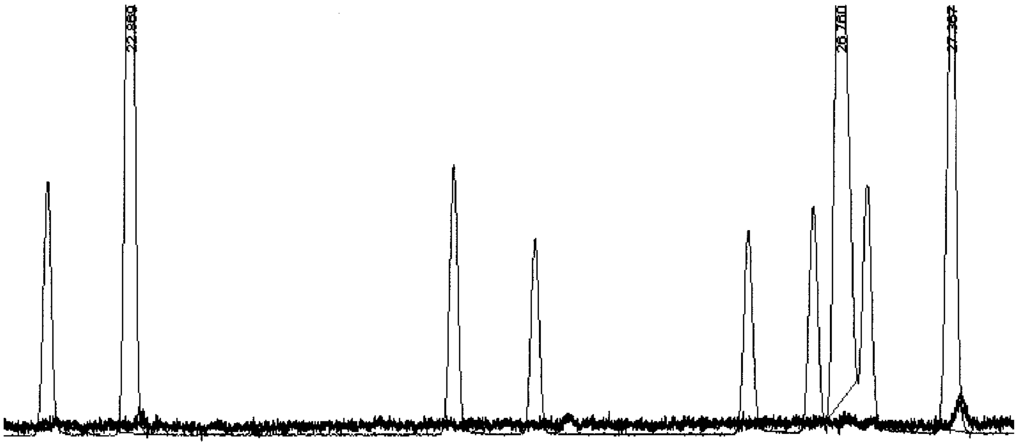

Figure 43 GC-FID spectra of fatty acid derivative: blue spectra is the method blank, the red spectra is the fatty acid sample and the green is the fatty acid standard.

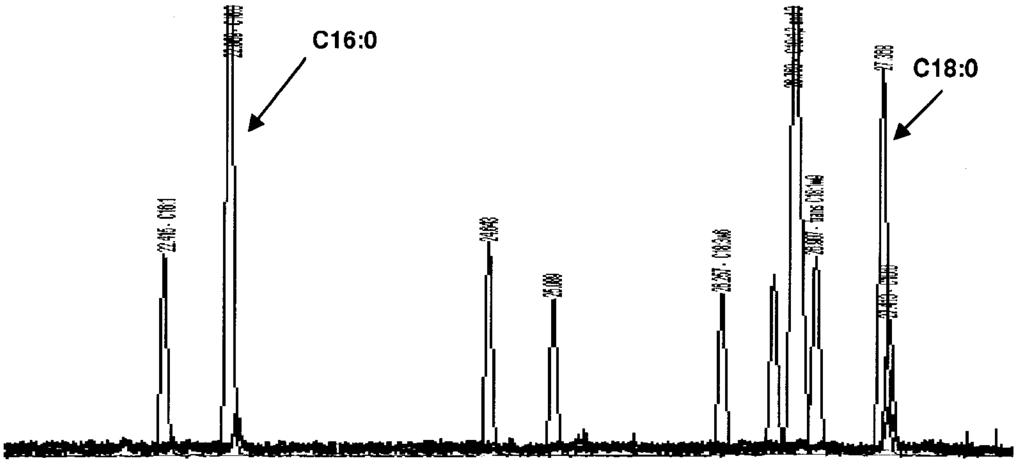

Figure 44 GC-FID spectra of lyso-PIH derivative: blue spectra is the method blank, the red spectra is lyso-PIH sample and the green is the fatty acid standard.

It has been confirmed that PIH does indeed contain 15% unsaturation. In addition, the dipalmitoyl-PI is not one of the components of PIH, as was determined by ESI-MS and confirmed by Jensen et al. This result has now eliminated one of the four possibilities, resulting in three remaining saturated components, C18:0/C18:0 (distearoyl-PI) and the asymmetric components, C16/C18-PI and C18/C16-PI. In addition, the asymmetric component, C16/C18-PI, might not be present in this lipid extract due to the reasoning given above. With these findings, PIH can now be characterized, where the phase behaviour of this unique lipid extraction will be investigating in the following chapter.

Chapter 5: Phase Behaviour of Hydrogenated Phosphatidylinositol at the Air-Water Interface.

In the following chapter a comparison of natural soy PI, hydrogenated soy PI and L-α-dipalmitoylphosphatidylinositol (DPPI) will be presented. To better understand the phase behaviour of PIH, a temperature study on temperatures ranging from 15 to 35 °C will follow in section 5.2 with a more detailed study at each of these temperatures in section 5.3. To assist in the interpretation of PIH the behaviour of DPPI will be reported in section 5.8. And finally, a discussion on the observed phase behaviour of PIH will be presented towards the end.

5.1 Comparison between Natural PI, Hydrogenated PI and DPPI

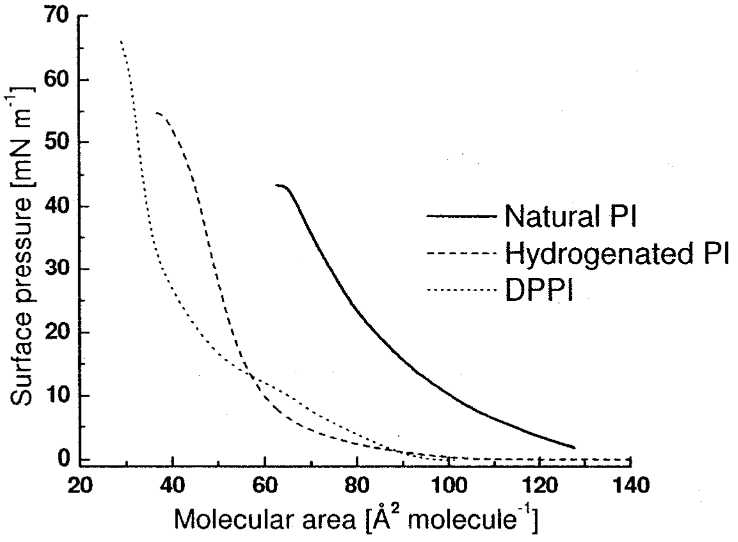

Figure 45 Comparison between monolayers natural soy PI and hydrogenated PI and DPPI on HEPES buffer at pH 7 and 25 °C. Note isotherm for natural PI provided by Yogita Patil-Sen at UMIST, UK.

Isotherms of natural soy PI, L-α-dipalmitoylphosphatidylinositol (DPPI) and hydrogenated soy PI at 25 °C were performed (see Figure 45) to compare their phase behaviour. At low surface pressures natural PI exhibits a gradual inclining slope which is characteristic of a liquid-expanded phase. As the molecular area decreases, the slope remains in, what appears to be, a liquid-expanded phase. Similarly, at low surface pressures, hydrogenated PI displays a gradual inclining slope that is characteristic of a liquid-expanded phase. By comparison to the natural PI the liquid-expanded region appears to be similar, however it does have a slight difference in slope, the film appears more compressible. As a result, this region (between 60 $Å^2$ and 100 $Å^2$) may be characteristic of a transition region as well. As the PIH monolayer is compressed to smaller molecular areas, the slope of the curve appears to have an increased incline, compared to natural PI. In addition, the molecular area, at which the critical area, A_c, is determined, shifted to smaller molecular areas. This difference indicates that hydrogenated PI has decreased compressibility, thus indicating the possibility of a condensed phase forming at high surface pressures. Most importantly, the PIH isotherm appears to exhibit either a transition region or an extended liquid-expanded phase, at low surface pressures. To confirm this, a temperature study is performed to enhance or suppress a transition region as is demonstrated for DPPC in Figure 46[4]. In addition an isotherm of DPPI was obtained, since it is a the only single component PI commercially available, it is fully saturated component similar to our PIH system and finally, it is known from phosphatidylcholines that stearoyl-palmitoyl PC shows similar phase behaviour to dipalmitoyl-PC, which might help in the interpretation of PIH. At low surface pressures the DPPI isotherm clearly displays a gradual inclining slope which is characteristic of a liquid-expanded phase. As the molecular area decreases, a change in slope is observed at approximately 10 mN m^{-1}. At this point it, the slope of the curve appears less inclined and almost horizontal, which is characteristic of a phase transition region. As the DPPI monolayer is compressed to smaller molecular areas, the slope of the curve appears to have an increased incline, and by 30 mN m^{-1} a kink in the isotherm can be seen. This kink is a possible transition point from one phase to another. However, what is quite clear is that the slope of the curve appears to have an increased incline compared to natural PI and hydrogenated PI. Note that the isotherm of DPPI is to extremely smaller molecular areas displaying a collapse area around 25 Å^{2} molecule^{-1}, which is impossible since a fatty acid chain has a diameter of approximately 19 Å across. Therefore, a concentration error is influencing the collapse area seen here.

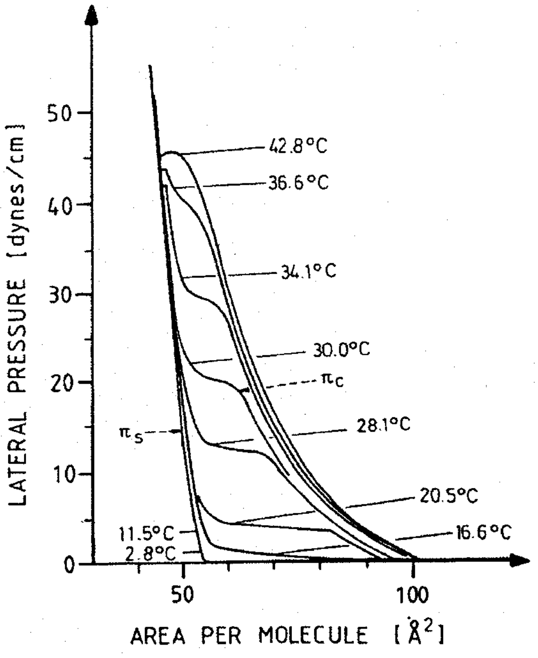

Figure 46 An example of an isotherm showing the effects of temperature on 1,2-dipalmitoyl-*sn*-glycero-3-phosphatidylcholine (DPPC) [4].

5.2 Temperature Study of PIH

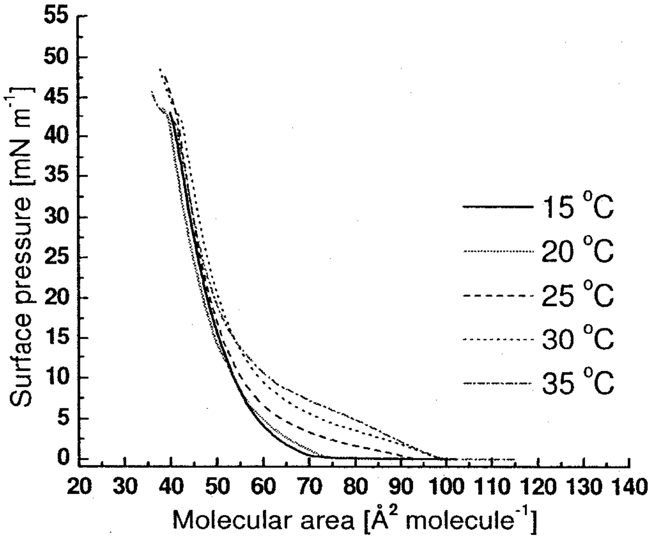

Figure 47 Overlay of isotherms of PIH monolayers on HEPES buffer, pH 7 at various temperatures (indicated).

Figure 47 displays isotherms of PIH at various temperatures. These isotherms show that as the temperature is increased, the critical area is shifted to larger molecular areas. This shift is due to an increase in compressibility of the film as the temperature increases. This implies that each molecule is occupying an increasing amount of space as the temperature increases. Therefore, PIH has an increased amount of fluidity with temperature. In addition, the appearance of a phase transition region becomes more prominent by 35 °C between 5 mN m^{-1} and 10 mN m^{-1}. This indicates that the extended plateau region seen at 25 °C in Figure 45 is indeed a phase transition region and not a liquid-expanded phase. Furthermore, PIH does not display an ideally horizontal phase transition region since it is a hydrogenated extract containing at least 3 components.

Note here that these isotherms were made with fresh solutions to ensure accurate concentration. However, due to the limited availability and high cost of the PIH, hysteresis curves and BAM isotherms shown in subsequent sections may not agree in molecular area, though do agree in shape. As a result, solutions were stored and their slight changes in concentration were observed, which might have had an influence on the critical area as well as the collapse area.

5.3 Analysis of PIH at 15 °C

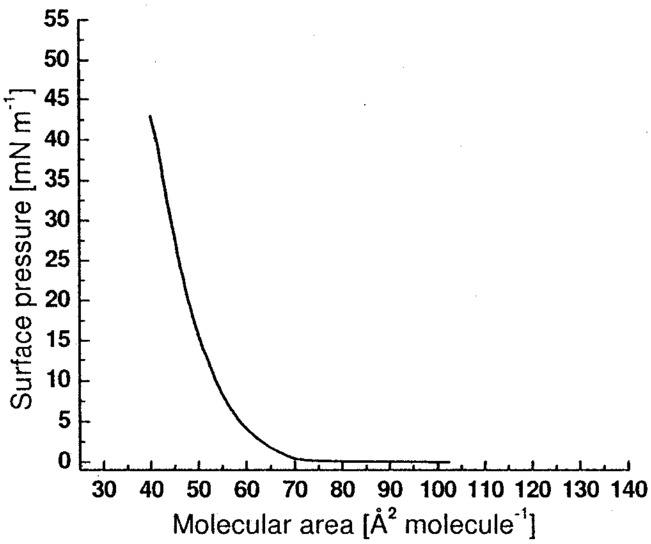

Figure 48 Isotherm of PIH monolayer at 15 °C.

At 15 °C the shape of the isotherm in Figure 48 suggests that PIH exhibits a condensed phase at all surface pressures above 0 mN m^{-1}. However, to confirm this behaviour a visual technique (BAM) is required.

Changes in the shape and/or the packing arrangement (molecular area) of an isotherm can be exhibited in compression-expansion cycles. The relaxation properties of a monolayer can be induced by compression, where molecular rearrangements can provide information about the self-assembly of PIH at the air-water interface.

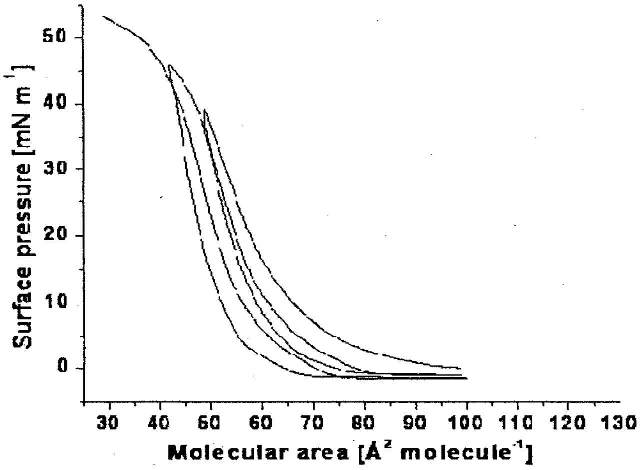

Figure 49 Hysteresis plot of PIH at 15 °C.

A monolayer of PIH was subjected to compression-expansion cycles at 15 °C (see Figure 49), where it was compressed to 38 mN m^{-1} during the first cycle and was then compressed to a surface pressure of (45 mN m^{-1}) in the second. In both cycles its reversed isotherms deviate to a smaller molecular area relative to the first one. The third compression, where monolayer is fully compressed, the isotherm deviates even further from the previous isotherms. This indicates that during both compression-expansion cycles, a loss of monolayer material at the air-water interface occurred. This type of behaviour is what is known as a hysteresis. A hysteresis is a term used when the reversible isotherm curve does not coincide with its compression isotherm curve[64]. As the monolayer goes through these cycles, re-orientation of the monolayer occurs, where molecules submerge into the subphase or form multi-layers at the interface; this behaviour is characteristic of a collapse phase.This loss of material at the interface creates a less densely packed surface, i.e. a lower surface concentration. Therefore, this decrease in the number of molecules at the interface causes the critical area, at which the pressure starts to increase, to occur at a smaller molecular area. From the hysteresis obtained at 15 °C, it appears as though a collapse does occur between 38 mN m^{-1} and 45 mN m^{-1} even though the slope of the curve gives no indication. In addition, a hysteresis was observed, which indicates that compression induces irreversible changes in the monolayer. In other words, this implies that favourable non-covalent interactions (lowered Gibbs free energy) are present within the multilayer which prevents or slows the reformation of a single monolayer.

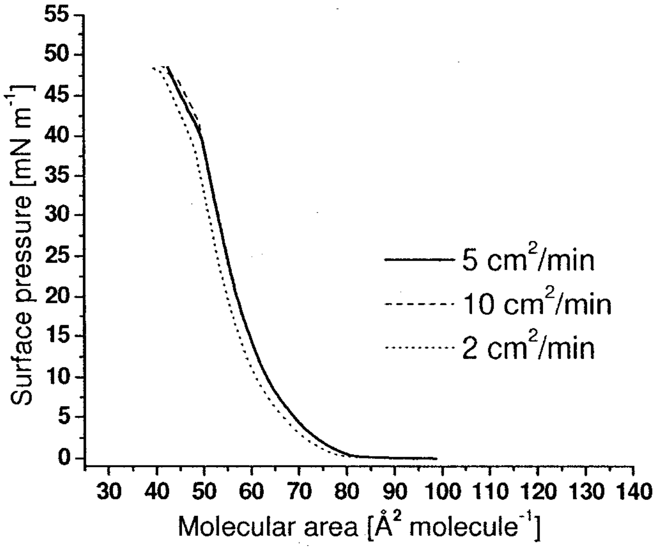

Figure 50 Isotherms displaying effects of compression speed on PIH monolayer at 15 °C (indicated).

As shown in Figure 50, when the barrier speed was increased, the collapse region (note kink in isotherm at approximately 42 mN m^{-1}) occurred at slightly higher surface pressures. According to Chen et al., a true collapse is speed dependent therefore as the speed increases the surface pressure of the collapse/plateau region should increase as well [48] (and references contained therein). Overall, the data obtained in Figure 49 and Figure

50 clearly indicates that the region between 38 mN m^{-1} and 45 mN m^{-1} is indeed a collapse. It must also be noted that the collapse pressure of a system depends on the level of the subphase, the lipid concentration (or $Å^2$ mol^{-1}) as well as the speed of compression. All precautions were taken to ensure that the amount of subphase added as well as the concentration was kept constant.

5.3.1 Brewster Angle images of PIH at 15 °C

BAM is used to study the homogeneity of the monolayer at the air-water interface in order to determine the miscibility of the individual PIH components. BAM images taken along the isotherm demonstrate the existence of aggregated material at high molecular areas and low surface pressures.

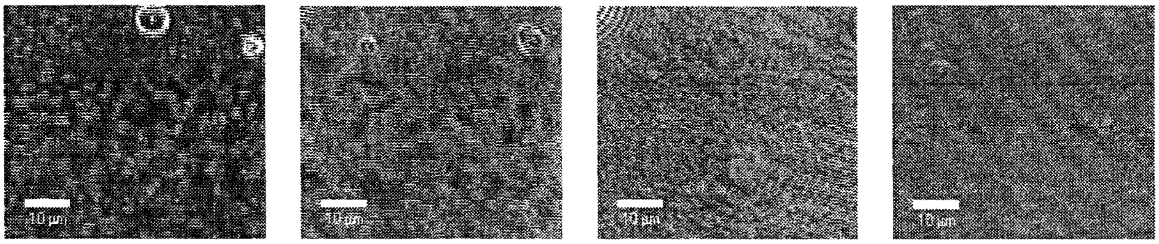

Figure 51 BAM images at 15 °C (from left to right): 1.6 mN m^{-1}, 16.8 mN m^{-1}, 20.5 and 38.0 mN m^{-1}.

This is indicative of a phase transition from the gaseous phase to an inhomogeneous, phase separated film in which liquid-expanded (LE) and condensed (C) phases co-exist. This phase co-existence at pressures above 0 mN·m^{-1} is evident from the BAM images taken around the critical area for the onset of pressure. As the pressure increases, the size of the domains increases until they begin to coalesce. The texture of the images at high pressures may be due to the anisotropy of a tilted condensed phase or may indicate that the monolayer is still inhomogeneous; however it is not possible with

BAM to elucidate the details of the domain structure since this technique has a limiting lateral resolution of 1 µm. Consequently, AFM was used to examine the topography of this structure in more detail.

5.3.2 AFM images of PIH at 15 °C

It is evident from the AFM images that phase separation occurs even at high pressures at 15 °C (Figure 52). Therefore, at least one component of PIH is able to form a condensed phase at all pressures above 0 $mN{\cdot}m^{-1}$ and at least one component remains liquid-expanded at all pressures. Given the fatty acid composition of PIH, as determined in Chapter 4, is likely comprised of symmetric lipids (distearoyl-PI), asymmetric lipids (palmitoyl-stearoyl-PI, with trace amounts of stearoyl-palmitoyl-PI), as well as up to 15% unsaturated PI phospholipids (see chapter 4), the fatty acid distribution could clearly influence the phase behaviour of PIH.

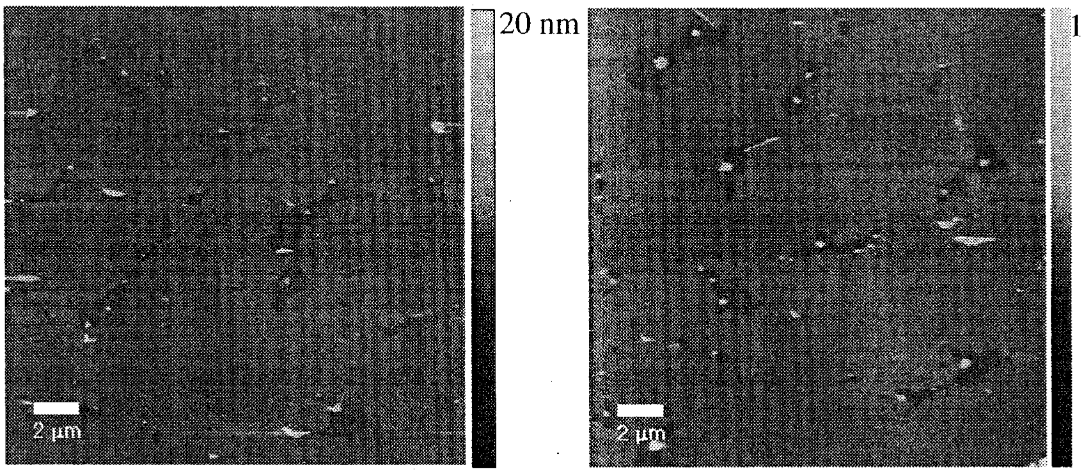

Figure 52 AFM scan of PIH monolayer deposited on mica at 15 °C and 40 $mN\ m^{-1}$ (left); and 45 $mN\ m^{-1}$ (right).

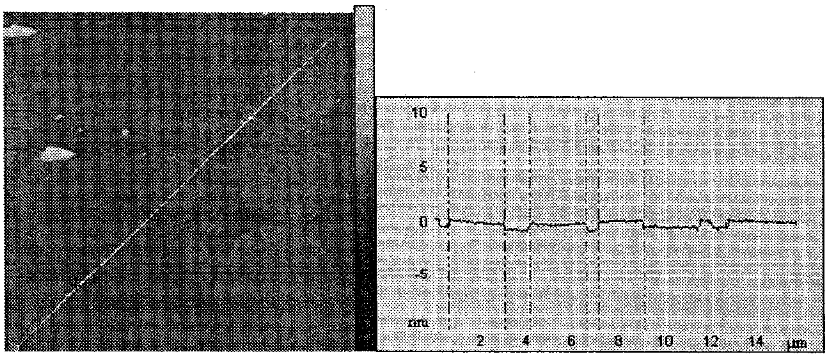

Figure 53 AFM scan of PIH monolayer deposited on mica at 15 °C and 8 mN/m.

For low pressures, the average size of domains ranges from 2 µm to 6 µm in diameter. In addition, the formation of collapse material appears to be consistently present in the liquid-expanded phase at low pressure. In contrast to the topography of PIH at low pressures, at higher pressures, these domains coalesce into large irregularly shapes and the amount collapsed material increases significantly throughout the liquid-expanded regions of the film. Similarly, the topography of PIH displays a height difference between the liquid-expanded and condensed phases to be approximately 1.3 nm, which is within the reported topographic range of phospholipids[65].

5.3.3 Ellipsometric measurements

At 15 °C, ellipsometric measurements yield a value of 0 ° in $\Delta\delta$ at high molecular areas (i.e. before the critical area), see Figure 54. Around the critical area, there is a sharp drop in $\Delta\delta$ to a value of – 3.0 ° and then decreases continuously. These measurements are likely related to an increase in optical thickness as the film is compressed. This abrupt change in optical thickness can also be related to a change in surface coverage of the monolayer, where as the monolayer becomes more densely packed, the film thickness changes. In addition, a change in surface pressure is also seen during the drop in

Δδ, which coincides nicely with critical area and with the observation of coherent film in BAM.

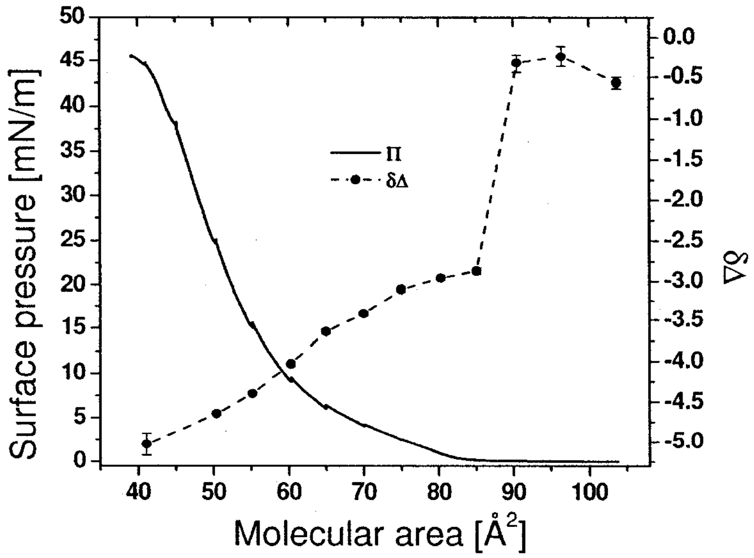

Figure 54 Ellipsometric isotherm of PIH at 15 °C.

5.4 Analysis of PIH at 20 °C

The isotherm obtained at 20 °C is similar to that obtained at 15 °C (see Figure 55) except the critical area is shifted to slightly larger molecular areas, yet this shift may not be significant as it lies within spreading error range (data not shown). Though hard to distinguish, the slope the curve at low surface pressures, between 0 mN m^{-1} and 10 mN m^{-1}, is slightly different from that at 15 °C (see Figure 45), which indicates that at 20 °C the film exhibits a decrease in compressibility.

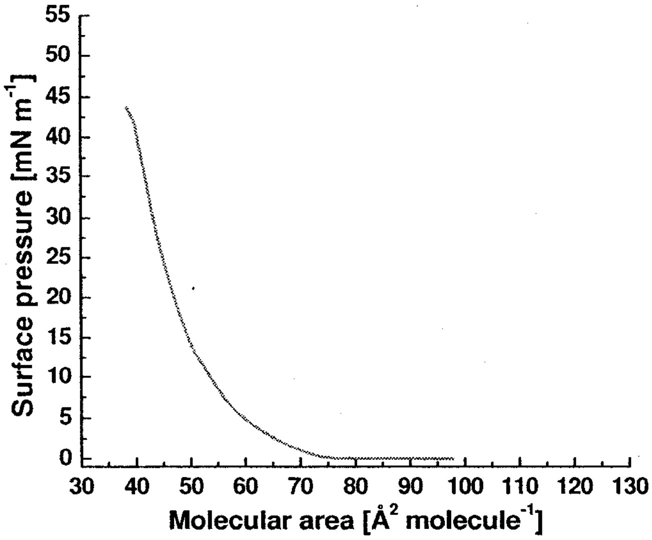

Figure 55 Isotherm of PIH monolayer at 20 °C.

5.4.1 BAM images of PIH at 20 °C

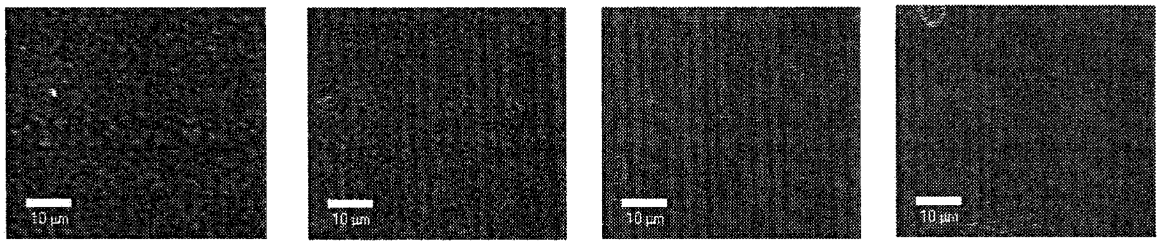

Figure 56 BAM images at 20 °C (from left to right): 4 mN m^{-1}, 8 mN m^{-1}, 20 mN m^{-1} and 30 mN m^{-1}.

BAM images at 20 °C exhibit phase co-existence at pressures above 0 mN m^{-1}, as seen previously at 15 °C. As the pressure increases domains coalescence and by 20 mN m^{-1}, only texture can be seen throughout the isotherm. This phase behaviour can be attributed to the anisotropy of a tilted condensed phase[44]. In addition, it may indicate that the monolayer may still be inhomogeneous, which is likely since similar images at 15 °C were obtained (see 5.3.1).

5.5 Analysis of PIH monolayers at 25 °C

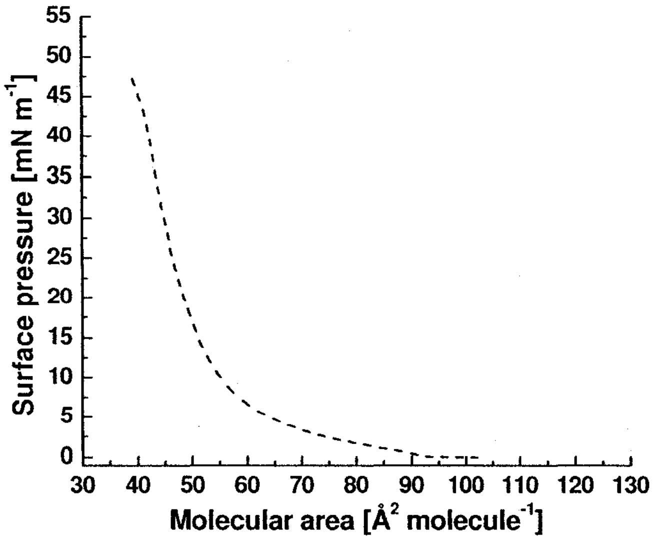

Figure 57 Isotherm of PIH monolayer at 25 °C.

An isotherm at 25 °C was obtained and thoroughly analyzed since this temperature displays the first indication of a phase transition (see

Figure 47 and Figure 57). The fatty acid analysis obtained on PIH revealed that 15 % unsaturated acyl chains still remained, which suggests that oxidation may affect the phase behaviour of PIH. It has been well studied that phospholipid mixtures or extracts containing units of unsaturation oxidize readily at the air-water interface[25]. To investigate whether oxidation contributes to the phase behaviour observed, isotherms of PIH with time are obtained (see Figure 58). From this graph, as the sample aged, from 2002 08 11, when it was freshly prepared, to 2003 01 15, five months later, no change in the shape of the curve was observed. However, the molecular area at which the collapse occurs deviates to larger areas (55 Å^2 mol^{-1}). Moreover, a year later, 2004 06 29, the shape of the curve as well as the critical area remain the same except for the collapse region, where a plateau is more prominent.

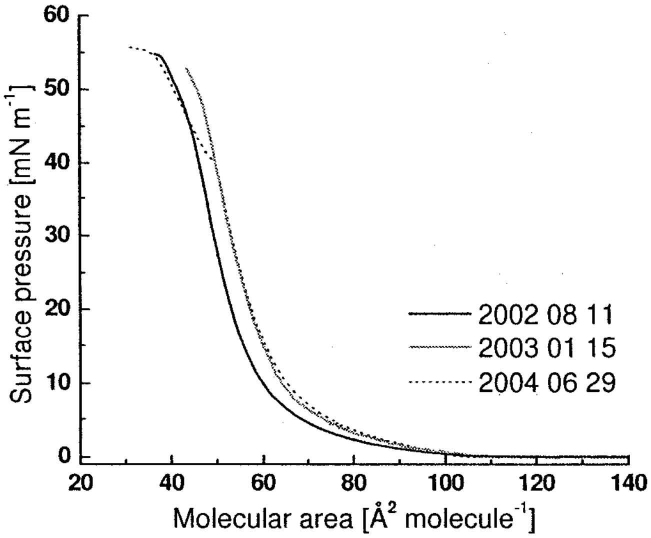

Figure 58 Overlay of isotherms displaying the aging effect of PIH monolayers at 25 °C.

From these isotherms, the only effects observed with time are an increase in concentration and a prominent plateau region at approximately 38 mN m^{-1}. The latter is likely due to the evaporation of solvent causing the concentration of PIH to be higher and therefore more molecules at the air-water interface are present. The plateau at approximately 38 mN m^{-1} the isotherm displays comparable results to those obtained for mixtures of PI with distearoylphosphatidylcholine (DSPC) [11] in which the plateau was attributed to the collapse of the fluid phase at 42 mN·m^{-1}.

To further confirm that a collapse is indeed observed at 38 mN m^{-1}, a hysteresis measurement was obtained at 25 °C (see Figure 59). In the first compression-expansion cycle, the monolayer was compressed to a surface pressure of 30 mN m^{-1}.

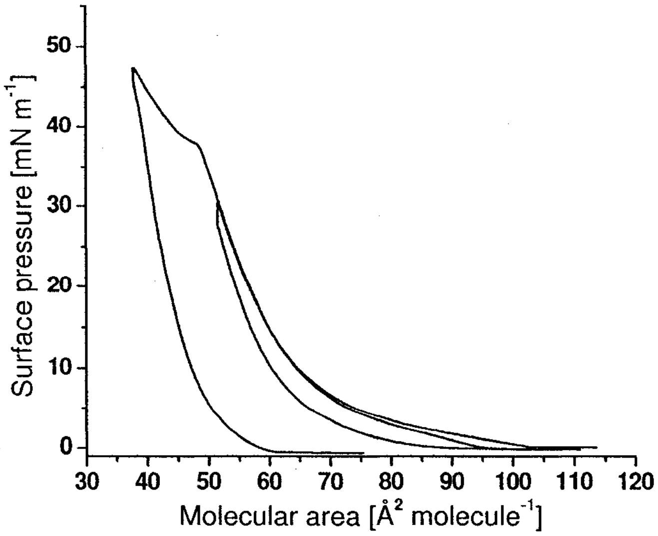

Figure 59 Hysteresis plot of PIH at 25 °C

Upon expansion, the reversed isotherm deviates to a smaller molecular area thus creating a hysteresis. The compression isotherm of the second cycle, which was fully compressed, deviates to a smaller critical area (or molecular area) from that seen in the compression isotherm of the first cycle. However, at high pressures the slope of the curve appears to have similar phase behaviour. This deviation, approximately 10 Å^2 mol^{-1}, is due to the fact that the expansion isotherm was not fully expanded to its initial area. This indicates that during both compression-expansion cycles, hardly any loss of material at the air-water interface occurred. From this data we can clearly see that the monolayer is able to recover after compression to 30 Å^2 mol^{-1}, since the second compression isotherm has relatively similar shape, molecular area and pressure. Collectively, the data obtained previously at 15 °C (see Figure 48) as well as that obtained in Figure 59, tells us that 38 mN m^{-1} is indeed a collapse. Furthermore, the phase behaviour of PIH with respect to compression speed observed at 25 °C indicates a similar trends to that obtained at 15 °C and correlates nicely with literature[11] (see Figure 50).

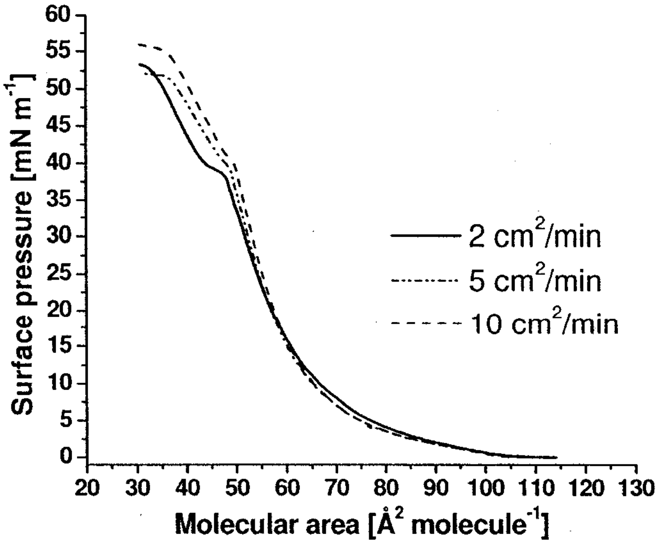

Figure 60 Isotherms displaying effects of compression speed on PIH monolayer at 25 °C (indicated).

5.5.1 BAM images of PIH at 25 °C

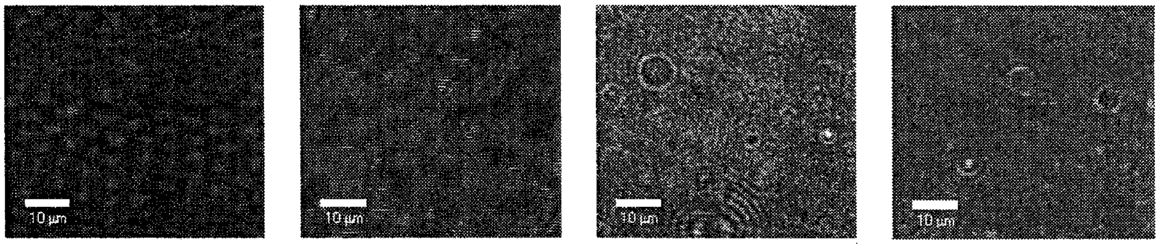

Figure 61 BAM images at 25 °C (from left to right): 6 mN m^{-1}, 20 mN m^{-1}, 30 mN m^{-1} and 42 mN m^{-1}.

BAM images in Figure 61 indicate the presence of condensed phase domains co-existing with fluid phase at all surface pressures above 0 mN·m^{-1} for 25 °C. As a result, the first order phase transition at 25 °C is indistinguishable from the onset of pressure.

5.5.2 AFM images of PIH at 25 °C

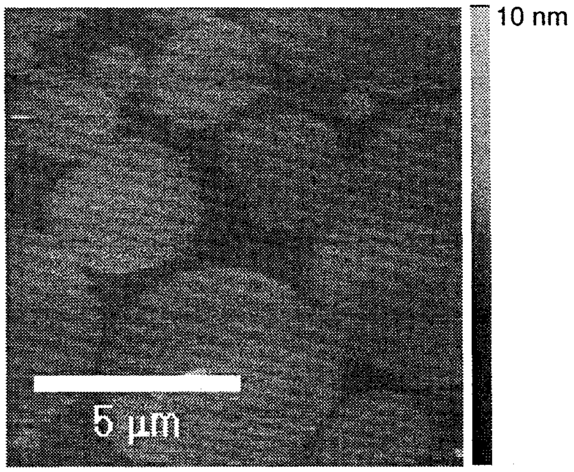

Figure 62 AFM image at 25 °C at 16 mN m^{-1} (20 × 20 µm scan).

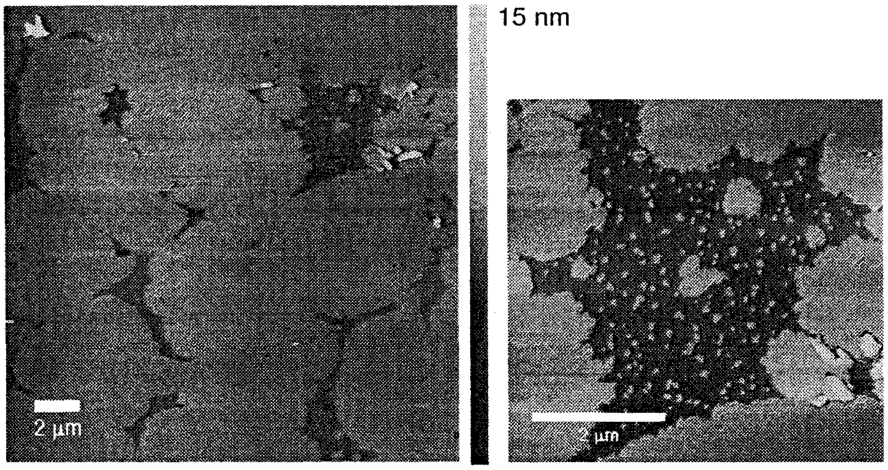

Figure 63 AFM images at 25 °C at 30 mN m^{-1}. Scan size: 20 × 20 µm (left) and 5.7× 5.7 µm (right).

Similar to BAM images taken at 20 mN m^{-1} (see Figure 61), where domain formation is observed, AFM results at 16 mN m^{-1} confirm the presence of condensed phase domains co-existing with a liquid-expanded phase at 25 °C (see Figure 62 and Figure 63). In addition, the average size of domains and height difference between the phases are comparable to that obtained at 15 °C as observed by AFM. Furthermore, at high surface pressures (30 mN m^{-1}), AFM clearly indicates coalescence of domains, where irregularly shaped and sized domains can be observed (see Figure 63). Within this image, the presence of small aggregates of condensed material can be found within the liquid-expanded phase. These aggregates have a similar height to the larger domains that encapsulate this liquid-expanded region. The presence of small aggregate formation is not unusual for it is known to be induced during the transfer and not a representation of the morphology of the film[21,35,39,66,67].

5.5.3 Ellipsometric measurements of PIH at 25 °C

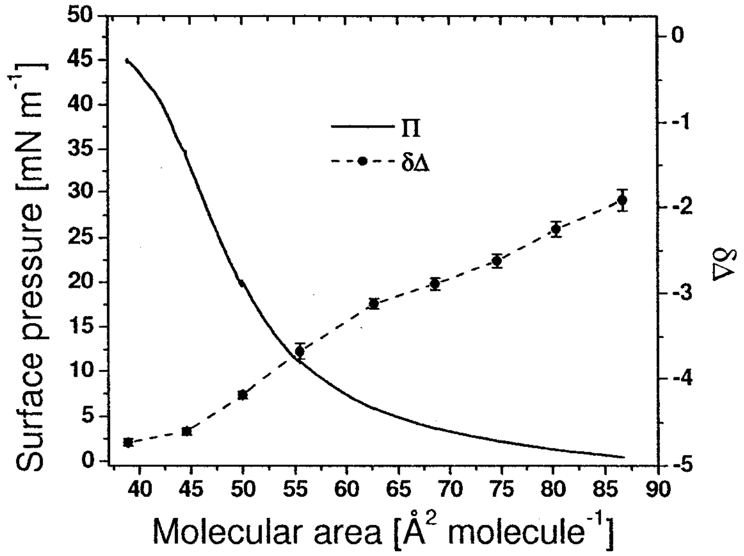

Figure 64 Ellipsometric Isotherm of PIH at 25 °C.

In Figure 64, the ellipsometric isotherm follows a comparable trend the isotherm at 25 °C, where as the surface pressure gradually increases, Δδ appears to be proportionally decreasing. Overall the shape of the ellipsometric isotherm does not indicate a linear decrease in Δδ. This gradual change indicates that the optical properties, of the monolayer do not change significantly, as was seen for the ellipsometric isotherm at 15

°C (see Figure 54). In addition, a slight change in slope, from a higher inclining curve to a lower inclined curve can be seen between 67 and 72 Å^2 and between 40 and 45 Å^2. This coincides nicely with the appearance of a liquid-expanded to a phase transition region isotherm and then a liquid-expanded to a phase separated phase.

5.5.4 Grazing Incidence X-ray Diffraction of PIH at 25 °C.

Measurements were carried out at various pressures along the isotherm at 25 °C (see Table 4). Diffraction patterns are only seen for condensed phases and not for liquid-expanded.

A structure is observed at all pressures above 0 mN m^{-1}, which confirms that a condensed phase is present (Figure 65). Therefore, the structures produced are attributed to the condensed phase domains that are observed in BAM and AFM (refer to Figure 61, Figure 62 and Figure 63).

Table 4 Peak positions, Q_{xy} and Q_z, as a function of the surface pressure.

Pressure [π]	$Q_{xy}1$ [Å^{-1}]	Q_z1 [Å^{-1}]	$Q_{xy}2$ [Å^{-1}]	Q_z2 [Å^{-1}]	$Q_{xy}3$ [Å^{-1}]	Q_z3 [Å^{-1}]
1.2	1.439	0.499	1.460	0.378	1.484	0.121
4.8	1.448	0.460	1.469	0.338	1.488	0.121
9.8	1.453	0.415	1.472	0.302	1.490	0.113
16.8	1.492	0.000	1.467	0.320	-	-
24.9	1.492	0.000	1.462	0.335	-	-
35.2	1.516	0	1.492	0.271	-	-
42.5	1.525	0	1.499	0.208	-	-

Table 5 Lattice dimensions *a*, *b* and γ, tilt angle with respect to the normal *t*, tilt azimuth (TA) (NN=Nearest Neighbour and Interm. = Intermediate), unit cell distortion d, unit cell area per chain A_{xy}, and cross section area A_o as a function of surface pressure π.

Pressure [π]	a [Å]	b [Å]	γ [°]	d [$\times 10^{-2}$]	t [°]	A_{xy}	A_o	TA
1.2	4.893	4.965	118.4	3.561	19.94	21.37	20.08	Interm.
4.8	4.873	4.947	118.6	3.226	18.23	21.16	20.10	Interm.
9.5	4.869	4.933	118.7	2.903	16.50	21.05	20.19	Interm.
16.8	4.84	4.91	118.8	2.89	16.1	20.80	20.00	Interm.
24.9	4.997	4.897	120.7	2.74	14.9	21.00	20.30	NN
35.2	4.880	4.810	120.5	2.140	11.90	20.23	19.83	NN
42.5	4.868	4.785	120.6	2.306	9.18	20.06	19.80	NN

The peak positions reported in Table 4 are used to calculate the dimensions of the unit cell for a given pressure (see Table 5). It is evident that at low pressure three peaks indicates an oblique unit cell. As the pressure is increased, the tilt angle reduces and the peaks shift to small Q_z values. Between 16.8 and 24.9 mN m^{-1} there appears to be a phase transition to a centered rectangular unit cell with a NN tilt however, it should be noted that with such a low tilt angle the peaks are highly overlapping and as a result makes it difficult to distinguish whether two or three peaks could be identified. Since the values of the cross-sectional area, A_o, should not vary significantly with pressure, an NN tilt is selected because it corresponds nicely with other A_o values at all other pressures. As the pressure increased the molecular area, A_{xy}, decreased with the exception of that obtained at 24.9 mN m^{-1}, which does not follow the general trend. However, it should be noted that preliminary fitting was unable to conclusively distinguish between oblique and centered rectangular peak, which suggests that this pressure lies very close to the transition pressure. Even at high pressure, near the collapse, a tilt of 9.18° is still present, indicating that a hexagonal packing of upright chains cannot be achieved.

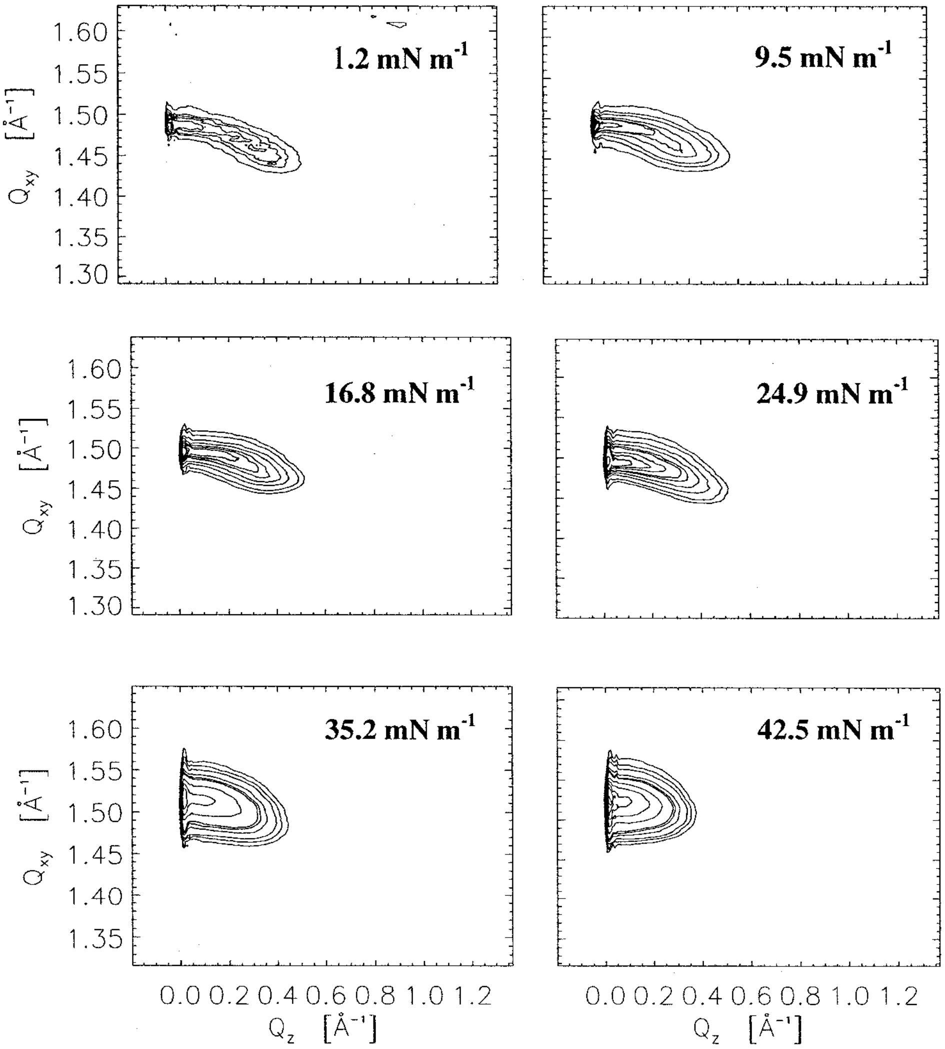

Figure 65 Contour plot of the corrected x-ray intensity as a function of the in-plane component Q_{xy} and the out-of-plane component Q_z of the scattering vector Q of PIH at various pressures (indicated).

5.6 Analysis of PIH at 30 °C

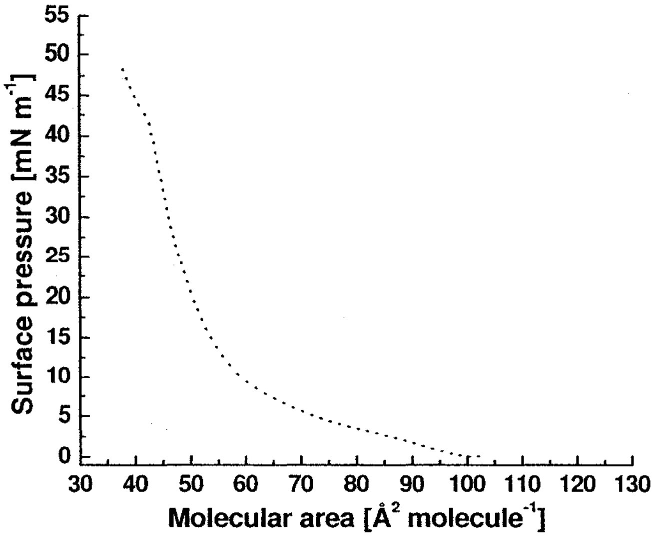

Figure 66 Isotherm of PIH at 30 °C

An isotherm at 30 °C is shown in Figure 66. From this isotherm, it is evident that a plateau region is seen, between 3 mN m^{-1} and 8 mN m^{-1}, which correspond to a phase transition.

5.6.1 BAM images of PIH at 30 °C

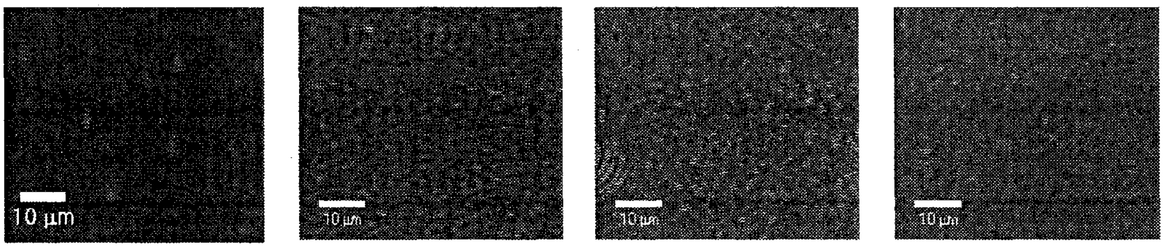

Figure 67 BAM images at 30 °C (from left to right): 0 mN m^{-1}, 5.2 mN m^{-1}, 17 mN m^{-1} and 29.8 mN m^{-1}.

In the isotherm obtained for PIH at 30 °C, the phases observed correlate to the BAM images (see Figure 67). At low surface pressures, approximately 0 mN m^{-1}, the BAM image indicates a non-ideal gaseous phase. It is not ideal in the sense that small aggregates can be seen at low pressures however have not accumulated enough to have a considerable effect on the surface pressure. As the monolayer is compressed to smaller areas, a gradual inclining slope can be seen which is characteristic of a liquid-expanded phase and images at this point along the isotherm do not differ from that shown at 0 mN m^{-1}. However, by 5.2 mN m^{-1}, where a phase transition region is seen, the formation of domains is detected (see Figure 67), which correlates nicely to its isotherm. By compressing the monolayer further the isotherm undergoes a change in slope while at the same time the coalescence of domains is seen at 17 mN m^{-1}. This indicates that PIH remains phase separated passed the plateau region and by 29.8 mN m^{-1} and all the way to collapse only texture can be seen. This texture, as was observed at 15, 20, and 25 °C, might be due to an inhomogeneous film or might be due to different types of condensed phases co-existing in this region[44].

5.7 Analysis of PIH at 35 °C

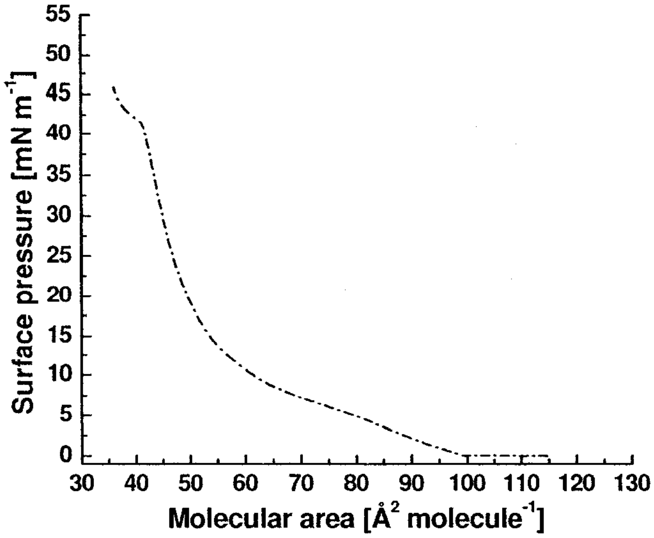

Figure 68 Isotherm of PIH at 35 °C.

By 35 °C (Figure 68), the phase transition region has shifted to higher surface pressure, between 5 mN m^{-1} and 10 mN m^{-1}. In addition, both liquid-expanded phase as well as the phase transition can be clearly distinguished.

5.7.1 BAM images of PIH at 35 °C

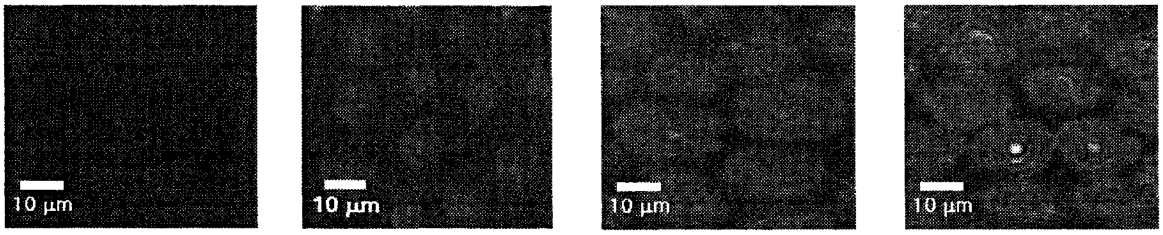

Figure 69 BAM images of PIH at 35 °C (from left to right): 0 mN m^{-1}, 5.8 mN m^{-1}, 19.8 mN m^{-1} and 31.3 mN m^{-1}.

At low surface pressures, the slope of the isotherm in Figure 68 appears to be, indicative of a liquid-expanded phase. Though BAM no evidence of domain formation below 5 mN·m^{-1} was seen, which shows a relationship to the isotherm shape. This finding confirms that all components form a fluid phase at low pressures at this temperature. As the monolayer is compressed to smaller areas, by 5.8 mN m^{-1} the formation of domains from the liquid-expanded phase occurs, where nucleation of these domains takes place at PIH sites in the monolayer. The plateau does indeed lie between 5 mN m^{-1} and 10 mN m^{-1}, which is exactly where domain formation is visualized. This region corresponds to a liquid-expanded-condensed phase transition and is likely for the saturated components as well as the unsaturated components (see Chapter 4). While the monolayer remains phase separated above this plateau region, the domains which vary in shape and size are well separated and clearly visible using BAM even at high pressures, as opposed to 15 °C where only texture could be observed. Additionally, no aggregated material was seen at high molecular areas at 35 °C, indicating a direct transition from the gaseous to the liquid-expanded phase.

5.7.2 AFM images of PIH at 35 °C

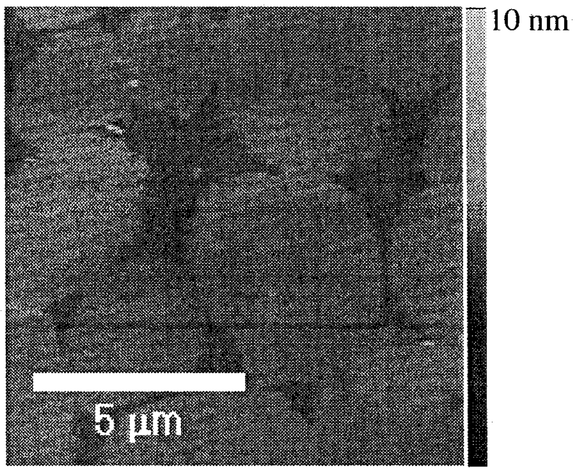

Figure 70 AFM image at 35 °C at 16 mN m^{-1} (20 × 20 µm scan).

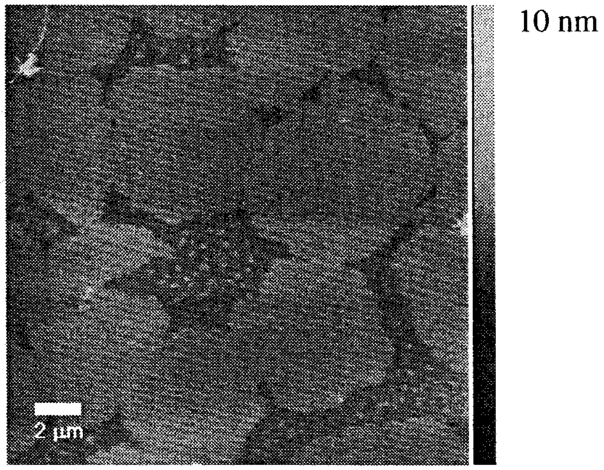

Figure 71 AFM of image at 35 °C at 30 mM m-1 (20 × 20 µm scan).

AFM images at 35 °C similar to those at 30 °C were obtained. Again, phase separating can be seen at low and high surface pressure along with small condensed material within the liquid-expanded region at higher pressures. In addition, collapsed material is observed exclusively along the liquid-expanded-condensed interface.

5.7.3 Ellipsometric measurements of PIH at 35 °C.

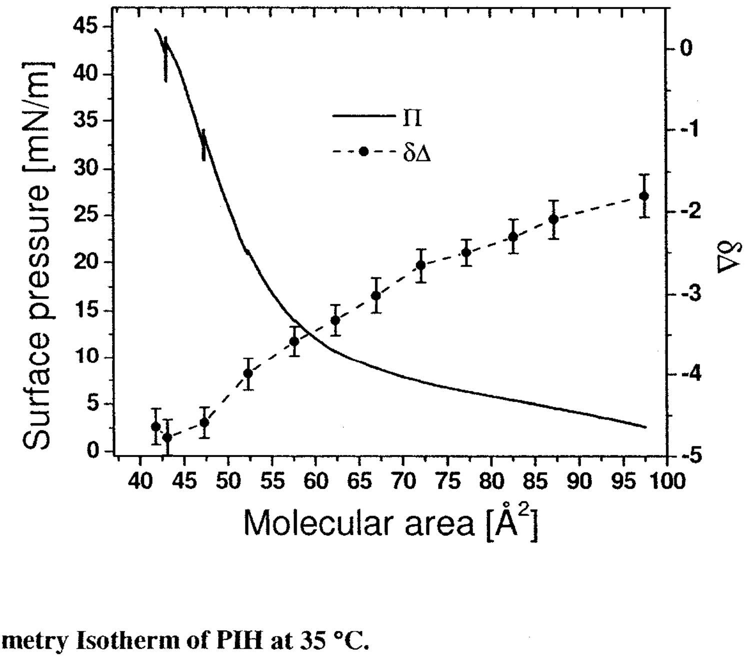

Figure 72 Ellipsometry Isotherm of PIH at 35 °C.

Similarly, at 35 °C, the ellipsometric isotherms also show a continuous decrease in $\Delta\delta$ from -1.8 ° after the critical area; however there is a distinct change in the shape of the isotherm. At this temperature, an inflection point becomes apparent at approximately 50 Å^2 molecule^{-1}, which corresponds with the end of the phase transition. It should be noted that the error in the $\Delta\delta$ measurement increases with increasing temperature. This can be attributed to increased Brownian motion within the film, thus making it difficult to obtain ten extremely precise recordings of the δ and ψ angles. The beginning of the collapse of the monolayer can be seen in the ellipsometric isotherms at molecular areas between 40 and 45 Å^2.

5.8 Isotherm of DPPI at 25 °C

By comparison with PIH in Figure 45, DPPI has phase behaviour similar to that of PIH at 35 °C as well as the reported isotherm of DPPC[68], with the exception that the phase transition region occurs at 15 mN m^{-1} instead of 5 mN m^{-1} (see Figure 46). Moreover, an isotherm of DPPI has been previously reported and dissimilar isotherms were obtained[10]. In particular, Mansour et al. report a liquid-expanded isotherm only, where the isotherm in Figure 73 clearly shows a transition from a liquid-expanded phase to a condensed phase. This difference in results is due mainly to the method of compression, where Mansour et al. obtain recordings of pressures after holding barriers at a given molecular area for up to approximately 24 hours. In contrast to their method, our pressure recordings were obtained under continuous compression, thus creating a non-equilibrated condition, which is the commonly used method. In addition, Mansour et al. reported their isotherm of DPPI at 25 °C on a Tris-HCl buffer at a pH of 7, while in our experiments a HEPES buffer was used as the subphase for comparison with PIH isotherms. It should be noted that whether a HEPES or Tris-HCl buffer is used, the phase behaviour of DPPI should not vary. This fact was confirmed when an isotherm was recorded on Tris-HCl under the same conditions reported by Mansour et al., and an identical isotherm to that performed on HEPES was observed (data not shown).

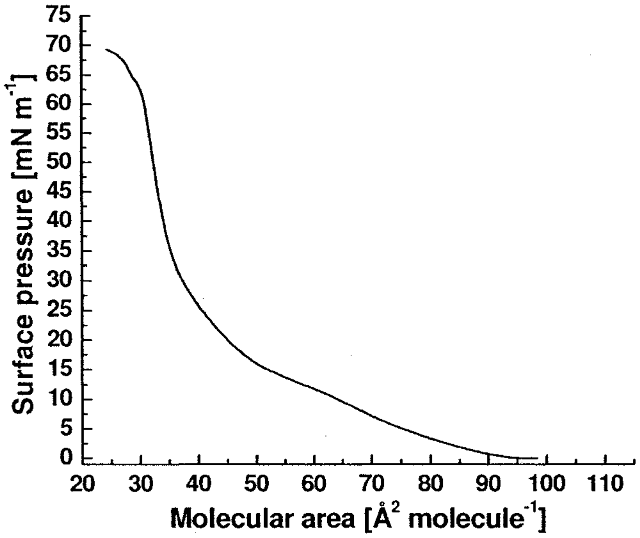

Figure 73 Isotherm of DPPI on HEPES buffer (pH 7) at 25 °C.

5.8.1 BAM images of DPPI at 25 °C.

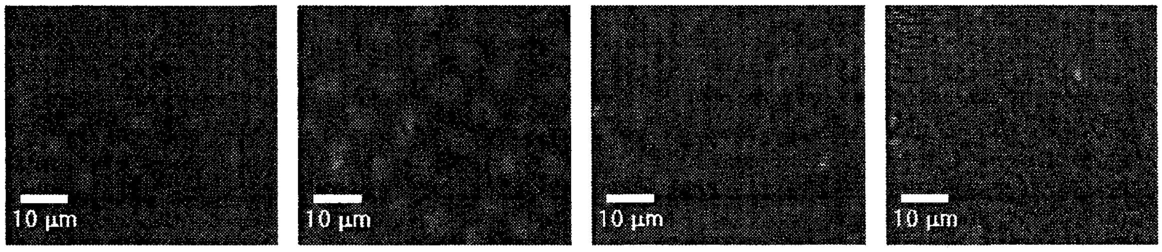

Figure 74 BAM images of DPPI at 25 °C (from left to right): 15 mN m^{-1}, 18 mN m^{-1}, 27 mN m^{-1} and 42 mN m^{-1}.

BAM images of DPPI confirm that that a phase transition is indeed present at approximately 15 mN m^{-1}. In contrast to this finding, Mansour et al.[10] report that no domains could be observed with fluoresce microscopy, however, this could be due to the presence of the fluorescence probe. BAM, on the other hand, has no requirement for an additional probe to visualize phase behaviour. At low surface pressures, near the gaseous phase and into the liquid-expanded region, the small aggregates of condensed phase can be seen periodically. As the pressure increased, the formation of domains was observed throughout the transition region, which coincides with the shape of the isotherm. This transition region persisted until the domains coalesced at approximately 27 mN m^{-1}. At high surface pressures, a condensed phase with a lot of texture can be seen. The appearance of this texture can be due to type of condensed phase formed[44]. Based on GIXD data obtained for PIH, one could expect to observe similar packing for the condensed phase since the area requirements are determine by the headgroup. This will need to be confirmed by GIXD.

5.8.2 Ellipsometric Isotherm of DPPI at 25 °C.

The ellipsometric isotherm for DPPI shows a decrease in $\Delta\delta$ as the surface pressure increases. A significant decrease in $\Delta\delta$ is observed at the critical area which is followed by a gradual decrease. Note that during the plateau region a large error is observed. This occurrence is due to the presence of domains that diffuse rapidly throughout the monolayer therefore making in difficult to obtain 10 consistent measurements.

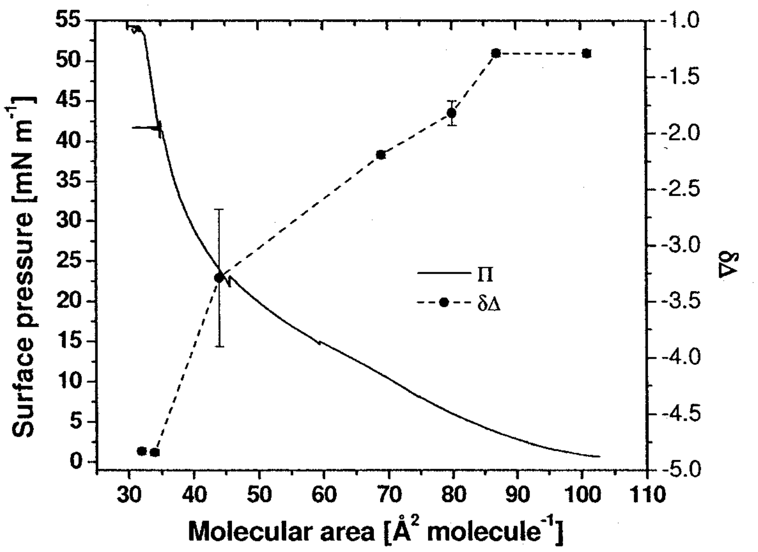

Figure 75 Ellipsometry Isotherm of DPPI at 25 °C on HEPES buffer.

5.9 Discussion

Phase separation is observed at high pressures and all temperatures by BAM and AFM. As determined in Chapter 4, the primary saturated components of PIH include distearoyl-PI, palmitoyl-stearoyl-PI and possibly trace amounts of stearoyl-palmitoyl-PI. In addition, it was found that up to 30% of the total PIH composition could be unsaturated. Within PIH, the components forming the condensed phase can be attributed to the saturated PI components which have alkyl chains that can be packed in an all trans conformation. The main asymmetric component, palmitoyl-stearoyl-PI, differs in length by two carbons from that of distearoyl-PI. In phosphatidylcholine, the palmitoyl-stearoyl-PC has been shown to form condensed phases[68]. Similarly, if one assumes the PIH system to exhibit analogous trends in phase behaviour to the phosphatidylcholines, the asymmetric PI components could contribute to the condensed phases and combine with the distearoyl-PI component. More specifically, palmitoyl-stearoyl-PC monolayers have been shown to be slightly more expanded than those of distearoyl-PC, which exhibits a condensed phase only[69]. However, it does not exhibit identical phase behaviour to stearoyl-palmitoyl-PC. Ali et al. demonstrated that the phase behaviour of stearoyl-palmitoyl-PC closely resembles that of dipalmitoyl-PC, which shows a liquid-expanded to condensed phase transition, rather than distearoyl-PC[68]. However, we have shown that dipalmitoyl-PI exhibits a liquid-expanded to a condensed phase transition which is similar to the phase behaviour of dipalmitoyl-PC. Without the individual components we can only speculate that stearoyl-palmitoyl-PI would exhibit similar phase behaviour to that of dipalmitoyl-PI. Therefore, the trace amounts of stearoyl-palmitoyl-PI, if present, may contribute to the condensed and/or liquid-expanded phase. It may be miscible with the liquid-expanded at low pressures and soluble in the condensed phase at high pressures. Assuming the assymetric PIs can form a condensed phase, it would combine with the distearoyl-PI[68]. The components forming the liquid-expanded phase can be attributed to the unsaturated PI components in which the unit of unsaturation induces a conformation preventing close packing. This was seen for the natural PI, which showed only a liquid-expanded phase due to the high degree of unsaturated chains (see Figure 45).

In addition, we cannot exclude the fact that components forming condensed phase may be miscible in the liquid-expanded phase or vice versa. In PIH, the amount of liquid-expanded phase observed at high pressures does not coincide with the maximum amount of unsaturated lipid as determined in chapter 4. This suggests two things: (i) that more than one unit of unsaturation is present per molecule, thus reducing the total amount of unsaturated lipid molecules to a minimum of 15% and/or (ii) that miscibility of the condensed phase in the liquid-expanded or vice versa can occur.

These findings report, for the first time, the presence of a condensed phase formed by PI. This condensed phase was found at all pressures and temperatures in a PI system. Moreover, this unique observation is confirmed in the crystallographic data (GIXD) obtained for PIH, where formation of a condensed phase even at low pressures was present. In comparison to the zwitterionic phosphatidylcholines, the phosphatidylinositols appear to produce a condensed phase which is significantly less tilted (reduced by more than 20°) and in which the molecules are more closely packed. The molecular areas determined by GIXD are 2-3 $Å^2$ less than those found for DPPC[70] and DSPC[11]. In direct contrast to the finding of Mansour et al. who proposed that the charged bulky inositol group would hinder packing of the alkyl chains and lead to a more expanded phase[10], we find that this lipid is able to pack more efficiently than PC. The apparent expansion in the isotherm shape at low pressures is due to the unsaturated components, which remain in a liquid-expanded phase as was shown by AFM.

However, at 35 °C and low pressures, below 5 mN m^{-1}, all components formed only a liquid-expanded phase. As the pressure increases, the formation of condensed phase domains initiate from the liquid-expanded phase during the phase transition region and continue to grow in size as the monolayer is compressed to smaller molecular areas. Assuming that the condensed phase is formed primarily by saturated PI, we have determined, for these components, that the critical temperature above which a transition from a gaseous to a liquid-expanded phase occurs (prior to the appearance of condensed phase domains) is between 30 and 35 °C, which is similar to the critical temperature for other distearoylphospholipids[68]. We have also demonstrated that within the temperature range of 15-35 °C, the components forming a liquid-expanded phase, namely unsaturated-PI, cannot form a condensed phase, where at high pressures this component of PI remains liquid-expanded (see AFM images, Figure 52).

The ability to form domains implies that the components forming the condensed phase may play a role in the formation of lipid rafts. To prove this hypothesis, we must but our findings into context, which would mean looking at the behaviour of PIH in a physiological environment. As discussed in Chapter 1:, PI only contributes to a small percentage of total phospholipids. Therefore, in the following chapter mixtures of PIH with DSPC and DSPE will be studied. In addition, it would be interesting to look at the possible effects PI has on the monolayer, where from this a better understanding of the phase behaviour of PIH might be obtained.

Chapter 6: Miscibility of Hydrogenated Soy L-α-Phosphatidylinositol

Now that the phase behaviour of pure PIH has been investigated in the previous chapter, it is clear that the saturated components of PI form condensed phase domains. These domains could most likely contribute to raft formation seen in the plasma membranes. The role of PI in this occurrence and its implication in a physiological relevant system still remains to be investigated. Which brings us to another key question: will domain occurrence still persist in a membrane system? In other words, does PI sequester into localized regions within a mixed bilayer. Based on their experiments with DOPC and bovine PI, Redfern et al. suggest a de-mixed system should still be seen[46]. Under similar conditions to those found in a membrane, the miscibility of PIH with inner leaflet lipids at various mole percentages will be performed as a preliminary investigation. This will be carried out using binary mixtures of 1,2-Distearoyl-*sn*-Glycero-3-Phosphatidylcholine (DSPC) and 1,2-Distearoyl-*sn*-Glycero-3-Phosphatidylethanolamine (DSPE) since both phosphatidylcholine and phosphatidylethanolamine are found in the inner leaflet of the membrane in high proportions (see Table 1). Using this system will enable us to study the role that the saturated components of PI play in this organization.

In addition to the physiological relevance of this investigation, miscibility with other phospholipids might give additional information about its physical behaviour. For example, both DSPC and DSPE are zwitterionic phospholipids, while PI has a bulky negatively charged headgroup. The headgroup interactions of binary mixtures of either lipid with PI could influence their miscibility. Also, since PIH is predominantly C18

(60%), similar length PCs and PEs were chosen to observe the influence of the headgroup versus that of the alkyl chains.

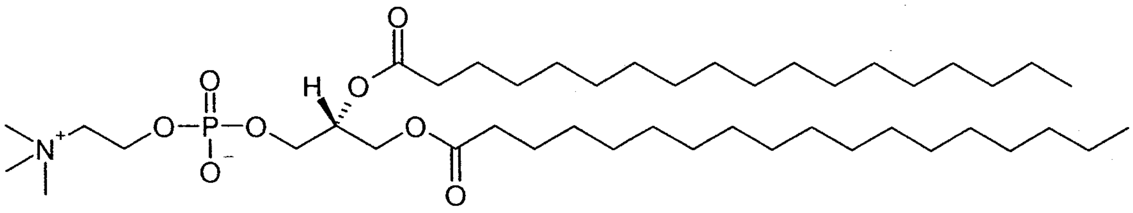

Figure 76 1,2-Distearoyl-*sn*-Glycero-3-Phosphatidylcholine (DSPC).

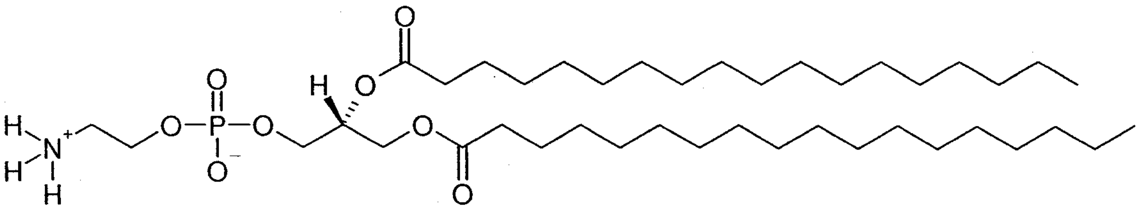

Figure 77 1,2-Distearoyl-*sn*-Glycero-3-Phosphatidylethanolamine (DSPE).

In addition, comparable PI miscibility studies conducted using DSPC[11] and DSPE[50] will aid in understanding the role PIH might have in the formation of lipid rafts as well as their lipid-protein interaction requirements.

6.1 Miscibility of PIH with DSPC

Only small physiologically relevant mixing ratios for PIH were implemented in miscibility studies. Higher mixing ratios (above 5 mol%) will not be reported since isotherms of PIH in DSPC above 5 mol% showed a similar trend (data not shown) to that of natural PI in DSPC[11]. DeWolf et al. found that by increasing the mole percentage of PI in DSPC, an increased in de-mixing of DSPC occurred. However, in contrast to these findings, isotherms of PIH in DSPC at low percentages (below 5 mol%) exhibit an interesting change in the trend (see Figure 78).

6.1.1 Isotherms

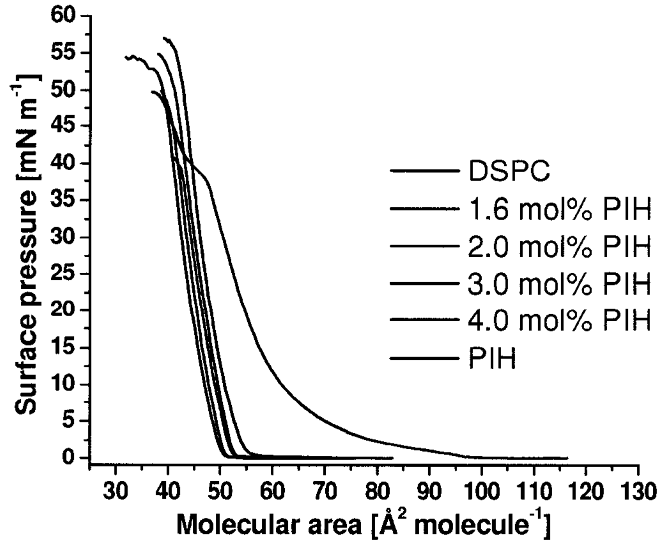

Figure 78 Overlay of PIH in various mixing ratios with DSPC (indicated).

Isotherms of pure DSPC with increasing mole percentages of PIH at 25 °C were overlayed to compare their phase behaviour in Figure 78. DSPC alone at low surface pressures exhibits a highly inclining slope which is characteristic of a condensed phase. As the molecular area decreases, the slope remains in, what appears to be, a condensed phase all the way up until collapse. As was previously investigated, PIH, at low surface pressures, exhibits a gradual inclining slope which is characteristic of a liquid-expanded phase followed by a non-ideal horizontal slope, which was determined to be a transition region and finally at high pressures displays a more inclined slope, which was reported as a phase separated region. Similar to DSPC, the isotherms of 1.6 to 4.0 mol% PIH, at low surface pressures, displays a highly inclining slope that is characteristic of a condensed phase. In addition to this, the slope of the isotherm does not change until collapse as the molecular area decreases. In contrast to this, the most important difference between

DSPC and its mixtures is the critical area, A_c, which shifted to smaller molecular areas. This occurrence indicates that at small mixing ratios of PIH a negative excess area, A^E, is observed which indicates a condensation of the monolayer. This implies that the mixture packs more efficiently that the individual components. Though this is quite possible, we cannot ignore the fact that all PIH mixtures isotherms are within spreading error of the DSPC isotherm and may not actually be affecting the phase behaviour of the condensed phase.

6.1.2 BAM images of PIH with DSPC

6.1.2.1 Pure DSPC

For comparison, BAM images where obtained for the pure components of this binary mixture. Since pure PIH was investigated in the previous chapter, those images will not be shown here. However, those of DSPC are shown in Figure 79. From these images it is clear that at zero surface pressure a gaseous phase can be seen, in which some condensed aggregates are formed. As the pressure increased to 1.3 mN m^{-1}, a homogeneous film was present and by 15 mN m^{-1}, a stable film with slight texture, due to the anisotropy film of the tilted phase, was observed all the way up until collapse. These images coincide nicely with its isotherm and confirm that the isotherm does indeed exhibit a predominantly condensed phase at all surface pressures above zero.

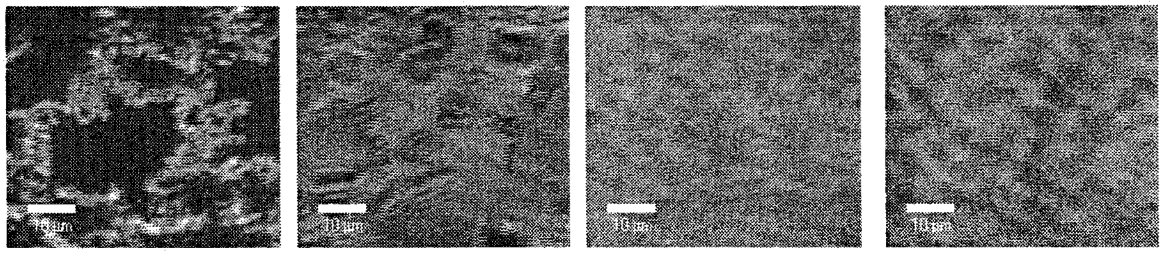

Figure 79 BAM images of pure DSPC at 25 °C (from left to right): 0 mN m^{-1}, 0.1 mN m^{-1}, 1.3 mN m^{-1} and 14.6 mN m^{-1}.

6.1.3 BAM and AFM images of binary mixtures

BAM images of DSPC with increasing mole percentage of PIH were obtained. As the percentage of PIH increased, an increase in the fluidity of the monolayer was observed at low surface pressures. Similar to DSPC, a condensed phase is seen by approximately 10 mN m^{-1} however, images do show an enhancement of texture. As discussed in Chapter 5, this texture can be due to the anisotropy of the condensed phase present or might imply that this system is phase separating at high surface pressures, as was seen for PIH. This uncertainty needs to be resolved by AFM and selected images will be presented and discussed for each mole percentage of PIH. The full range of BAM images for all mixtures at various pressures can be found in appendix 1.

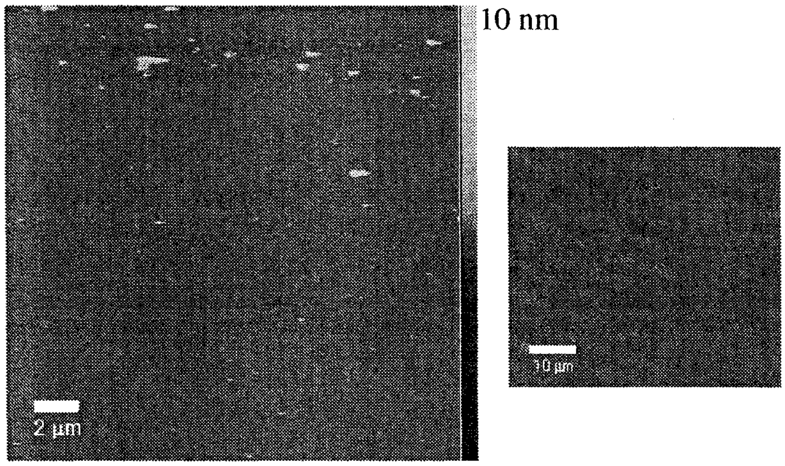

Figure 80 20 µm × 20 µm AFM scan of 1.6 mol% PIH in DSPC monolayer deposited on mica at 25 °C and 16 mN m^{-1} (left) and its corresponding BAM image at 25 °C and 18.2 mN m^{-1}.

In particular at 1.6 mol%, the AFM image confirms that only a condensed phase is present and that the texture seen by BAM is due to the presence of an anisotropic condensed phase (see Figure 80). This AFM image also shows that 1.6 mol% PIH appears to be fully miscible in the condensed phase of DSPC.

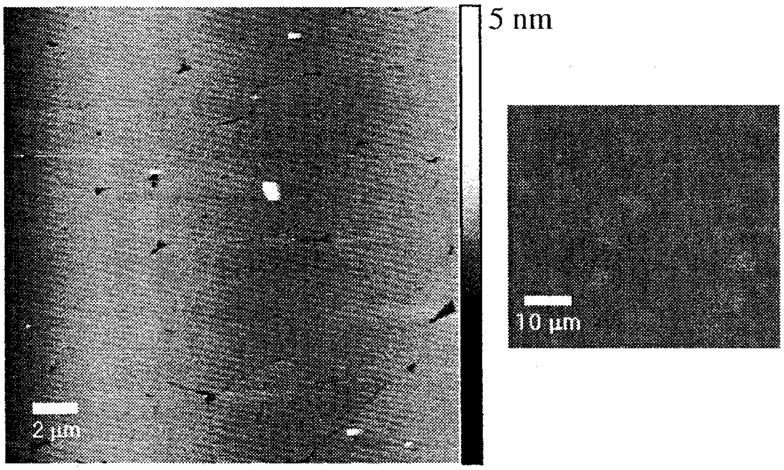

Figure 81 20 µm × 20 µm AFM scan of 2 mol% PIH in DSPC monolayer deposited on mica at 25 °C and 16 mN m^{-1} (left) and its corresponding BAM image also at 25 °C and 16 mN m^{-1}.

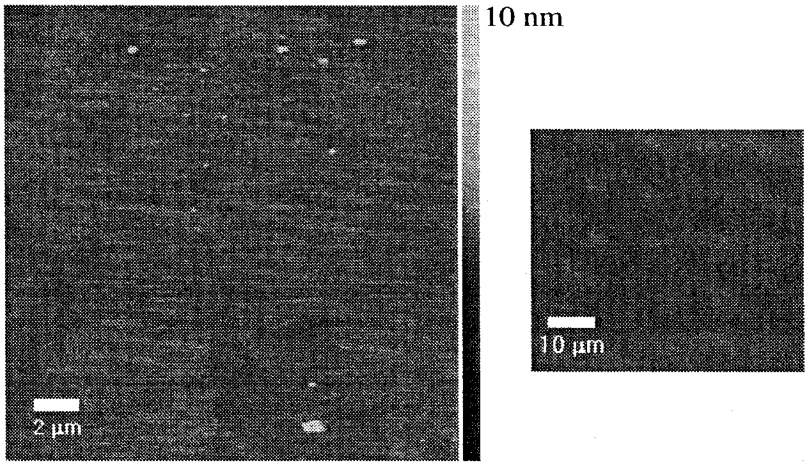

Figure 82 20 µm × 20 µm AFM scan of 2 mol% PIH in DSPC monolayer deposited on mica at 25 °C and 30 mN m^{-1} (left) and its corresponding BAM image at 25 °C and 37 mN m^{-1}.

On the other hand, at 2.0 mol%, where texture can also be seen, a phase separated system is detected at 16 mN m^{-1} and again at 30 mN m^{-1} by AFM (see Figure 81 and Figure 82, respectively), although at the higher pressure the contrast between the different regions within the film is significantly reduced. Despite the small height difference, we can clearly see that there are co-existing regions which may be due to partial miscibility of the components. This would also explain the texture observed by BAM. However, by 2.5 mol% phase separation cannot be seen by AFM (see Figure 83) and only one phase is seen. However, there are some small crystalline aggregates which are formed at this higher pressure.

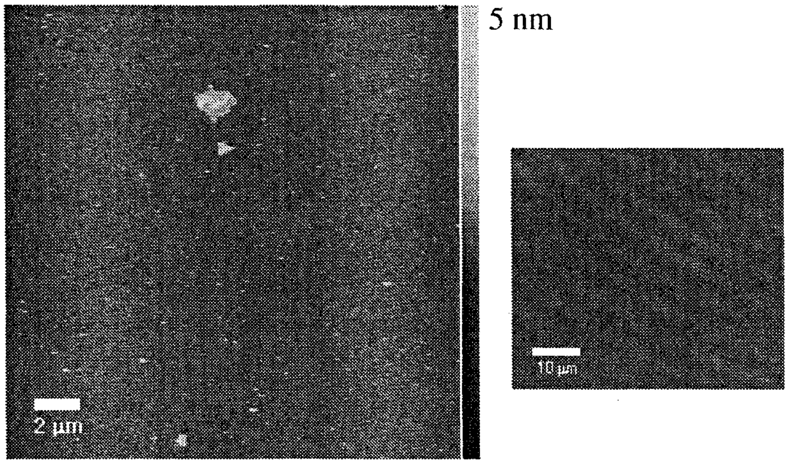

Figure 83 20 µm × 20 µm AFM scan of 2.5 mol% PIH in DSPC monolayer deposited on mica at 25 °C and 30 mN m^{-1} (left) and its corresponding BAM image at 25 °C and 31.2 mN m^{-1}.

More interestingly, by 4.0 mol% PIH different regions can once again be observed by AFM.

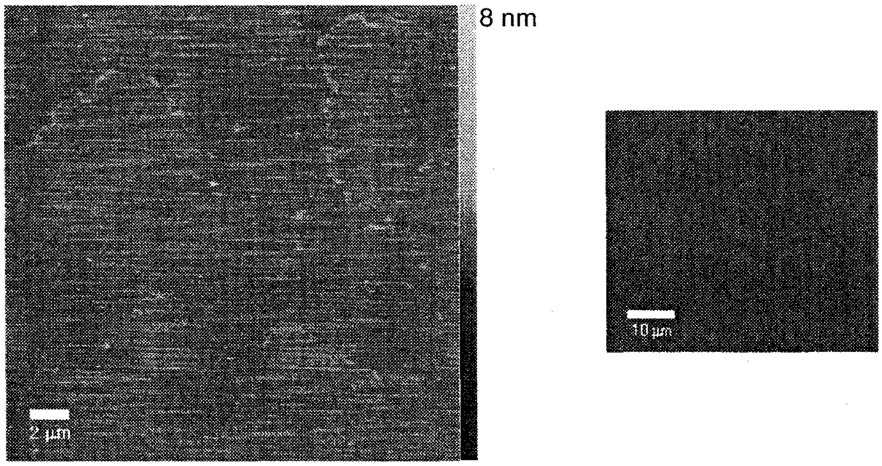

Figure 84 20 µm × 20 µm AFM scan of 4.0 mol% PIH in DSPC monolayer deposited on mica at 25 °C and 16 mN m^{-1} (left) and its corresponding BAM image at 25 °C and 28 mN m^{-1}.

Although there is no general trend seen in the AFM images, it should be noted that multiple scans were obtained for each mixing ratio and any single image does not represent the morphology of the whole film. However, at mole percentages between 2 and 4 mol% PIH, there is still some interesting behaviour that arises. One might expect to see a single phase at high pressure for this system however the AFM images indicate otherwise. On the other hand, the different regions that are observed do not appear to be due to the co-existence of liquid-expanded and condensed phases. This is in agreement with Redfern's experiments[46], who have shown that DPPC and DPPI form a de-mixed system in bilayers. It is also interesting that this phenomenon is observed at physiologically relevant mixing ratios. The behaviour of the system within this small range of mixing ratios will require further analysis.

6.1.4 Ellipsometric Isotherm of PIH with DSPC

The ellipsometric isotherm of DSPC, coincides nicely with the isotherm obtained where at low pressures the gaseous phase has low $\delta\Delta$ value, which implies that not a significant difference in Δ from water (buffer in this case) (see Figure 85). As the molecular area decreases, at approximately the same location of the critical area, A_c, there is a sudden drastic decrease in $\delta\Delta$. As the monolayer in compressed even further, a gradual decrease in $\delta\Delta$ is now observed. Similar ellipsometric isotherms are observed for PIH mixtures from 1.6 to 2.5 mol% (see appendix). However, a significant change in the shape occurs at 3.0 mol% (Figure 86) and is also seen in 3.5 and 4.0 mol% PIH mixtures (see appendix). These ellipsometric isotherms inform us that there is indeed a change in phase behaviour since there is no longer a drastic decrease $\delta\Delta$ in at the critical area, and a gradual decrease is observed instead. A similar gradual decrease was observed for PIH 25 °C, which corresponded to a liquid-expanded condensed phase co-existence region. This may influence the behaviour once sufficient mole ratios of PIH are present. It may also explain the different regions observed by AFM, which could be due to DSPC-rich condensed phase forming directly from the gaseous phase and the PI-rich condensed phase forming only at pressures above zero.

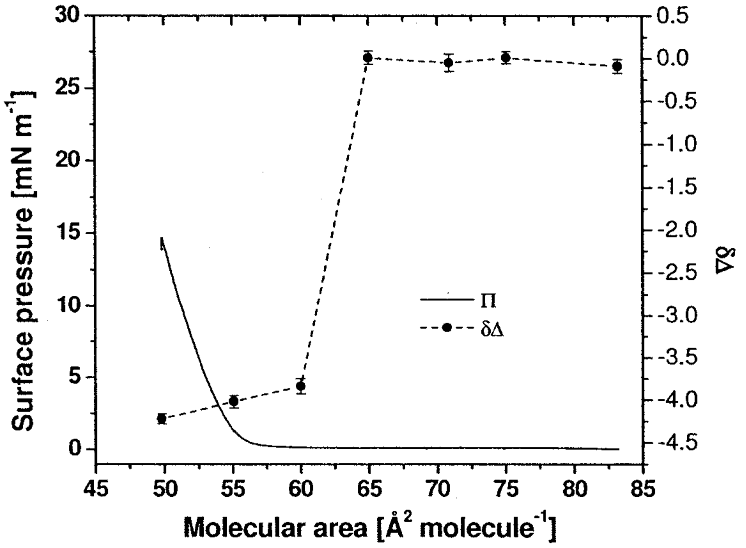

Figure 85 Ellipsometric isotherm of pure DSPC at 25 °C.

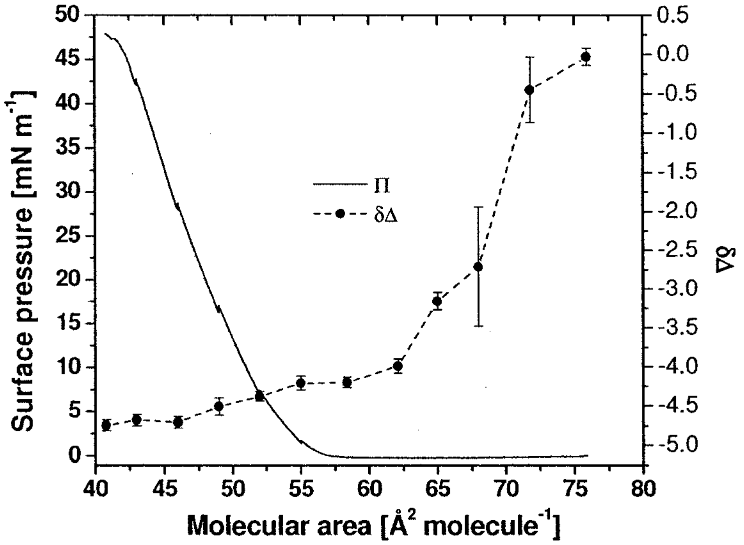

Figure 86 Ellipsometric isotherm of 3.0 mol% PIH in DSPC at 25 °C.

6.2 Miscibility of PIH with DSPE

In contrast to DSPC, DSPE will be reported over a broader range of mole percentage to determine if a trend could be established. In this section, the phase behaviour of DSPE with mole percentages ranging from 1 to 20 mol% PIH is investigated. Preliminary observation of the phase behaviour of these binary mixtures will be reported in the following section.

6.2.1 Isotherms

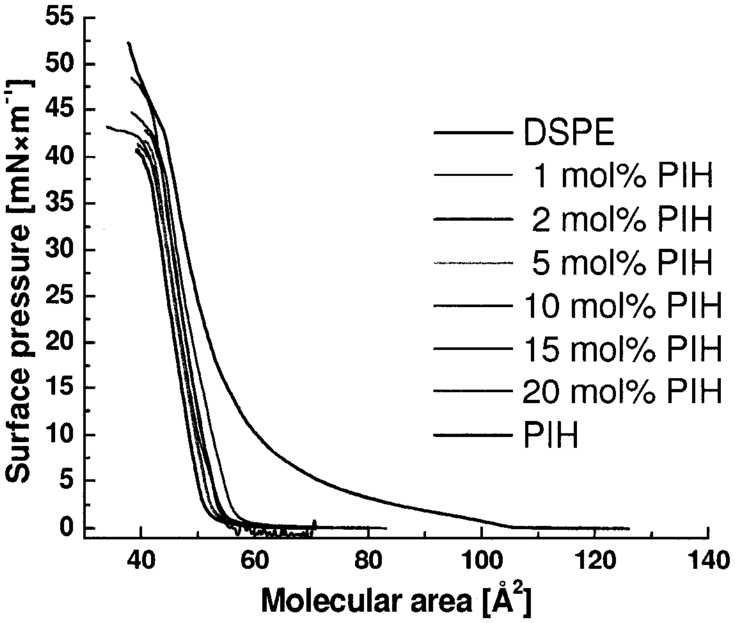

Figure 87 Overlay of PIH in various mixing ratios with DSPE (indicated).

Isotherms of pure DSPE with increasing mole percentages of PIH at 25 °C were overlayed to compare their phase behaviour Figure 87. DSPE is an extremely rigid film and its isotherm at low surface pressures exhibits a highly inclining slope which is characteristic of a condensed phase. As the molecular area decreases, the slope remains in, what appears to be, a condensed phase all the way up until collapse. As was discussed in section 6.1, the phase behaviour of PIH goes from a liquid-expanded phase to a phase separation with two co-existing phases, namely liquid-expanded and condensed. Similar to DSPE, the isotherms of 1 to 15 mol% PIH, at low surface pressures, displays a highly inclining slope that is characteristic of a condensed phase. However, 20 mol% exhibits a more compressible monolayer with a slight shift in the critical area, A_c. The slope of the isotherm does not change until collapse as the molecular area decreases. Again, in these series of isotherms the difference in molecular area at the A_c is small. However, by 20% one would expect to see a more significant shift in molecular area, indicated that once again a negative excess area is observed. However, there is not a trend of increasing molecular area proportional to the amount of PIH present.

6.3 Discussion

Previous findings of binary mixtures of DSPE with natural PI, show an increase excess area, A^E, as the mole percentage of PI increases[50]. It is quite possible that a similar trend could be seen in our system. However, from the isotherms in Figure 87 this is not likely the case since no obvious trend can be observed, unlike that reported by Patil-Sen et al.[50] To investigate whether this is due to phase separation, will require BAM and AFM. Also, ellipsometric measurements will be required to observe whether optical properties of the film can be compared to that of the pure components.

There is however evidence of de-mixing of DSPC and PIH at physiologically relevant mixing ratios, which is in agreement with Redfern et al. who also see de-mixing of inositols, and phosphatidylcholines[46]. Rerfern et al. state that the phase behaviour is not chain dependent and that the headgroup governs the observed phase separation.

Similarly, our results show phase separation in a system where the chains are similar in length and units of unsaturation are present. Moreover, his result also indicated that phase separation will occur even at low PI content, which is in agreement with our findings. These results support the proposal that inositol may form rafts due to the biophysical interactions of the lipid rather than being sequestered by proteins. One might expect that charged PIs would show charge repulsion between the headgroup, which might induce miscibility rather than phase separation. Redfern et al.[46] suggest that the repulsion may be overcome by favourable intermolecular interactions between the inositol ring or between the inositol ring and the neighbouring charged phosphate. The structure of the PI's headgroup plays an important role in its ability to cluster, which is the requirement for raft formation.

Chapter 7: Conclusions and Future Work

The phase behaviour of PI in monolayers at the air-water interface has been investigated in this thesis according to our objectives. These objectives were to qualitatively and quantitatively analyze PIH, to study its phase behaviour at temperatures ranging from 15 to 35 °C and finally to investigate the miscibility of PIH with DSPC and DSPE. In this section, the key findings will be summarized followed by the future directions of each study.

Initially, the analytical analysis revealed that the primary saturated components of PIH included distearoyl-PI, palmitoyl-stearoyl-PI and possibly trace amounts of stearoyl-palmitoyl-PI. The quantity of stearoyl-palmitoyl-PI compared to palmitoyl-stearoyl-PI still remains unknown. Even though it has been suggested that possible trace amounts of stearoyl-palmitoyl-PI are found in PIH, a quantitative study still needs to be performed to confirm our suggestion. This will be done using phospholipase A_2, where hydrolysis of PIH will result in cleavage at the *sn*-2 position only. Selective hydrolysis will enable us to quantitate the asymmetric components and determine the actual amount present within this extract. As discussed, the optimization of this hydrolysis experiment will be carried out, where a better extraction procedure will enable improved quantification.

In addition, 15% unsaturation was quantified, using GC-FID, which equates to a maximum of 30% of the total PIH composition being unsaturated. Since the commercially available PIH was not completely hydrogenated, a procedure needs to be developed to enable us to complete the hydrogenation of PIH. By doing this, a comparison between the phase behaviour of a fully saturated system and the commercially available PIH could be investigated. Xi-jiang outlines this hydrogenation experiment in great detail, therefore the protocol and requirement for this experiment should be quite successful since we have access to the required instrumentation[71].

The effect of this unsaturation played a role in the phase behaviour, where a richer polymorphism for PIH compared to that of natural PI was observed[10,11]. It was found that PIH phase separated at high pressures for all temperatures studied. Overall these findings report, for the first time, the presence of a monolayer condensed phase formed by PI. This condensed phase was found at all pressures and temperatures in the PIH system. Moreover, this unique sighting is confirmed in the crystallographic (GIXD) data obtained for PIH, where a condensed phase was formed even at low pressures. In addition, at high temperatures and low pressures, below 5 mN m^{-1}, all components formed only a liquid-expanded phase. The critical temperature, above which a transition from a gaseous to a liquid-expanded phase occurs, has never been reported for inositol extracts and in our study we report this temperature to be between 30 and 35 °C.

Given that PIH is a charged lipid, one future direction for this study would be to look at the effect pH and salt concentration has on the behaviour of PIH at temperatures ranging from 15 to 35 °C. As well, since it is believed that stearoyl-palmitoyl-PI exhibits similar behaviour to that of DPPI, the GIXD of pure DPPI would help to determine the type of condensed phase that might be observed for the stearoyl-palmitol-PI component of PIH, thus determining how this component would influence the condensed phase.

Binary mixtures of DSPE with natural PI showed a negative excess area, A^E. Though, no obvious trend can be observed, we can say that our system is able to condense more efficiently in a mixture. To investigate whether this phase behaviour is due to phase separation, will require BAM and AFM. Also, ellipsometric measurements should be performed to observe whether optical properties of the film can be compared to that of the pure components. In contrast, evidence of de-mixing of DSPC and PIH at physiologically relevant mixing ratios was obtained, which is in agreement with Redfern et al. who also reports de-mixing of inositols, and phosphatidylcholines. To complete this characterization, the AFM images need to be closely studied where height differences along with area of fluid phase covered will need to be calculated. GIXD would aid in the determination of the miscibility in both DSPC/PIH and DPSE/PIH mixtures. If there is a PIH miscible in the DPSC phase (and vice versa) this would affect the packing and the resulting diffraction pattern. This technique will also provide information with regards to the condensing effect which was observed for both DSPC and DSPE mixtures. It has been suggested that the presence of other phospholipids namely, phosphatidylserine (PS), induces raft formation. If such is the case, binary mixtures of PI with PS along with ternary mixture of PI, PS and DSPC should be studied.

In the longer term, the aim will be to study the biophysical aspects of the phospholipid effect. Since PIH forms condensed phase domains, hydrolysis at the air-water interface using PLA_2 would be easy to visualize throughout the enzymatic reaction over time. In addition, other interfacial enzymes could be studied using PIH, such as PI-3K, which phosphorylates PIH at the 3-position of the inositol ring or PLC, which cleaves PIH at the phosphodiester bond. This reaction could also be monitored, using the visual capabilities of BAM which would enable one to study the effects of lipid-protein binding and the enzymatic reaction on the monolayer with time. GIXD can also be used to observe the structural changes upon reaction. This would also require knowledge of phase behaviour of products, e.g. PI-3P which would also need to be characterized.

There are two opposing ideas regarding the interaction of phosphoinositide rafts with proteins. One idea is that raft formation is induced by the presence of a protein, while the other believes that raft formation is initially required for lipid-protein binding to occur. Our findings support the idea that raft formation is possible without the presence of proteins, which establishes a foundation for the study of this enzymatic pathway. This foundation will contribute to the study of the miscibility of PI with key membrane phospholipids, in providing a better understanding of the behaviour of PI. This understanding will then leads to a long term study to uncover the biophysical properties required for raft formation by PI's. Moreover, this can then lead to a greater knowledge of the phospholipid effect.

References

(1) Karp, G. *Cell and Molecular Biology: Concepts and Experiments.*; John Wiley & Sons, Inc.: U.S, 1996; Vol. Second Edition.

(2) Evans, D. F.; Wennerstrom, H. *The Colloidal Domain Where Physics, Chemistry, Biology, and Technology Meet*, Second ed.; Wiley-VCH: New York, 1999.

(3) Office of Technology for Education 2005, *http://telstar.ote.cmu.edu/Hughes/tutorial/cellmembranes*.

(4) Cevc, G. *Phospholipids Handbook*; Marcel Dekker, Inc: New York, 1993.

(5) Thompson, W. *Biochimica et Biophysica Acta* 1969, *187*, 150-153.

(6) Holmberg, K.; Shah, D. O.; Schwuger, M. J. *Handbook of Applied Surface and Colloid Chemistry*; Wiley: New York, 2002; Vol. 1.

(7) Cullen, P. J.; Cozier, G. E.; Banting, G.; Mellor, H. *Current Biology* 2001, *11*, R882-R893.

(8) Berridge, M. J. *Biochemical Journal* 1984, *220*, 345-360.

(9) Vanhaesebroeck, B.; Leevers, S. J.; Ahmadi, K.; Timms, J.; Katso, R.; Driscoll, P. C.; Woscholski, R.; Parker, P. J.; Waterfield, M. D. *Annual Review of Biochemistry* 2001, *70*, 535-602.

(10) Mansour, H.; Wang, D.-S.; Chen, C.-S.; Zografi, G. *Langmuir* 2001, *17*, 6622-6632.

(11) DeWolf, C.; Leporatti, S.; Kirsch, C.; Klinger, R.; Brezesinski, G. *Chemistry and Physics of Lipids* 1999, *97*, 129-138.

(12) Squire, L. R. *Fundamental Neuroscience*, Second ed.; Elsevier Science: Amsterdam, 2003.

(13) Bear, M. F.; Connors, B. W.; Paradiso, M. A. *Neuroscience: Exploring the Brain*, Second Edition. ed.; Lippincott Williams & Wilkins: U.S, 2001.

(14) James, S. R.; Demel, R. A.; Downes, C. P. *Biochemical Journal* 1994, *298*, 499-506.

(15) Souvignet, C.; Pelosin, J. M.; Daniel, S.; Chambaz, E. M.; Ransac, S.; Verger, R. *Journal of Biological Chemistry* 1991, *266*, 40-44.

(16) Rao, C. S.; Damodaran, S. *Langmuir* 2002, *18*, 6294-6306.

(17) Dahmen-Levison, U.; Brezesinski, G.; Mohwald, H. *Thin Solid Films* 1998, *327-329*, 616-620.

(18) Hirasawa, K.; Irvine, R. F.; Dawson, R. M. *Biochemical Journal* 1981, *193*, 607-614.

(19) Hubner, S.; Couvillon, A. D.; Kas, J. A.; Bankaitis, V. A.; Vegners, R.; Carpenter, C. L.; Janmey, P. A. *European Journal of Biochemistry* 1998, *258*, 846-853.

(20) Brown, D. A.; London, E. *Annual Review of Cell and Developmental Biology* 1998, *14*, 111-136.

(21) Caroni, P. *EMBO Journal* 2001, *20*, 4332-4336.

(22) Bradshaw, J. P.; Bushby, R. J.; Giles, C. C. D.; Saunders, M. R.; Saxena, A. *Biochimica et Biophysica Acta* 1997, *1329*, 124-138.

(23) Zhou, C.; Garigapati, V.; Roberts, M. F. *Biochemistry* 1997, *36*, 15925-15931.

(24) Peters, G. H.; van Aalten, D. M. F.; Edholm, O.; Toxvaerd, S.; Bywater, R. *Biophysical Journal* 1996, *71*, 2245-2255.

(25) Stottrup, B., L.; Veatch, S., L.; Keller, S., L. *Biophysical Journal* 2004, *86*, 2942-2950.

(26) Brown, D. A.; London, E. *Biochemical and biophysical research communications* 1997, *240*, 1-7.

(27) Chen, J.; Feng, L.; Prestwich, G. D. *Journal of Organic Chemistry* 1998, *63*, 6511-6522.

(28) Dietrich, C.; Bagatolli, L. A.; Volovyk, Z. N.; Thompson, N. L.; Levi, M.; Jacobson, K.; Gratton, E. *Biophysical Journal* 2001, *80*, 1417-1428.

(29) Yun, H.; Choi, Y.-W.; Kim, N. J.; Sohn, D. *Bulletin of the Korean Chemical Society* 2003, *24*, 377-383.

(30) Brown, D. A.; London, E. *Journal of Biological Chemistry* 2000, *275*, 17221-17224.

(31) Jacobson, K.; Dietrich, C. *Trends in Cell Biology* 1999, *9*, 87-91.

(32) Ikonen, E. *Current Opinion in Cell Biology* 2001, *13*, 470-477.

(33) Kurzchalia, T. V.; Parton, R. G. *Current Opinion in Cell Biology* 1999, *11*, 424-431.

(34) Hurley, J. H.; Meyer, T. *Current Opinion in Cell Biology* 2001, *13*, 146-152.

(35) Tall, E. G.; Spector, I.; Pentyala, S. N.; Bitter, I.; Rebecchi, M. J. *Current Biology* 2000, *10*, 743-746.

(36) Cockcroft, S.; De Matteis, M. A. *Journal of Membrane Biology* 2001, *180*, 187-194.

(37) Bankaitis, V. A.; Aitken, J. R.; Cleves, A. E.; Dowhan, W. *Nature* 1990, *347*, 561-562.

(38) Eberhard, D. A.; Cooper, C. L.; Low, M. G.; Holz, R. W. *Biochemical Journal* 1990, *268*, 15-25.

(39) Tuominen, E. K. J.; Holopainen, J. M.; Chen, J.; Prestwich, G. D.; Bachiller, P. R.; Kinnunen, P. K. J.; Janmey, P. A. *European Journal of Biochemistry* 1999, *263*, 85-92.

(40) Foster, W. J.; Shih, M. C.; Pershan, P. S. *Journal of Chemical Physics* 1996, *105*, 3307-3315.

(41) Gascard, P.; Sauvage, M.; Sulpice, J. C.; Giraud, F. *Biochemistry* 1993, *32*, 5941-5948.

(42) Glaser, M.; Wanaski, S.; Buser, C. A.; Boguslavsky, V.; Rashidzada, W.; Morris, A.; Rebecchi, M.; Scarlata, S. F.; Runnels, L. W.; et al. *Journal of Biological Chemistry* 1996, *271*, 26187-26193.

(43) Barnett, S. F.; Ledder, L. M.; Stirdivant, S. M.; Ahern, J.; Conroy, R. R.; Heimbrook, D. C. *Biochemistry* 1995, *34*, 14254-14262.

(44) Knobler, C. M. *Molecular Crystals and Liquid Crystals Science and Technology, Section A: Molecular Crystals and Liquid Crystals* 2001, *364*, 133-140.

(45) Ter-Minassian-Saraga, L.; Madelmont, G. *Journal of Colloid and Interface Science* 1982, *85*, 375-388.

(46) Redfern, D. A.; Gericke, A. *Biophysical Journal* 2004, *86*, 2980-2992.

(47) Hansbro, P. M.; Byard, S. J.; Bushby, R. J.; Turnbull, P. J. H.; Boden, N.; Saunders, M. R.; Novelli, R.; Reid, D. G. *Biochimica et Biophysica Acta* 1992, *1112*, 187-196.

(48) Chen, L.; Johnson, M. L.; Biltonen, R. L. *Biophysical Journal* 2001, *80*, 254-270.

(49) Bradshaw, J. P.; Bushby, R. J.; Giles, C. C.; Saunders, M. R. *Biochemistry* 1999, *38*, 8393-8401.

(50) Patil-Sen, Y.; Tiddy, G. J. T.; Brezesinski, G.; DeWolf, C. *Physical Chemistry Chemical Physics* 2004, *6*, 1562-1565.

(51) Nanofilm Surface Analysis. In *I-Elli2000 Manual*, 2002.

(52) Nima Technology 2005, *http://langmuir-blodgett.com/basics/basics0.htm*.

(53) Teknillinen Korkeakoulu 2005, *http://www.tkk.fi/Yksikot/Paperi/laitteet.html#10*.

(54) Kaganer, V. M.; Mohwald, H.; Dutta, P. *Reviews of Modern Physics* 1999, *71*, 779-819.

(55) Leporatti, S. *PhD Thesis*, University of Potsdam, Germany, 1999.

(56) Wakeham, S. G. *Lipid Analysis in Marine Particle and Sediment Samples*; Skidaway Institute of Oceanography: Savannah, 2002.

(57) Barenholz, Y.; Gibbes, D.; Litman, B. J.; Goll, J.; Thompson, T. E.; Carlson, R. D. *Biochemistry* 1977, *16*, 2806-2810.

(58) Menashe, M.; Romero, G.; Biltonen, R. L.; Lichtenberg, D. *Journal of Biological Chemistry* 1986, *261*, 5328-5333.

(59) Egberts, J.; Sloot, H.; Mazure, A. *Biochimica et Biophysica Acta* 1989, *1002*, 109-113.

(60) Avanti Polar Lipids Inc. 2005, *http://www.avantilipids.com/index.htm*.

(61) Jensen, N. J.; Tomer, K. B.; Gross, M. L. *Lipids* 1987, *22*, 480-489.

(62) Hsu, F.-F.; Turk, J. *Journal of the American Society for Mass Spectrometry* 2000, *11*, 986-999.

(63) Holub, B. J.; Kuksis, A.; Thompson, W. *Journal of Lipid Research* 1970, *11*, 558-564.

(64) Shaw, D. J. *Introduction to Colloid and Surface Chemistry*, 3rd edition ed.; Butterworths & Co Ltd: London, 1980.

(65) Moraille, P.; Badia, A. *Langmuir* 2002, *18*, 4414-4419.

(66) Chi, L. F.; Anders, M.; Fuchs, H.; Johnston, R. R.; Ringsdorf, H. *Science* 1993, *259*, 213-216.

(67) Chi, L. F.; Fuchs, H.; Johnston, R. R.; Ringsdorf, H. *Thin Solid Films* 1994, *242*, 151-156.

(68) Ali, S.; Smaby, J. M.; Momsen, M. M.; Brockman, H. L.; Brown, R. E. *Biophysical Journal* 1998, *74*, 338-348.

(69) Evans, R. W.; Williams, M. A.; Tinoco, J. *Biochemical Journal* 1987, *245*, 455-462.

(70) Dahmen-Levison, U. *PhD Thesis*, University of Potsdam, Germany, 1998.

(71) Jin, X.-j. *Jingxi Huagong* 1999, *16*, 5-6.

Appendix:

Miscibility of PIH with DSPC (Chapter 6:)

BAM images of PIH with DSPC

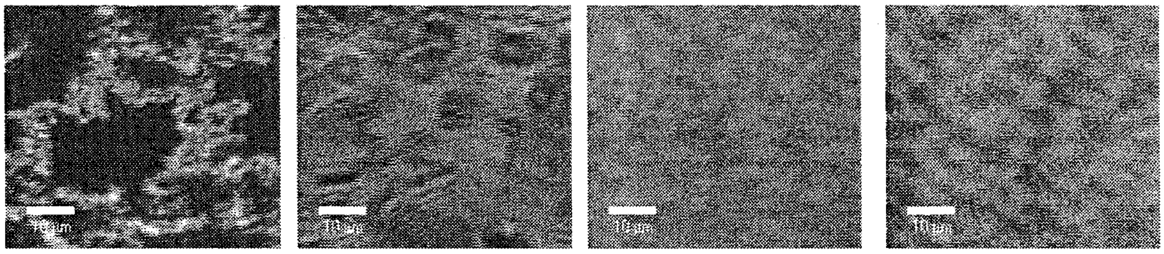

Figure 88 BAM images of pure DSPC at 25 °C (from left to right): 0 mN m^{-1}, 0.1 mN m^{-1}, 1.3 mN m^{-1} and 14.6 mN m^{-1}.

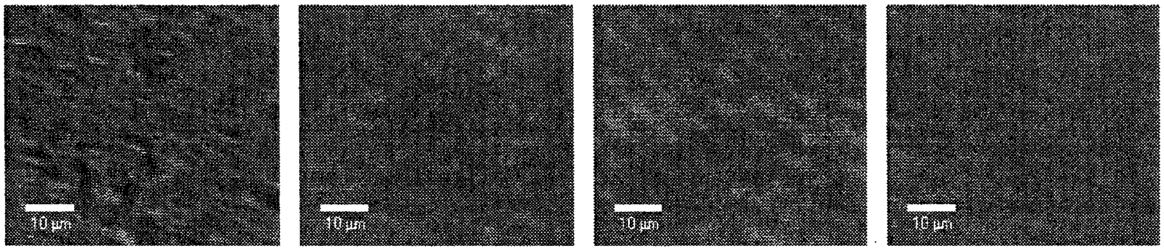

Figure 89 BAM images of 1.6mol% PIH in DSPC at 25 °C (from left to right): 0 mN m^{-1}, 4.2 mN m^{-1}, 18.2 mN m^{-1} and 43 mN m^{-1}.

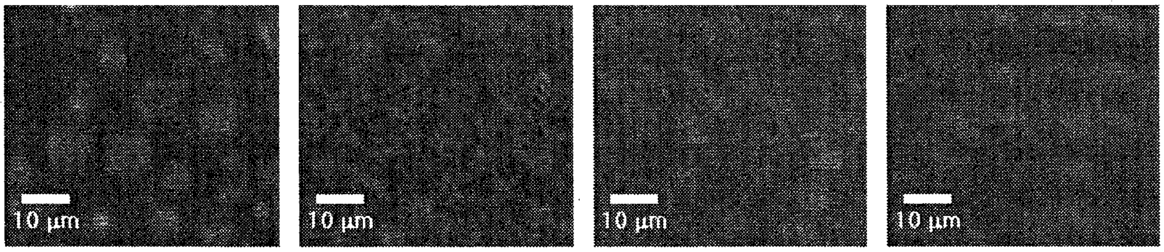

Figure 90 BAM images of 2.0mol% PIH in DSPC at 25 °C (from left to right): 0 mN m^{-1}, 9 mN m^{-1}, 16 mN m^{-1} and 37 mN m^{-1}.

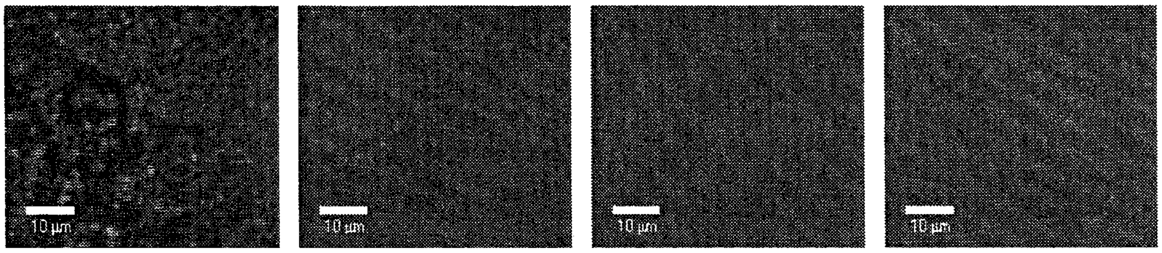

Figure 91 BAM images of 2.5mol% PIH in DSPC at 25 °C (from left to right): 0 mN m^{-1}, 8.6 mN m^{-1}, 20.3 mN m^{-1} and 31.2 mN m^{-1}.

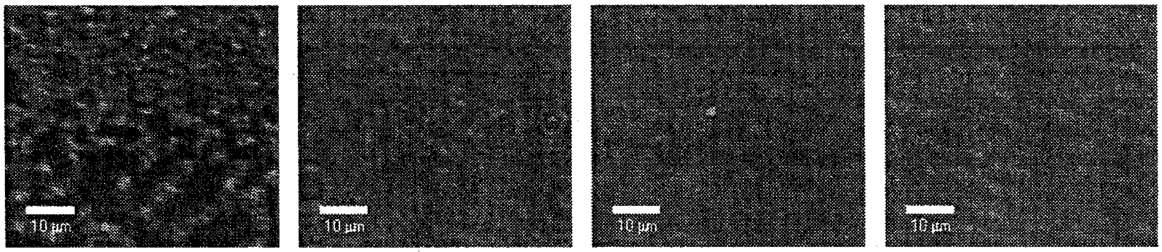

Figure 92 BAM images of 3.0mol% PIH in DSPC at 25 °C (from left to right): 0 mN m^{-1}, 1.6 mN m^{-1}, 10.4 mN m^{-1} and 42.6 mN m^{-1}.

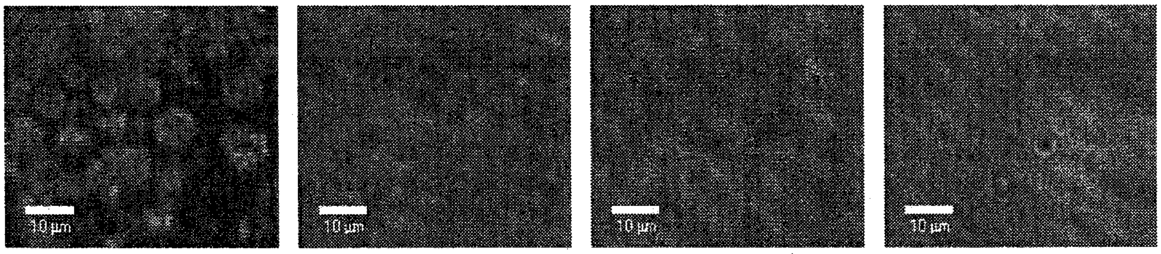

Figure 93 BAM images of 3.5mol% PIH in DSPC at 25 °C (from left to right): 0 mN m^{-1}, 2.4 mN m^{-1}, 9.6 mN m^{-1} and 24.9 mN m^{-1}.

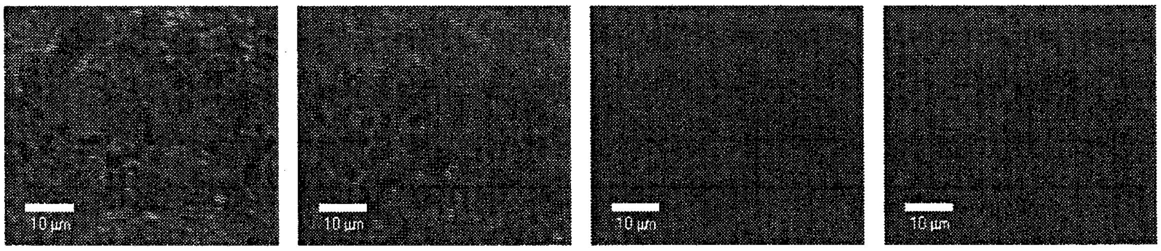

Figure 94 BAM images of 4.0mol% PIH in DSPC at 25 °C (from left to right): 0 mN m^{-1}, 2.5 mN m^{-1}, 28 mN m^{-1} and 45.3 mN m^{-1}.

Ellipsometric Isotherms of PIH with DSPC

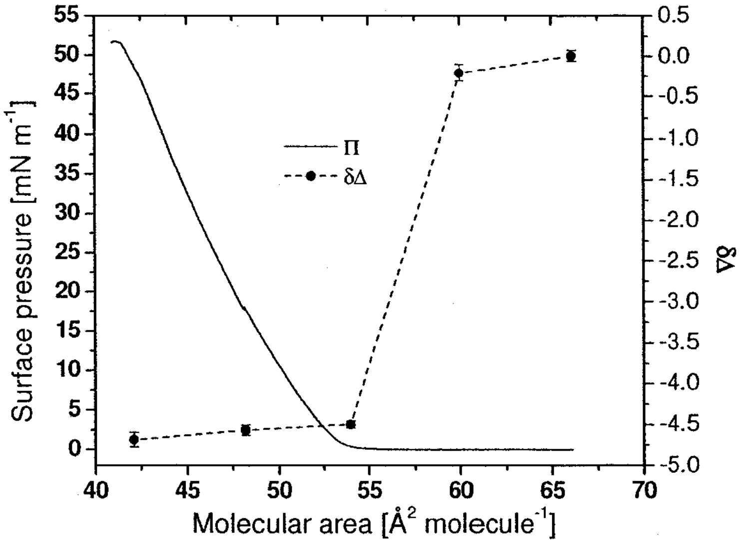

Figure 95 Ellipsometric isotherm of 1.6mol% PIH in DSPC at 25 °C.

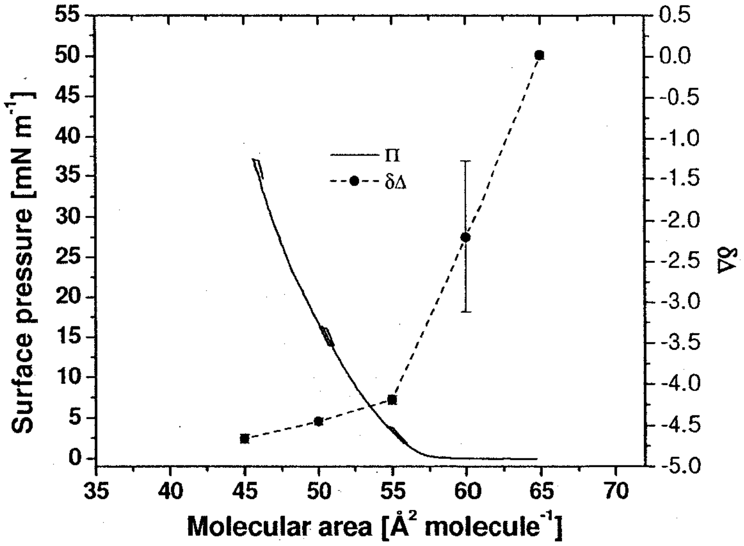

Figure 96 Ellipsometric isotherm of 2mol% PIH in DSPC at 25 °C.

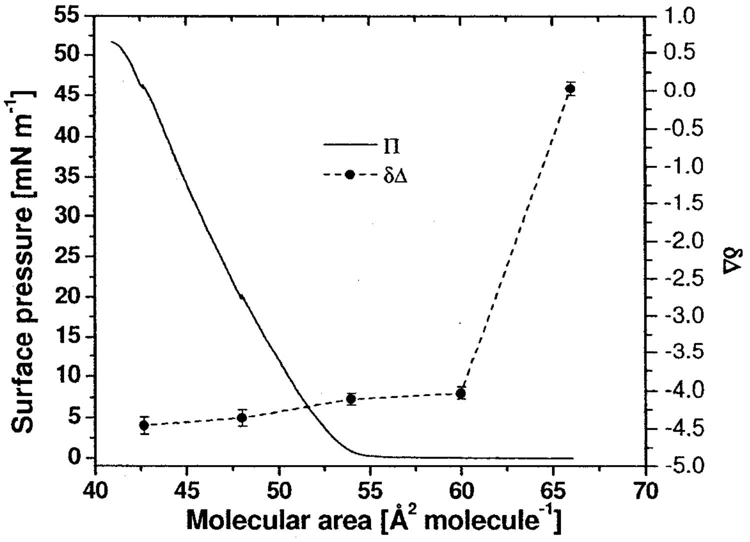

Figure 97 Ellipsometric isotherm of 2.5mol% PIH in DSPC at 25 °C.

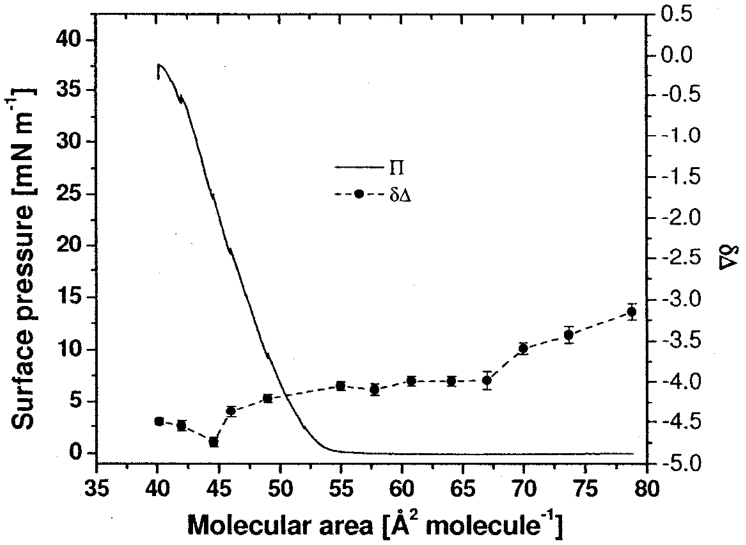

Figure 98 Ellipsometric isotherm of 3.5mol% PIH in DSPC at 25 °C.

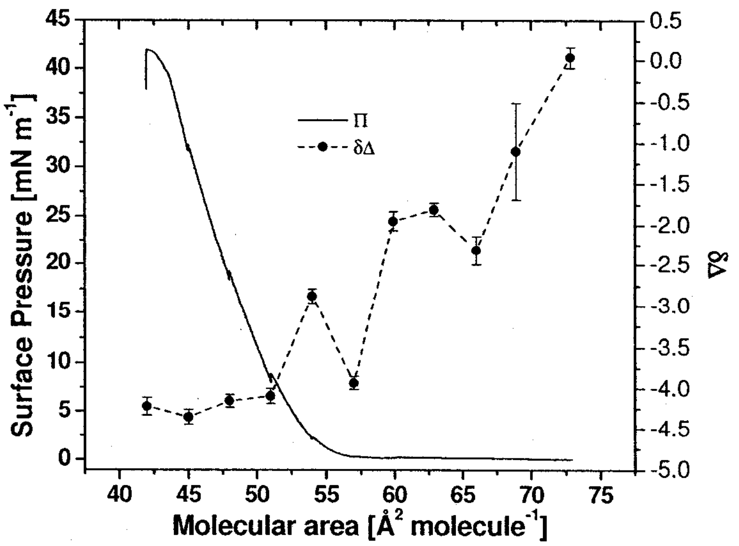

Figure 99 Ellipsometric isotherm of 4.0mol% PIH in DSPC at 25 °C.